Electrical Engineering

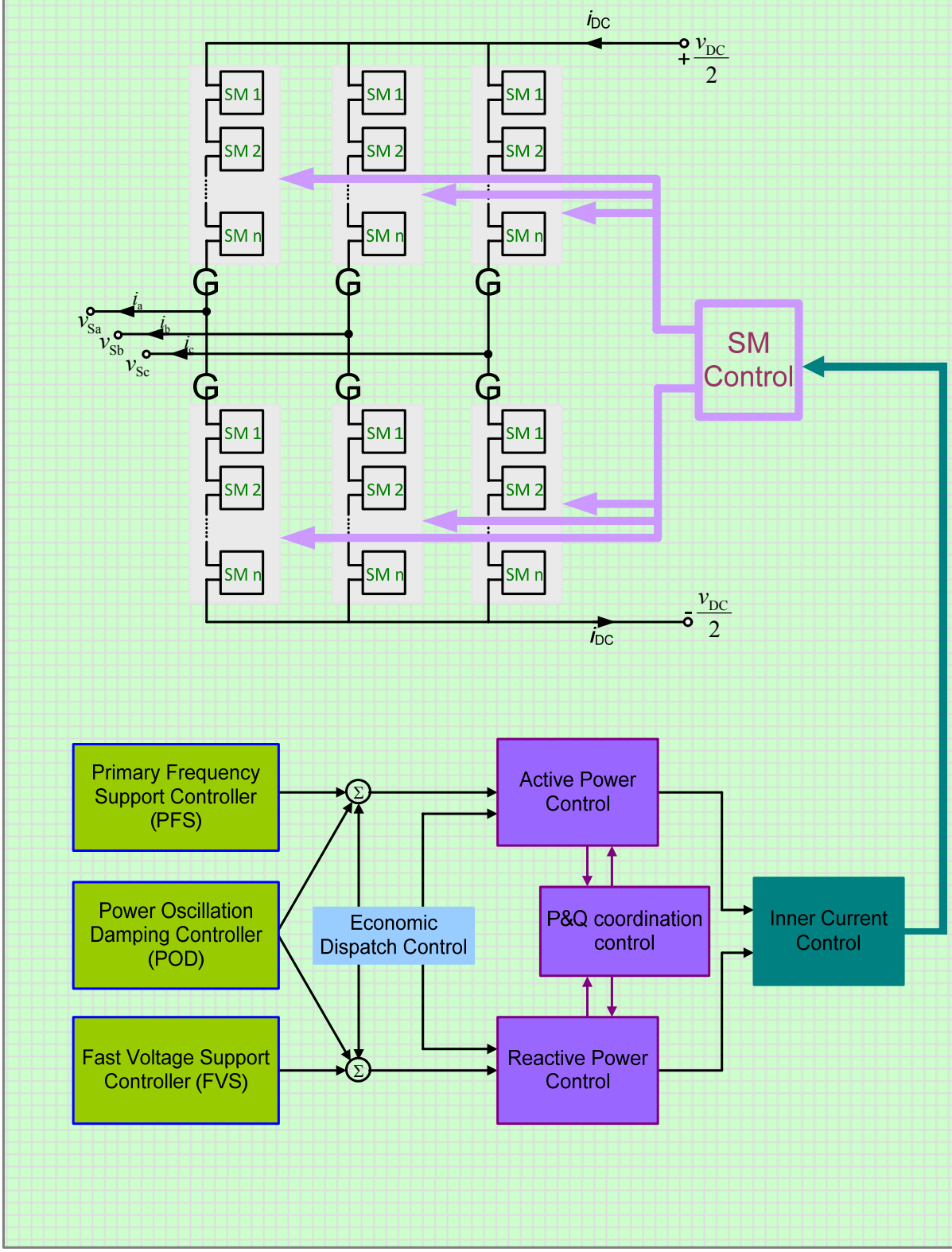

Enhancement of Grid Dynamic Performance using MMC-VSC-MTDC Systems

Ngoc-Tuan Trinh

Enhancement of Grid Dynamic Performance using VSC-based Multi-terminal HVDC Systems in Multilevel Modular Converter Topology

Von der Fakultät für Ingenieurwissenschaften der
Abteilung Elektrotechnik und Informationstechnik
der Universität Duisburg-Essen

zur Erlangung des akademischen Grades eines

Doktors der Ingenieurwissenschaften (Dr.-Ing.)

genehmigte Dissertation

von

Ngọc-Tuấn Trịnh

aus

Nghe An, Vietnam

Tag der Einreichung:	02.06.2016
Tag der mündlichen Prüfung:	02.11.2016
1st Gutachter:	Prof. Dr.-Ing. Habil. Istvan Erlich
2nd Gutachter:	Prof. Dr. Dirk Van Hertem
Prüfer und Vorsitzender:	Prof. Dr. rer. nat. Roland Schmechel
Prüfer:	Prof. Dr.-Ing. Rainer Kokozinski
Prüfer:	Prof. Dr.-Ing. Andreas Czylwik

Abstract

Modern power systems have expanded, both in size and complexity. More challenges will emerge with the integration of an increasing number of renewable generation sources to the existing power systems, which are driven to operate closer to their technical limits under pressure from economic objectives in deregulated markets and environment impacts. The transmission systems must be strengthened to transmit a larger amount of power from the remote renewable generation sources to load centers while ensuring a higher degree of flexibility and stability in operating the power systems. The Voltage-Source Converter (VSC) in Modular-Multilevel Converter (MMC) topology for High-Voltage Direct Current (HVDC) application has been recently developed and has become an attractive solution to address the new challenges to the existing power system.

This thesis deals with the utilizations of MMC-VSC-HVDC systems in Multi-Terminal Direct Current (MTDC) configuration to enhance the dynamic performance of AC power systems. In this framework, several supplementary controllers are integrated into the standard VSC station controller to exploit the distinct advantages in the areas of controllability and flexibility of the MMC-VSC-MTDC systems. The integrated supplementary controllers are developed to address most of the dynamic stability aspects in the power systems: small-signal stability (SSS), transient stability including frequency and voltage stabilities. The main contributions of this work include: the development of a generic RMS model of the MMC-VSC-MTDC system and its corresponding linearization; the development of a novel frequency controller which enables the MMC-VSC-MTDC system to effectively support the power flow in primary frequency control; the investigation of several major factors influencing the contribution of the VSC-MTDC system to the damping of system oscillations and the demonstration of the capability of supporting system voltage during symmetrical grid faults. The thesis also proposed the design as well as appropriate methodologies for selecting parameters of the supplementary controllers. The controllers are firstly investigated in individual studies under consideration of several influence factors to explore their main features. Furthermore, possible interactions between the investigated supplementary controllers which may influence their effectiveness's are identified. Based on the investigation, proper counter-measures are proposed to mitigate the interactions.

Zusammenfassung

Moderne elektrische Energieversorgungssysteme sind bei zunehmender Größe und Komplexität erweitert worden. Mit der Integration einer wachsenden Anzahl von erneuerbaren Erzeugungsquellen werden weitere Herausforderungen in den bestehenden elektrischen Energieversorgungssystemen entstehen Diese werden unter Druck von wirtschaftlichen Zielen in deregulierten Märkten und Umweltauswirkungen näher an ihren technischen Grenzen betrieben. Die Übertragungssysteme müssen gestärkt werden, um eine größere Menge an elektrischer Energie von den entlegenen, erneuerbaren Erzeugungsquellen zu den Lastzentren zu übertragen, während gleichzeitig ein höheres Maß an Flexibilität und Stabilität in der Betriebsführung der elektrischen Energieversorgungssysteme gewährleistet sein soll. Der spannungsgeführte Umrichter (englisch: Voltage Source Converter, VSC) mit modularer Multilevel-Umrichter (englisch: Modular Multilevel Converter, MMC) Topologie für Hochspannungs-Gleichstrom-Übertragungs- (HGÜ) Anwendung wurde vor kurzem entwickelt und wurde eine attraktive Lösung für die neuen Herausforderungen an das bestehende elektrische Energieversorgungssystem.

Diese Arbeit beschäftigt sich mit der Nutzung der MMC-VSC-HGÜ-Systeme in Multi-Terminal-Gleichstrom (englisch: Multi Terminal Direct Current, MTDC) Konfiguration, um das dynamische Verhalten von Drehstromsystemen zu verbessern. In diesem Rahmenwerk sind zu der Standard-VSC Stationsregelung einige, zusätzliche Reglungsfunktionen hinzugefügt worden, um so deutliche Vorteile in den Bereichen der Regelbarbarkeit und Flexibilität der MMC-VSC-MTDC-Systeme zu nutzen. Die integrierten, zusätzlichen Regelungsfunktionen wurden entwickelt um die meisten der dynamischen Stabilitätsaspekte in elektrischen Energieversorgungssystemen zu behandeln: Kleinsignalstabilität, transiente Stabilität einschließlich Frequenz- und Spannungsstabilität. Die wichtigsten Beiträge dieser Arbeit sind: die Entwicklung eines generischen RMS Modells des MMC-VSC-MTDC-Systems und seiner entsprechenden Linearisierung; die Entwicklung eines neuartigen Frequenzreglers, der dem MMC-VSC-MTDC-System ermöglicht, den Leistungsfluss während der Primärregelung effizient zu unterstützen; die Untersuchung von mehreren, wichtigen Faktoren, die den Beitrag des VSC-MTDC Systems zur Dämpfung von Systemschwingungen beeinflussen und die Demonstration der Fähigkeit zur Unterstützung der Systemspannung während symmetrischer Netzstörungen. Diese Arbeit schlägt auch den Entwurf sowie geeignete Methoden zur Parameterbestimmung der zusätzlichen Reglungsfunktionen vor. Die Regler wurden zunächst in einzelnen Studien unter Berücksichtigung von mehreren Einflussfaktoren untersucht, um so ihre wichtigsten Merkmale zu erkunden. Darüber hinaus wurden mögliche Wechselwirkungen zwischen den untersuchten, zusätzlichen Regelungsfunktionen, die ihre Wirksamkeit beeinflussen können, identifiziert. Auf Grundlage der Untersuchung wurden geeignete Gegenmaßnahmen vorgeschlagen, um die Wechselwirkungen abzuschwächen.

Acknowledgements

This thesis was written during my time as a researcher at the institute of Electrical Power Systems (EAN) of the University Duisburg-Essen and as a consultant at Siemens PTI in Erlangen between 2012 and 2016.

First of all, I want to express my highest regards, and deepest respect, to my daily supervisor, Prof. Dr. Istvan Erlich. It is an honor and a pleasure for me to have Prof. Dr. Istvan Erlich as my supervisor. His patience and support helped me to go through the hardest moments of the research work. Without his guidance and encouragement, the contents of the thesis cannot reach the same level as it is today. Hereby, I would also like to thank Prof. Dr. Dirk Van Hertem and the other members of my Ph.D. defense committee for their time to appraise, and comment on the contents of this work.

This work was supported in part by the German Federal Ministry for the Environment, Nature Conservation and Nuclear Safety within the 'ACCESS2Grid' project (0325663). The financial support is greatly acknowledged. I also want to thank my project partners Dr. Klaus Würflinger and Dr. Marcus Zeller from Siemens EM TS for the fruitful discussions and their inputs for developing suitable models for the project.

My acknowledgement also goes to my colleagues in Siemens in Erlangen. My most sincere thankfulness goes to Dr. Ronald Völzke (PTI), who initiated the three-year research project between EM TS and PTI and supported me to successfully complete the project during my study in Duisburg. I would like to give a special thank to my dear friend, Dr. Simon Teeuwsen (EM TS), who introduced me to Prof. Erlich and supported me to publish the first paper together with him at IEEE PES GM 2014. I would like to thank another special friend, Dr. RodrigoTeixeira Pinto (EM TS), for reviewing the manuscript of the thesis with all of his excellent language skill and carefulness. My sincere thankfulness also goes to my close friends, Adham Atallah and Dr. Cuong Nguyen-Mau, who always welcomed me and provided the warmest stay every time I came back Erlangen for reporting the progress of the project.

I would like to thank my colleagues in the EAN institute in Duisburg who directly or indirectly contributed to this work by their good suggestions and their kind help. In particular, my sincere thankfulness goes to Dr. Fekadu Shewarega for his advices and proofreading of my papers published during this time. I would like to thank Tobias Neumann for his help when I started my work at the EAN institute, for his coordination in publishing scientific papers and for reviewing the German version of the abstract in my thesis.

More than a dissertation, I also made good friends during my staying in Duisburg. I want to thank a very special team of friends, Fischnull group, with whom I have shared opinions, sport passion and have done social activities for Vietnamese community in Duisburg. I would also like to give a sincere thank to family Ngoc-Ha and family Mai Hong-Steffen for being with my family at many special moments of life, and making us feel at home. They were, and will continue to be, very good friends of my family.

This work is dedicated to my parents and my parents-in-law, who always wanted to have a Doctor in the family! Thank you very much for your love and encouragement for all the time. I also want to thank my brothers and sisters for their love and for putting your trust in me. I wish to be an example to my brothers and sisters that hard work does pay off, as much as my parents have been a role model of hard work to me all my life.

Finally, I would like to thank my beloved wife and son. Thank you, Nga, so much for your endless love, support and understanding. Thank you, Titie, for the joys you have brought to my life.

Erlangen, November 2016 Ngoc-Tuan Trinh

Contents

Figures ..... **iii**

Tables ..... **v**

Abbreviation ..... **vi**

1 Introduction **1**
1.1 Motivation 1
1.2 Objective of the thesis 2
1.3 Outline of the thesis 5

2 MMC-VSC in HVDC application **7**
2.1 MMC-VSC-HVDC features 7
2.2 Working principle of MMC-VSC 8

3 MMV-VSC-HVDC modeling **11**
3.1 Averaged EMT model of MMC-VSC 12
3.1.1 Averaged EMT representation 12
3.1.2 MMC-VSC control for EMT model 14
3.2 Generic RMS model of MMC-VSC 16
3.2.1 Generic RMS representation 16
3.2.2 MMC-VSC control for RMS model 17
3.3 Generic RMS model identification 19
3.3.1 Parameter identification algorithm 20
3.4 Simulation results 22
3.5 Dynamic performance of the generic RMS model of MMC-VSC-HVDC system 23
3.5.1 Test network 23
3.5.2 Simulation results 25

4 Power oscillation damping controller **29**
4.1 Linearized model of an embedded MMC-VSC-MTDC power system 30
4.2 POD controller for a MMC-VSC-MTDC system 31
4.2.1 Input/output selection algorithm 32
4.2.2 Parameter optimization 33
4.3 Test system 34
4.3.1 Modal analysis 35
4.3.2 POD input/output selection 36
4.4 Damping support capability of MMC-VSC-MTDC systems equipped with POD controllers 38
4.4.1 Effect of system load characteristics 40
4.4.2 Effect of using global signals 41
4.4.3 Effect of communication delay 41
4.4.4 Effect of active power loading levels 43
4.5 Summary 44

5 Primary frequency support controller **47**
5.1 Dynamic response of MTDC systems following power reference change 48
5.2 Exchanged powers between areas in AC grids in primary frequency control 51
5.3 Primary frequency support controller in VSC-MTDC-embedded network 52
5.3.1 PFS gain determination 52
5.3.2 Transient component 53

5.3.3 Controller activation scheme 55
5.4 Test system 57
5.5 Simulation results 59
5.5.1 Performance of the proposed static gain 59
5.5.2 Performance of transient component 63
5.5.3 Parameter sensitivity analysis 66
5.5.4 PFS control application on MTDC systems connecting isolated systems 68
5.6 Summary 69

6 Fast voltage support controller 71
6.1 FVS controller structure 71
6.2 P&Q coordination control 72
6.3 STATCOM mode 73
6.4 Test system 74
6.5 Simulation results 75
6.6 Summary 80

7 Controller coordination 81
7.1 Test system 81
7.2 Small-signal stability analysis 82
7.3 Large disturbance analysis 84
7.3.1 Control coordination on reactive power channel 85
7.3.2 Control coordination on active power channel 89

8 Conclusions and future work 91
8.1 Conclusions 91
8.2 Future work 93

References 95

Publications 101

Appendixes 103

Figures

Figure 1.1: High level of a VSC-HVDC station control system 3

Figure 2.1: Overview of the Modular-Multilevel Converter topology [5] 8

Figure 3.1: MMC-VSC generic EMT model [10] 12

Figure 3.2: MMC-VSC control scheme 15

Figure 3.3: MMC-VSC generic RMS model 16

Figure 3.4: Test network for parameter identification of the RMS model 19

Figure 3.5: Flowchart of the MVMO algorithm. 21

Figure 3.6: Comparison of simulation results of 150-ms 3PSC at PCC1. 22

Figure 3.7: Test network for RMS model validation 24

Figure 3.8: Simulation result in time domains using averaged EMT and generic RMS models 25

Figure 4.1: PSS-based POD controller for a MMC-VSC-MTDC system 31

Figure 4.2: Test network for the POD analysis. 34

Figure 4.3: Observability measure results 36

Figure 4.4: Controllability measure results (x10-4) 37

Figure 4.5: Joint Controllability/Observability measure results ($x10^{-4}$): BEST-L and BEST-G are the best combination of input/output using local and global bus angle inputs, respectively, described in Table 4.2 37

Figure 4.6: Modal analysis results of different POD options 39

Figure 4.7: Time domain simulation results of different POD options 39

Figure 4.8: Effect of load characteristic on controllability measures of POD controllers on P and Q channels of VSC2 ($x10^{-4}$) 40

Figure 4.9: Effect of communication time delay to observability of bus angle input 42

Figure 4.10: Effect of communication time delay to damping support capability of MMC-VSC-MTDC system 42

Figure 4.11: Effect of random deviation of communication time delay to damping support capability of MMC-VSC-MTDC system 43

Figure 4.12: Effect of active power VSC-loading on damping support capability of POD equipped on: a) active power channel (P-BEST-G option) b) reactive power channel (Q-BEST-G option) 44

Figure 5.1: Schematic structure of the proposed PFS controller 52

Figure 5.2: Simplified power-frequency model of embedded VSC-MTDC grid 54

Figure 5.3: Novel PFS controller using feed-forward control technique 55

Figure 5.4: Activation scheme applied for PFS controller 56

Figure 5.5: Test network for the primary frequency control analysis 58

Figure 5.6: Turbine governor block diagram 58

Figure 5.7: Case 1a: PFS controller without $G_{PFS}(s)$, 240 MW generation outage in area 260

Figure 5.8: Case 1b: PFS controller without GPFS(s), 240 MW generation outage in area 1 62

Figure 5.9: Case 2a: PFS controller with $G_{PFS}(s)$, α_{DC}=1.0, generation outage of 240 MW in area 2 64

Figure 5.10: Case 2b: PFS controller with $G_{PFS}(s)$, α_{DC}=1.0, generation outage of 240 MW in area 1 65

Figure 5.11: Case 3: PFS controller with $G_{PFS}(s)$, α_{DC}=1.0, generation outage of 160 MW in area 1 67

Figure 5.12: Case 4: VSC-MTDC connecting isolated areas, PFS controller with $G_{PFS}(s)$, α_{DC}=1.0, generation outage of 240MW in area 2 69

Figure 6.1: FVS controller structure 72

Figure 6.2: Limitation allocation options 72

Figure 6.3: Structure of the P&Q Coordination Control 73

Figure 6.4: Full-bridge configuration 74

Figure 6.5: Test system for voltage stability analysis 75

Figure 6.6: Simulation results of a 150-ms 3PSC applied at Bus 9 77

Figure 6.7: Simulation results of a 150-ms 3PSC applied at bus 4 78

Figure 6.8: Simulation results of a line-to-line fault in DC grid 79

Figure 7.1: Test system for control coordination study 82

Figure 7.2: Relative damping results of control coordination study 83

Figure 7.3: Time-domain simulation results of control coordination study 84

Figure 7.4: Fault scenarios considered for control coordination study 85

Figure 7.5: Simulation results of control coordination study on Q channel 86

Figure 7.6: The proposed POD controller with additional blocking scheme 87

Figure 7.7: Simulation results of control coordination study on Q channel with the blocking scheme 88

Figure 7.8: Comparison of the resulted terminal voltages of cases with and without the blocking scheme 89

Figure 7.9: Simulation results of control coordination study on P channel 90

Tables

Table 3.1: Components of the DC active power 18

Table 3.2: Eigen value analysis results 26

Table 4.1: Eigenvalue analysis results without POD controller 35

Table 4.2: The best input-output combination for POD controller by applying the geometric approach 38

Table 5.1: Parameters for governors, load model and VSC control 59

Table 5.2: Control parameters for PFS controllers 59

Table 5.3: Simulation result of case 1a at quasi-steady state 61

Table 5.4: Simulation result of case 1b at quasi-steady state 63

Table 5.5: Simulation result of case 3 at quasi-steady state 68

Table 6.1: Setting parameters for FVS controller 75

Table 6.2: Study cases for voltage stability analysis 76

Table 7.1: Results of modal analysis without POD controller 83

Table 7.2: Study cases for control coordination study 85

Abbreviation

HVDC	High-Voltage direct current
HVAC	High-Voltage alternating current
MTDC	Multi-terminal High-Voltage direct current
VSC	Voltage-Source converter
MMC	Modular-multilevel converter
SM	Submodule
LCC	Line-commutated converter
IGBT	Insulated gate bipolar transistor
AC	Alternating current
DC	Direct current
POD	Power oscillation damping
PODp	Power oscillation damping controller equipped on the active power channel
PODq	Power oscillation damping controller equipped on the reactive power channel
PFS	Primary frequency support
FVS	Fast voltage support
RMS	Root mean square
EMT	Electromagnetic transient
PCC	Point of common coupling
P&Q	Active and reactive power
P	Active power
Q	Reactive power
PI	Proportional-integral
ctr	Control
ref	Reference
ord	Ordered
cap	Capacitor
qs	Quasi steady state
CONV	Converter
3PSC	Three-phase short-circuit

GOV	Speed governor
AVR	Automatic voltage regulator
PSS	Power system stabilizer
SVC	Static Var Compensator
MVMO	Mean-variance Mapping Optimization
MLQG	Modal linear quadratic Gaussian
WAMS	Wide area measurement signal

1 Introduction

1.1 Motivation

HVDC transmission technology has been utilized in the electrical power systems for more than 50 years, offering new dimensions for long distance transmissions [1]. Its development started with the transmission of power in a range of less than a hundred MW and has grown since. The HVDC transmission technology provides essential features to avoid technical problems in power systems. They increase the transmission capacity and enhance stability of power systems in an efficient way [2].

HVDC transmission started with the first commercial HVDC link between Sweden's mainland to Gotland island in 1954. At that time, the mercury-arc valve was used [2]. With the introduction of the thyristor valve converters in 1970s, the HVDC transmission technology became more attractive. The utilization of thyristor valves has enabled to build Line-Commutated Converters (LCC) for HVDC transmission with higher power rating. These converters are famous for their low operational losses, their overload capability and robustness of the thyristors against surge currents. Therefore, the LCC-HVDC connections are still the most attractive option for bulk power transmission in future HVDC projects [3].

In the late 1990s, the insulated-gate bipolar transistor (IGBT) was further developed to a sufficiently high rating that was economical to build high-voltage valves. The introduction of the IGBT as the main building block of the valves started a new era in the HVDC technology with the Voltage-Source Converter (VSC). VSC stations facilitate a more compact design and provide a high degree of controllability [4]. The new technology offers more advanced features which are not available in the classical LCC-HVDC technology.

The VSC converters with two-level or three-level converters for the HVDC applications introduced in 1997 have offered the possibility to control the active and reactive powers independently [1]. The VSC-HVDC connections are able to connect to weak or even passive networks, which is not possible with the LCC-HVDC technology. This controllability makes them attractive to power transmission and distribution applications. A main disadvantage is however, that the power losses in VSC stations are higher.

Only recently, Modular-Multilevel Converter (MMC) topologies have been applied for VSC-HVDC technology. This new MMC-VSC in the HVDC application possesses not only the well-proven advanced features, but also eliminates several drawbacks of the VSC converters with the two- or three-level topologies [5]. For instance, the operational power losses are

significantly reduced and the need for harmonic filter is obviated [4-5]. Owing to the rapid development of power electronic devices, the MMC-VSC-HVDC technology has reached the GW range to become available for bulk power transmission applications, i.e. 2x1 GW connection between France and Spain in INELFE project [5]. The distinct advantages in the areas of controllability and flexibility of the VSC-HVDC technology ensure it as an attractive solution to face the new challenges of existing power systems [6]. The challenges are related with the integration of an increasing number of renewable generation sources to the existing power systems, which are driven to operate closer to their limits due to pressure of economic objectives in deregulated markets and due to more strict environment impact regulations. The transmission systems must then be strengthened to transmit a larger amount of power from the remote renewable generation sources to load centers while ensuring a higher degree of flexibility and stability in operating the power systems. Since the first installation of point-to-point MMC-VSC-HVDC connection went operational in 2010, the number of the MMC-VSC-HVDC projects keeps continuously increasing [7]. In recent years, there has been an increased interest in MMC-VSC-HVDC systems in multi-terminal (MTDC) configuration as a prospective alternative for strengthening the transmission system [8]-[9].

The probable investigations on impacts of MMC-VSC-MTDC systems on existing power systems must be carried out in order to enable any feasible integration planning of a MMC-VSC-MTDC system. This is the motivation of this thesis, which focuses on investigations of the interactions between integrated MMC-VSC-MTDC systems and interconnected AC power systems. In this thesis, several methods to explore the controllability offered by the MMC-VSC-HVDC technology in multi-terminal configuration to enhance the dynamic stability of AC power systems are proposed and described.

1.2 Objective of the thesis

As mentioned in the previous part, the focus of this work is the converter station control system utilized in VSC-HVDC systems. Such control system is designed not only to protect the VSC station, but also to actively strengthen the dynamic stability of the power systems (within the scope of the thesis) and provide auxiliary control functions (outside the scope). Figure 1.1 shows the overview of the converter control structure and its functional modules which can be classified into two groups: principle control and supplementary control.

The principle control is a group of core control modules of a converter control structure. It aims to ensure and establish a stable operation of the whole power system including AC and DC grids. It involves all activities of the VSC-HVDC station control. The principle control

comprises of Inner Current Control, Active Power Control, Reactive Power Control and Control Channel Coordination. The principle control provides reference voltages for the converter operation level of the VSC control system through the Inner Current Control. The Inner Current Control is a high dynamic performance controller, working on the *dq* co-ordinate system. It ensures a fast and accurate tracking of the reference currents provided by the Active and Reactive Power Controls.

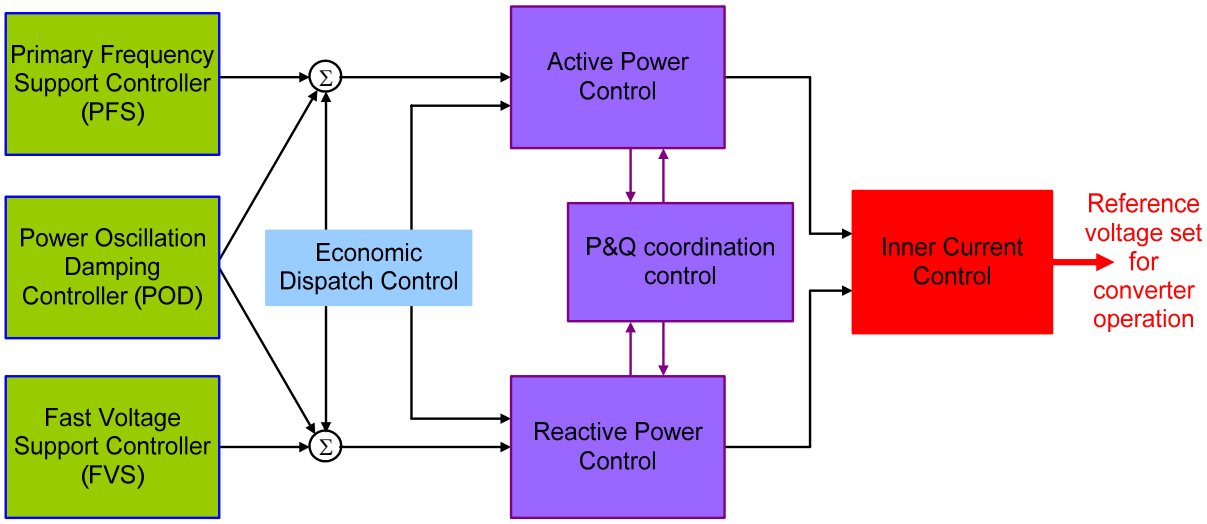

Figure 1.1: High level of a VSC-HVDC station control system

The Active Power Control defines the active power exchange between areas or buses of the AC power system interconnected by the VSC-HVDC system in normal operation. In abnormal operation and post-disturbance conditions, the control acts in combination with other supplementary controls to support the system frequency and improve the damping to counteract the system oscillations. For the DC grid side of the VSC-HVDC system, the Active Power Control plays also a crucial role. Similarly to the frequency in the AC system, DC voltage is an indicator of the power balance in a DC system. The Active Power Control is organically related to the DC voltage control. It involves in the primary control action to enable to set up a continuous operating equilibrium in the DC grid with well-defined operating points for all converter stations. It should also enable to establish a new equilibrium following a stable transition under small changes of loads/ network configuration or under large disturbances. Therefore, the Active Power Control at one converter station has to work in touch with the ones at other converter stations within a DC grid.

The Reactive Power Control aims to fulfill the inter-connected grid requirements for the converter station at the point of common coupling (PCC). Under normal operations, it can follow reference settings (ac reference voltage and reference reactive power) given by system

operators. The reference settings are always extracted from the activity of the Economic Dispatch Control located at system control centers. Under abnormal operations, the voltage system steps out of the continuous operating range. The Reactive Power Control co-operates with supplementary controls, i.e. fast voltage support controller, on the reactive power channel to bring the fast reactive power regulation capability of the VSC converter station into play. The coordination provides a fast voltage support locally at the PCC bus, thus participates in enhancing the system stability.

The P&Q Coordination Control has a special task. It manages the converter station limitations posed on the Active and Reactive Power Controls to maximize the VSC converter capability on controlling active and reactive power. The control gives out the priority of using the bigger constitution part of the converter limitation for either to the Active Power Control or the Reactive Power Control in different transient situations happening in the operating system. By doing so, the transient stability of power systems can be considerably improved.

In contrast to the principle control, the supplementary control provides application functional controllers to enhance the dynamic performance of AC power systems. They are inactive in steady-state operation, but active in dynamic transient stage through the principle controls by offering additional reference values to the principle controls. The use of the supplementary control depends on the installation request from the investors and in the same time depends on the situations in the inter-connected AC power systems. Several studies are ongoing to include more functional controllers into the supplementary control.

There are three functional controllers in Figure 1.1, which are the focus of this thesis. These functional controllers are: the Power Oscillation Damping (POD) controller; the Primary Frequency Support (PFS) controller; the Fast Voltage Support (FVS) controller. They are designed to support power systems during and after disturbances. The POD controller is to improve the damping inherent to AC power systems. The PFS control is used to support the primary frequency control following outages of large generation units. The FVS controller is used to support the recovery of the positive sequence voltage after short-circuit incidents.

In this thesis, the capability of the MMC-VSC-HVDC system equipped with the supplementary controllers in enhancing the dynamic performances of AC power systems is investigated. Firstly, the effect of each supplementary controller is individually analyzed taking into consideration several influence factors. The controllers design and appropriate methodologies for selecting their parameters are proposed. Analytical methods together with time-domain simulations are employed to validate the proposed methodologies. At last,

possible interactions between the investigated supplementary controllers which may influence their effectiveness are investigated.

1.3 Outline of the thesis

The thesis starts with a general introduction of its motivations and objectives in **chapter 1**.

Chapter 2 gives an overview of features and the working principle of the MMC-VSC technology in HVDC applications.

In **chapter 3**, modeling of MMC-VSC in HVDC applications for transient stability analysis is discussed. A generic RMS model of a MMC-VSC-HVDC system is proposed based on an existing averaged EMT model. Chapter 3 also presents a linearized model of the MMC-VSC-HVDC system for analytical modal analysis. The performance of the proposed RMS model is verified by both time- and frequency- domain simulations using a typical high-voltage transmission test network. These models are used in the different studies carried out in the following chapters.

Chapter 4 investigates the capability of MMC-VSC-MTDC systems for enhancing damping of inter-area oscillations. The Power Oscillation Damping controller is incorporated into both the active and reactive power modulation channels of the MMC-VSC station controls. In this chapter, the POD controller structure, input/output selection method and the parameter optimization method are described. Several influencing factors to the damping support capability, such as the voltage characteristics of the system loads, the active power loading level, the communication delay and the sensitivity to random delay variations are studied and the results are reported.

Chapter 5 deals with the utilization of MMC-VSC-MTDC systems for supporting power flows during the primary frequency control in large high-voltage transmission systems. The investigated MTDC system interconnects synchronous areas within an AC power system. A novel PFS controller is incorporated into the active power modulation channel of the VSC station control to enable the VSC-MTDC system taking part in the primary frequency control under severe generation outages. An analytical method to determine the gain of the PFS controller is also proposed to assure an accurate schedule of exchanged powers through the VSC-MTDC system according to residual transferable margins of parallel HVAC lines. The proposed PFS controller uses the feed-forward control technique to forestall undesirable effects of the transient frequency deviation on the system dynamic performance. The PFS controller is then validated on a test system similar to the one used in chapter 4.

Chapter 6 presents a study on the capabilities of MMC-VSC-MTDC systems in enhancing the transient stability of a large power system in fast and large voltage fluctuation events. A FVS controller is equipped to the reactive power modulation channel of the MMC-VSC station. The use of the FVS controller together with the active/reactive power (P&Q) coordination control to maximize the capability of the MMC-VSC-MTDC system in supporting the system voltage is analyzed. Furthermore, the performance of the MMC-VSC station control operated under a special operational mode, the STATCOM mode, during short circuits in the DC grid is also discussed and highlighted.

Chapter 7 studies the interactions between the supplementary controllers. The MMC-VSC-MTDC system is designed as a larger test system where events involving the actions of several controllers at the same time can be created. Hence, the interactions between the supplementary controllers can be evidently observed. Through this study, possible problems related to controller coordination are identified and counter measures are proposed.

Chapter 8 summarizes the main results and conclusions achieved from this thesis, and gives an outlook on possible further related research topics.

2 MMC-VSC in HVDC application

2.1 MMC-VSC-HVDC features

The new modular-multilevel converter topology for HVDC applications possesses the most well-proven advanced features of the existing VSC topologies with two-level or three-level converters (here classical VSC) [4,5,10]. Amongst the advanced features is: the decoupled control of the active and reactive powers; the interconnection capability to weak or passive AC networks; compact design of converter stations. Furthermore, with the new approach, many drawbacks of the classical VSC for the HVDC applications can be eliminated and additional performance improvements can be provided as well.

As the principle operation in the classical VSC technology using PWM modulation, the operational switching occurs between two or three voltage levels causing high and steep voltage steps, which poses high stresses on components and requires filtering [10]. By applying the new MMC topology, the voltage-source converter is constructed up by a series connection of a number of identical, but individually controllable submodules. The new topology enables both the switching voltage steps and the switching voltage gradients to be reduced or minimized. As a result, the MMC-VSC can generate nearly ideal desired sinusoidal waveforms at the terminal voltage and, therefore, almost entirely reduce the need of the harmonic filters. In addition, the significantly low switching frequency in each submodule and the low voltage across each switch results in low operational losses of the converter. The reduced switching voltage gradients also enable the use of ordinary transformers with lower insulation requirements. The modular design in hardware and software gives MMC-VSC high flexibility and easy scalability with low engineering efforts for power ranges up to 1000 MW and up to the highest transmission voltages.

With one high-capacitance capacitor in each submodule, the MMC-VSC generally has a relatively high energy-storage capacity. During disturbances in AC systems, the energy-storage capacity helps the DC voltage substantially remain constant, thus allowing a more continuous and stable converter operation. Therefore, the dynamic performance of the MMC-VSC is improved over conventional VSC- HVDC [4]. In the MMC-VSC topology, there is no need for a DC-link capacitance. The MMC-VSC topology is capable of handling internal and external faults more effectively than the other VSC topologies. For instance, a short circuit between the two DC poles of the transmission line does not lead to a complete discharge of

the capacitors. Other advantages of MMC-VSC for HVDC applications which are not described here can be found in numerous research reports.

2.2 Working principle of MMC-VSC

The basic idea of the MMC-VSC is to create a controllable Voltage-Source which can generate a nearly ideal sinusoidal voltage waveform at the AC terminals. The idea is realized by the MMC topology approach in which a number of identical but individually switched converter submodules are connected in series.

Figure 2.1a shows the three-phase MMC which has two arms (upper and lower arm) per phase. Each arm is formed by n-identical submodules connected in series.

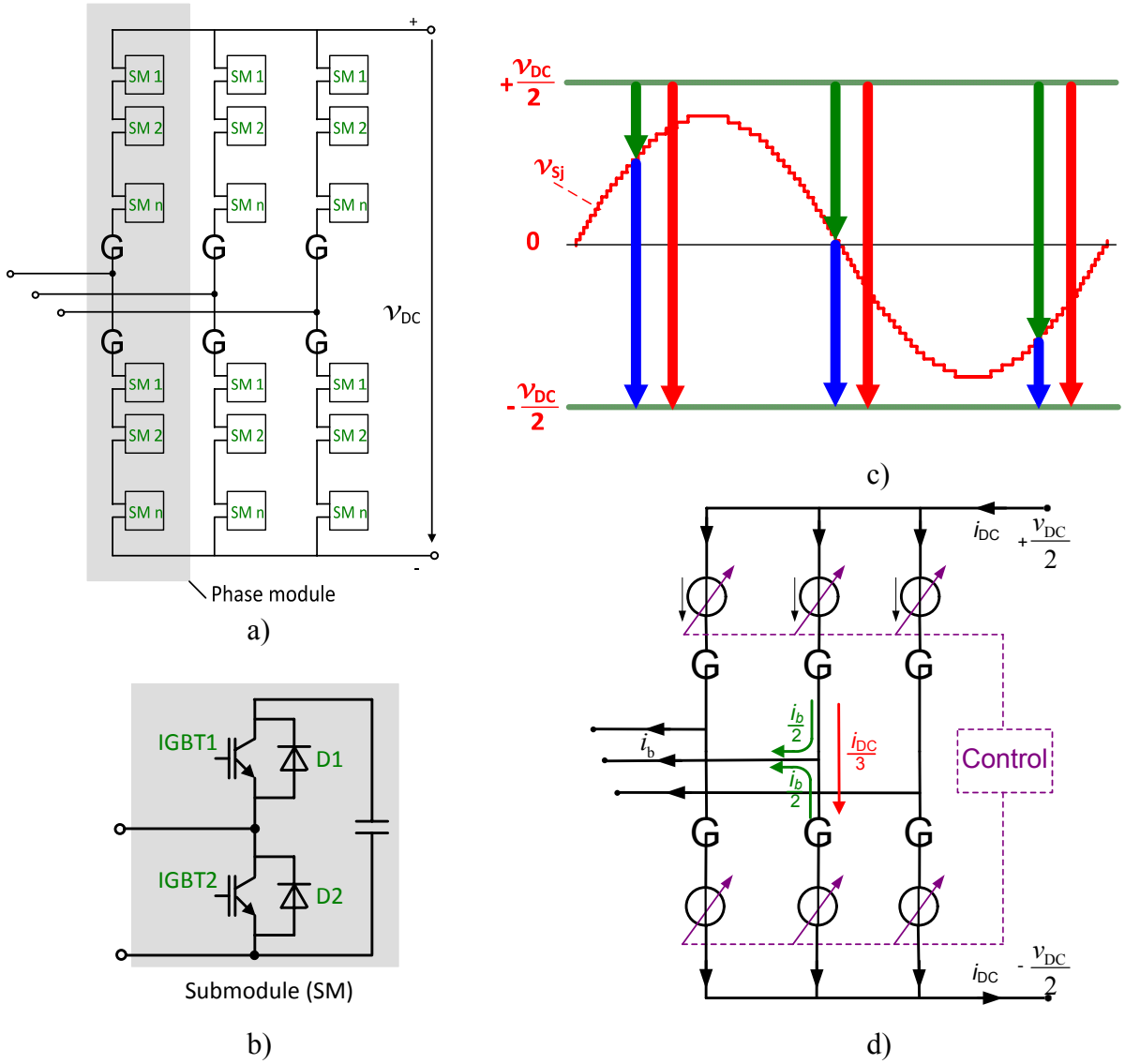

Figure 2.1: Overview of the Modular-Multilevel Converter topology [5]

The submodules in the MMC can either be two-level half-bridge submodules, each capable of producing +V or zero voltage, or two-level full-bridge submodules, producing ±V or zero voltage [4].

Figure 2.1b shows the basic structure of two-level half-bridge submodules. It consists of two IGBT 1&2 and a capacitor. The control of the half-bridge submodules is implemented by inserting or bypassing the capacitor. In this way, the voltage over the submodule can be at the full module voltage equal the capacitor voltage (IGBT 1 = ON, IGBT 2 = OFF: the capacitor is inserted) or at zero module voltage (IGBT 1 = OFF, IGBT 2 = ON: the capacitor is bypassed) in both current directions.

The total voltage of the two converter arms in each phase unit equals the DC voltage. The sum of the inserted submodules indexes in one phase accounted for both arms should be kept equal to n in normal operation. In any switching operation to be executed, an insertion of a submodule in one arm corresponds to a bypassing of a submodule in the other arm in the same phase.

The desired sinusoidal voltage at the AC terminal can be achieved by adjusting the ratio of the converter arm voltages in one phase unit. A typically implemented voltage waveform is depicted in Figure 2.1c. In the picture, the DC voltage, upper-arm and lower-arm voltages in one phase at a given time are denoted by red, green and blue arrows respectively.

The selection of the individual submodule within each phase to be bypassed or inserted is done by an appropriate selection mechanism. The objective of the selection mechanism is to distribute a uniform voltage across the individual submodule capacitor. At the same time, it should stabilize the capacitor voltages in all submodules and simultaneously suppress second harmonic current circulating between the converter phase legs.

In principle, a converter arm represents a controllable Voltage-Source in every converter arm, allowing independent control of the three AC voltages and the DC voltage (see Figure 2.1d).

3 MMV-VSC-HVDC modeling

Since the MMC-VSC has been introduced and applied in power systems, modeling the MMC-VSC in HVDC applications has increasingly drawn the attention of researchers for different types of study. Detailed MMC-VSC models include a very large number of switching devices. The use of the detailed model is restricted only to component studies due to the high computational burden because of the required small simulation time steps. Efforts have been recently made in developing simplified models, which can lessen the high computational burden but at the same time accurately reproducing the dynamic performance of the detailed models. For the electromagnetic-transient (EMT) type simulations, averaged EMT models were developed [11-13]. Reference [11] proposed an efficient time-varying Thévenin equivalent for the converter part. An averaged EMT model was proposed in [13]. In comparison to the detailed model, the averaged model is a hundred times faster for the same simulation time step while the dynamic performance is still accurately reproduced. The simulation time step is typically in the range of tens to hundreds of microseconds.

For a study focusing on slow dynamic stability phenomena and performance analysis of MMC-VSC-HVDC systems within a large-scale AC network, the simulation using the average EMT model is still quite time-consuming in the simulation time range of interest (from tens of seconds to several minutes). There is a practical demand for a generic RMS model of the MMC-VSC in these studies. To build the RMS model, proper simplifications have been made to allow the model to work with larger simulation time while keeping reasonable dynamic response accuracy. A generic RMS model (phasor model) of the conventional VSC-HVDC system was introduced and used in several publications, including [14-17] among others. The RMS model includes voltage-controlled sources on the AC side and current-controlled sources on the DC side. The RMS model considers only the fundamental-frequency-controlled voltage source on the AC side. The controlled current source is derived using the power balance principle between AC and DC sides. For a MMC-VSC-HVDC system, a simplified positive sequence RMS model was introduced in [18]. However, details of the RMS model are not provided.

In this chapter, a generic RMS model of a MMC-VSC-HVDC system, developed based on an existing averaged EMT model, for transient stability analysis is described. The investigated MMC-VSC station control employs a particular control structure with two separate AC and DC control parts. The control structure differs from the well-known cascaded control structure applied in conventional VSC-HVDC system. The proposed RMS model is similar to the

existing RMS model for conventional VSC-HVDC systems. Some suitable modifications are made in the control structure. The model representation and its control structure are discussed in detail. A linearized model of the generic RMS model is also provided for analytical modal analysis. The RMS model is then validated against the established averaged EMT model, and the performance of the proposed RMS model is investigated in both the time- and frequency-domains.

3.1 Averaged EMT model of MMC-VSC

3.1.1 Averaged EMT representation

The topology of the averaged EMT model of an MMC-VSC is shown in Figure 3.1. In the averaged EMT model, the IGBTs are not explicitly modeled. Instead, they are represented by six controllable voltage sources, two in series per each phase. Each Voltage-Source represents the total controlled voltage across all submodules in each converter arm.

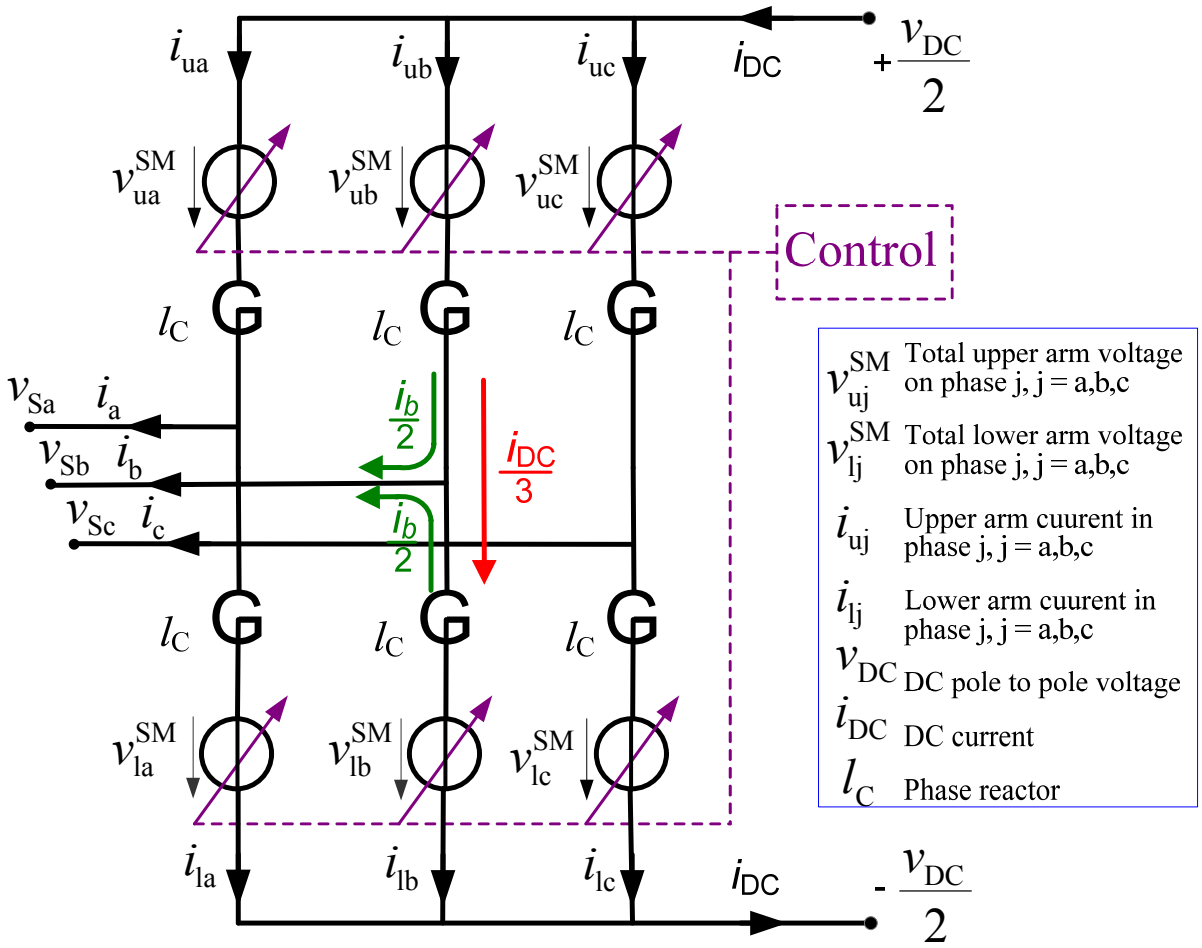

Figure 3.1: MMC-VSC generic EMT model [10]

Based on Figure 3.1, the total upper (denoted by u) and lower (denoted by l) arm voltages for phase j (j = a, b, c) can be calculated using the equations:

$$v_{uj}^{SM} = \frac{v_{DC}}{2} - v_{Sj} - l_C \frac{di_{uj}}{dt} \tag{3.1}$$

$$v_{lj}^{SM} = \frac{v_{DC}}{2} + v_{Sj} - l_C \frac{di_{lj}}{dt} \tag{3.2}$$

Assuming balanced voltages across all capacitors at any given time, the second harmonic circulating currents are zero [13]. Therefore, the arm current in each phase can be expressed as:

$$i_{uj} = \frac{i_{DC}}{3} + \frac{i_j}{2} \tag{3.3}$$

$$i_{lj} = \frac{i_{DC}}{3} - \frac{i_j}{2} \tag{3.4}$$

By subtracting (3.1) from (3.2), the AC terminal voltage in phase j (j= a, b, c) can be computed as follows:

$$v_{Sj} = v_{Cj} - \frac{l_C}{2} . \frac{di_j}{dt} \tag{3.5}$$

where

$$v_{Cj} = \frac{(v_{lj}^{SM} - v_{uj}^{SM})}{2} \tag{3.6}$$

Substituting (3.5), (3.3) into (3.1) results in:

$$v_{uj}^{SM} = \left(\frac{v_{DC}}{2} - \frac{l_C}{3} \frac{di_{DC}}{dt} \right) - v_{Cj} = \frac{v_{DC}^*}{2} - v_{Cj} \tag{3.7}$$

The total lower arm voltage can be derived by applying the same approach on (3.5), (3.4) and (3.2), which leads to:

$$v_{lj}^{SM} = \left(\frac{v_{DC}}{2} - \frac{l_C}{3} \frac{di_{DC}}{dt} \right) + v_{Cj} = \frac{v_{DC}^*}{2} + v_{Cj} \tag{3.8}$$

As can be seen from the above equations, the AC terminal voltage can be regulated through the difference between the total upper and lower arm voltages, whereas the DC terminal voltage can be controlled by regulating the sum of the total upper and lower arm voltages. The control of the AC voltage and DC voltage can be implemented through v_{Cj} and v_{DC}^*, respectively.

3.1.2 MMC-VSC control for EMT model

The control system of the VSC-HVDC system with two- or three- level converters mostly employs vector-current control method in combination with pulse-width modulation (PWM) control [20-21]. The control method offers high speed and independent controls of the active and reactive powers and a capability of limiting the converter current during disturbances. The control system using this control method has a cascaded control structure, including a fast inner current control loop and slower outer controllers. The inner current control loop controls the AC current using the current references supplied by outer controllers. In the outer controllers, different control strategies for the active and reactive power controls are implemented. The output of the inner current control loop is the reference voltage fed to the converter level of the VSC control. This control system can be successfully applied for the MMC-VSC-HVDC system [22]. In [12], a similar control system with additional submodule capacitor voltage controller is also used.

This chapter introduces a different control structure applied for a practical MMC-VSC, whose conceptual control structure is illustrated in Figure 3.2. This control structure has two control modules generating the reference AC voltage part (v_{Cj} by the AC control module) and reference DC voltage part (v_{DC}^{*} by the DC control module). The reference voltages of the converter arms are created according to (3.7) and (3.8). This control structure enables an independent control of the AC and DC terminal voltages. Through the DC control module, the ability to control the DC terminal voltage via high-value capacitor in each submodule of the MMC-VSC is exploited.

In the AC control module, the vector-current control method is utilized. The module has a cascaded control structure, including an inner current control loop and outer controllers. The inner current control loop generates the reference AC voltage corresponding to the ordered currents coming from the outer controllers. Here the control action is done in the synchronous rotating frame attached to the terminal voltage (here voltage-oriented d-q frame) enabling independent control of active and reactive power. The quadrature reference current is formulated in the reactive power control. The direct reference current of the inner current control is calculated from the output of the energy balance control instead of the active power control, which is implemented in the other control module. The energy balance control is employed to ensure a fast establishment of the energy balance over all submodule capacitors during any electrical transient excursion. An integral characteristic is used inside the energy balance control.

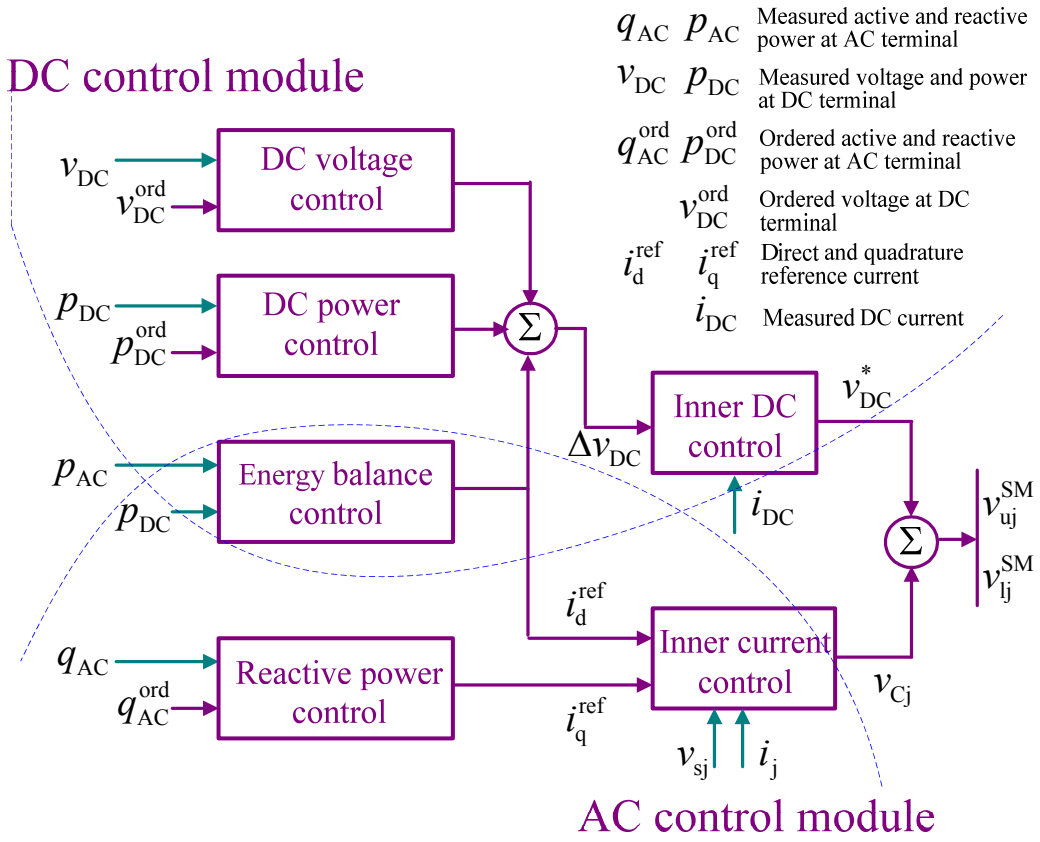

Figure 3.2: MMC-VSC control scheme

In the DC control module, the active power control strategy of the MMC-VSC is implemented via two control blocks, DC voltage control and DC power control. Several control strategies can be applied, such as constant DC voltage control, constant DC power control and voltage – power droop control strategies [23]. The energy balance control is also included in this control module. The outputs of these three blocks are then combined to form the input to the inner DC control. Here a proportional-integral (PI) function is then used to derive the corresponding reference DC voltage. Note that, the modular capacitors are not explicitly modeled. Instead, the dynamic behavior of the modular capacitor is included into the control model of the total arm Voltage-Source through the DC control module.

To protect the MMC-VSC in case of a nearby three-phase short circuit at the AC terminal against over-current, dynamic limiters as a function of AC terminal voltage are also implemented on both control modules.

In the EMT simulation using this averaged model of MMC-VSC, the DC cables are connected directly to the DC terminal of the MMC-VSC. To guarantee the accuracy of the simulation result, a small simulation time step should be taken. Typical values are in the range of 1 to 50 µs.

3.2 Generic RMS model of MMC-VSC

3.2.1 Generic RMS representation

The proposed transient stability model (so-called generic RMS model) representing the behavior of an MMC-VSC for transient stability studies is depicted in Figure 3.3.

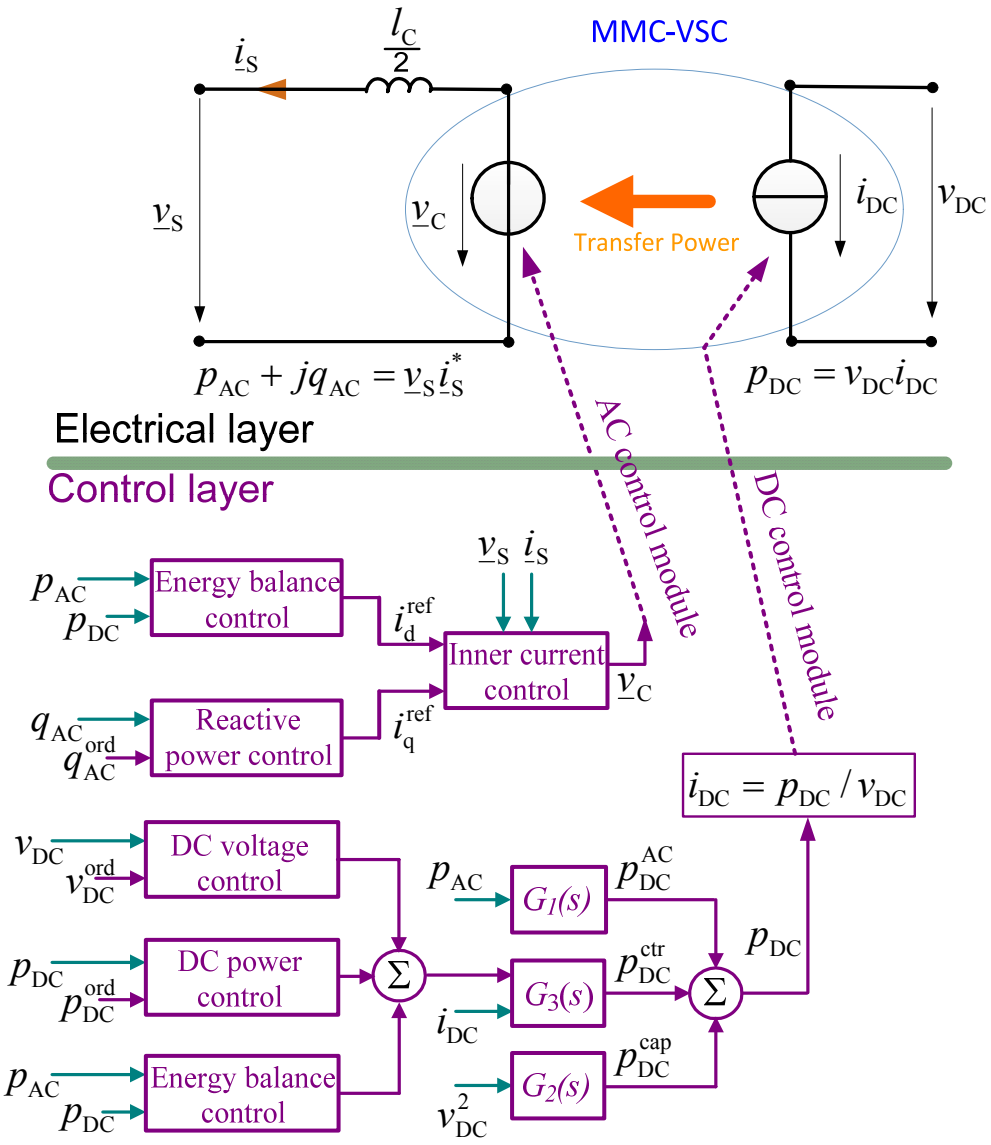

Figure 3.3: MMC-VSC generic RMS model

The generic RMS model includes a phase reactor, controlled voltage and current sources. The controlled sources represent the behavior of the MMC-VSC on the AC and the DC sides, respectively. The RMS model considers only the fundamental frequency controlled Voltage-Source on the AC side. The modeling using voltage and current sources is similar to the

existing RMS model developed for conventional VSC-HVDC system. Differences lie in the control structure incorporated into the controlled sources. The entire control system with a separate DC control module cannot be directly incorporated into the controlled Voltage-Source on the AC side. This is the case in the existing RMS model developed for conventional VSC-HVDC system. Furthermore, the separate DC control module, whose output is the reference DC voltage, cannot be directly included into the controlled current source on the DC side. Suitable adaptations shall be considered at this point. This chapter proposes such adaptations based on the power transfer from the DC to the AC side and derived from power balance principle.

3.2.2 MMC-VSC control for RMS model

The interface of the generic RMS model with the interconnected AC system is described by equation (3.5). The controlled voltage $\underline{v}_C$ is the output of the AC control module in averaged EMT model applied to the AC side of the generic RMS model. On the DC side, the control module of the current source can be derived by using the principle of power balance between the AC and DC sides.

In the averaged EMT model, at any time instant, the instantaneous power p_{DC} at the DC terminal is the sum of the instantaneous AC active power at the AC terminal p_{AC}, the instantaneous powers resulting from derivative of energy of the phase reactors p_{LC} and the module capacitors p_{CONV}. Here the phase reactor losses and converter losses are neglected. This relationship can be described using the following equation:

$$p_{DC} = p_{AC} + p_{LC} + p_{CONV} \tag{3.9}$$

p_{CONV} results from the variation in time of the controlled DC voltage, which is the voltage across the submodule capacitors. In steady state, this controlled DC voltage is equal to the DC voltage at the terminal of the MMC-VSC. In the transient excursion, due to the control action of the DC control module, the controlled DC voltage can be different from the terminal DC voltage. In the averaged EMT model, the control strategy of the DC side is implemented via the controlled DC voltage as a constituent component of the controlled arm voltages.

In the generic RMS model, the behavior of the MMC-VSC on the DC side is represented by a controllable current source. The controlled DC voltage is absent in this model. Therefore, p_{CONV} has to be estimated differently based on DC control module and the terminal DC voltage. Some simplifications have to be made. In this work, p_{CONV} is calculated by two

power components p_{DC}^{ctr} and p_{DC}^{cap} as shown in Fig. 3.3. The first component p_{DC}^{ctr} represents the influence of the DC power control module on p_{CONV} and is its main part. A PI controller replaces the inner DC power control of the DC control module, so that the adapted DC power control module outputs the power component p_{DC}^{ctr} instead of the reference DC voltage. The second component p_{DC}^{cap} gives the remaining (complementary) part of p_{CONV}. This component is estimated by the derivative of the squared DC terminal voltage.

Further assumption is made for the computation of p_{LC}. This transient component results - supposedly - only from the fluctuation of the AC power p_{AC} in the simulation using the EMT model. So that p_{LC} is here estimated using the AC power. Consequently the sum of p_{AC} and p_{LC}, represented by p_{DC}^{AC}, can be estimated through only p_{AC}. Now, the DC power can be reformulated as follows:

$$p_{DC} = p_{DC}^{AC} + p_{DC}^{cap} + p_{DC}^{ctr} \tag{3.10}$$

The newly introduced power components (see Figure 3.3), which are moderately coupled to the existing physical components, also include supplementary built-in transfer functions to better tune the behavior to that of the EMT model. Table 3.1 summarizes the supplementary transfer function for each power component.

Table 3.1: Components of the DC active power

Components in (3.9) EMT model		Components in (3.10) RMS model	Supplementary transfer function in Figure 3.3
Instantaneous AC active power at the AC terminal	p_{AC}	p_{DC}^{AC}	$G_1(s) = 1 + \frac{sk_{W1}T_{W1}}{1+sT_{W1}}$
Instantaneous power resulted from derivative of energy of phase reactors	p_{LC}	p_{DC}^{cap}	$G_2(s) = \left(\frac{sk_{W2}T_{W2}}{1+sT_{W2}}\right)\left(\frac{1+sT_{21}}{1+sT_{22}}\right)$
Instantaneous power resulted from derivative of energy of module capacitors	p_{CONV}	p_{DC}^{ctr}	$G_3(s) = k_{PDC} + \frac{1}{sT_{PDC}}$

The proposed generic RMS model and its control structure resemble the existing control structure of the averaged EMT model. Almost all control blocks (such as DC voltage control, DC power control, reactive power control) are similar to that of the EMT model. The controller settings of these control blocks in the EMT model can be used directly in the

corresponding ones in the RMS model. Only the inner DC control part is substituted by the tuned built-in transfer functions. Therefore, the following parameters (i.e. k_{W1}, T_{W1}, k_{W2}, T_{W2}, T_{21}, T_{22}, k_{PDC}, T_{PDC} seen in Table 3.1) of the built-in transfer functions require a fine-tuning to match the behavior to that of the EMT model. Any change at the inner DC control leads to a need of retuning the parameter settings of the built-in transfer functions. Changing the control strategies of active and reactive powers is the most common activity in investigating the interaction between HVDC systems and AC systems. For this activity, the proposed structure allows using directly the controller settings in the EMT model for the RMS model without re-tuning other parameters.

It is important to note that to enable the proposed generic RMS model of the MMC-VSC for HVDC applications running in the transient stability simulation, the DC circuit is modeled and integrated as part of the DC control module of the dynamic model. A DC cable can be modeled by a lumped simplified model comprising its resistance, and capacitances in a Π-circuit configuration.

Based on this generic RMS model, a linearized model of a MMC-VSC-HVDC system for small-signal stability analysis is also developed. Detailed description for the linearized model is given in the Appendix A.3.

3.3 Generic RMS model identification

To calibrate the parameters set for the proposed generic RMS model of the MMC-VSC, a test network shown in Figure 3.4 was used. A point-to-point MMC-VSC-HVDC system connects two 400kV power grids (each with short-circuit capacity S_{k3p}"= 43 GVA, R/X=0.1). The MMC-VSC-HVDC system transmits 675MW (75%) from Grid 1 to Grid 2. The structure of the two MMC-VSC stations is identical. In this study, the voltage-power droop control strategy is applied at both MMC-VSC stations. The reactive power control is set in constant power factor control mode.

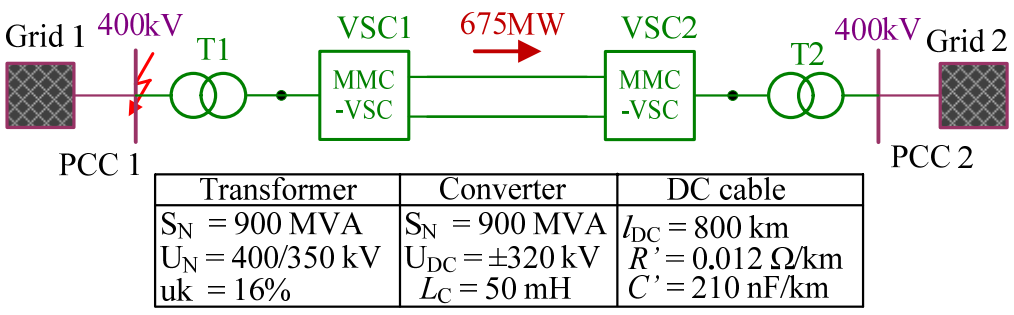

Transformer	Converter	DC cable
S_N = 900 MVA	S_N = 900 MVA	l_{DC} = 800 km
U_N = 400/350 kV	U_{DC} = ±320 kV	R' = 0.012 Ω/km
uk = 16%	L_C = 50 mH	C' = 210 nF/km

Figure 3.4: Test network for parameter identification of the RMS model

A 150 ms metallic three-phase short-circuit (3PSC) at the point of common coupling (PCC) of the MMC-VSC 1 is simulated with both the averaged EMT and generic RMS models. With the EMT model, the simulation is performed in EMT type simulation with the DC cables modeled using distributed parameters. The simulation time step is 0.01 ms. The result of this simulation is used as the reference for tuning the parameters of the generic RMS model in the second simulation. In contrast to the EMT type simulation, DC cables in the RMS type simulation are modeled as a lumped Π model due to the integration into the RMS model. A larger time step of 5 ms is used.

3.3.1 Parameter identification algorithm

The parameter identification problem can be defined as follows:

$$\text{Minimize OF} = \sum_{i=1}^{2} \int_{0}^{\tau} \left[w_1 (p_{DC,i} - p_{DC,i}^{ref})^2 + w_2 (v_{DC,i} - v_{DC,i}^{ref})^2 \right] dt$$

$$\text{subject to} \qquad \mathbf{x}_{min} \le \mathbf{x} \le \mathbf{x}_{max} \tag{3.11}$$

where OF is objective function. $v_{DC,i}^{ref}, p_{DC,i}^{ref}$ are the resulted voltage and power of simulation using the averaged EMT model at DC terminal of i-th VSC. $v_{DC,i}$, p_{DCi} are the resulted voltage and power of simulation using the generic RMS model at DC terminal of i-th VSC. w_1, w_2 are corresponding weighting factors. τ is the simulation period and vector **x** constitutes the solution to the parameter identification problem, that is, the set of identified parameters (gains and time constants in Table 3.1). Vectors $\mathbf{x}_{min}$ and $\mathbf{x}_{max}$ are given to define the search space for the identified parameters. The constraint (3.11) imposes minimum and maximum limits to the gains and time constants.

The parameter identification task was done using a heuristic optimization algorithm called Mean-Variance Mapping Optimization (MVMO). The theoretical background of MVMO can be found in [27-28]. The optimization method shares certain similarities to other heuristic approaches. However, the MVMO operates on a single solution rather than a set of solutions as in many heuristic algorithms. The internal searching space of all variables in MVMO is restricted in [0, 1]. Hence, the real min/max boundaries of variables have to be normalized. During the iteration it is not possible that any component of the solution vector violates the corresponding boundaries. To achieve this goal, a special mapping function was developed. The inputs of this function are the mean and the variance of the best solutions that the MVMO has discovered so far. The most elegant property of the MVMO is its ability to search around the local best-so-far solution with a small chance of being trapped into one of the local

optimums. This feature is contributed to the strategy for handling the zero-variance [27]. The flowchart of the MVMO algorithm is shown in Figure 3.5. Applications of the algorithm in power systems are found in [29-30]. The MVMO algorithm is particularly suited for solving the optimization problem here presented, because it shows excellent convergence behavior in comparison to other heuristic methods, especially in terms of convergence speed [30].

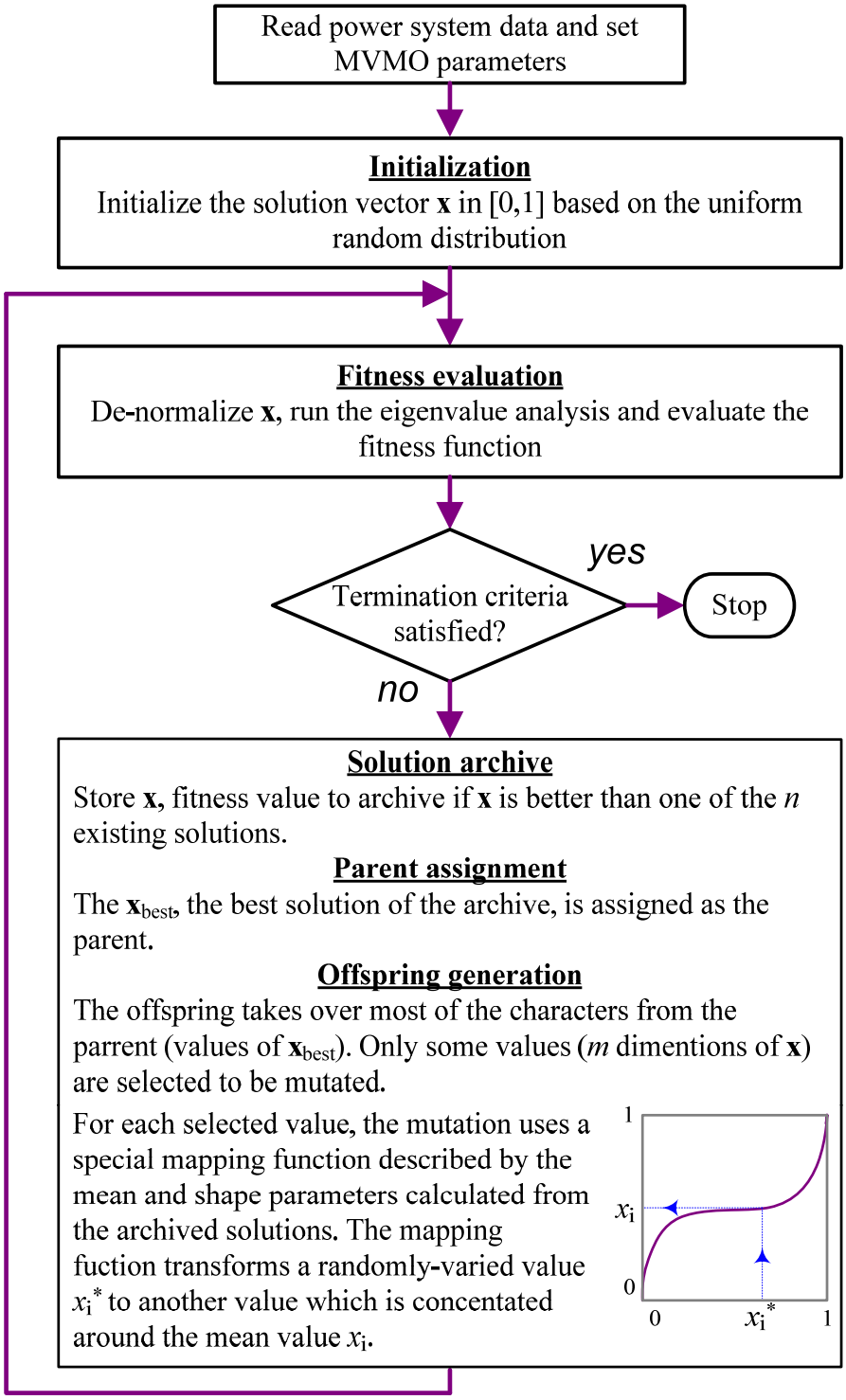

Figure 3.5: Flowchart of the MVMO algorithm.

3.4 Simulation results

The above-mentioned 150-ms 3PSC fault scenario applied in the test system is firstly simulated with the MMC-VSC-HVDC system modeled by using the averaged EMT model. The same fault scenario is carried out in RMS simulation using the generic RMS model with the identified parameters from the previous step (The identified parameters can be found in Appendix A.1). Figure 3.6 shows the simulated system responses to the above-mentioned 3PSC using the averaged EMT model and the generic RMS model. The figure includes the DC and AC voltages as well as the active and reactive powers at both PCCs.

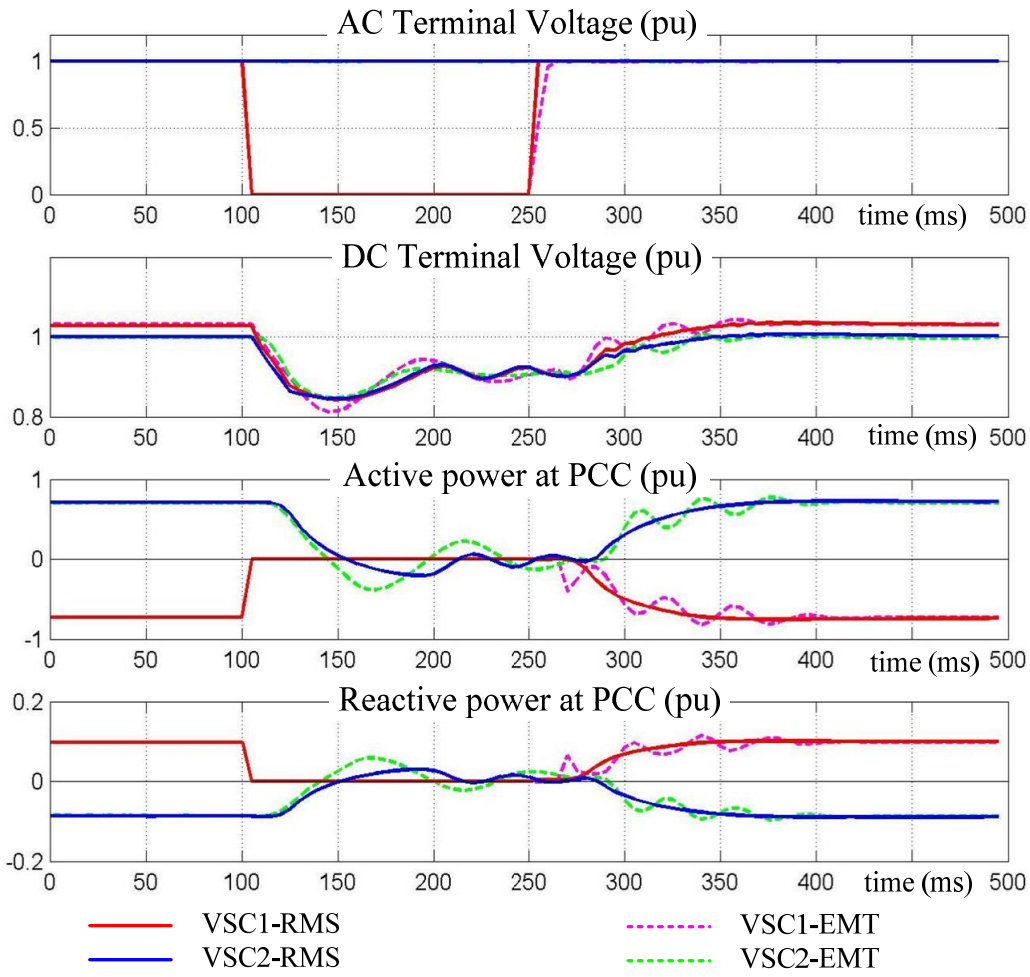

Figure 3.6: Comparison of simulation results of 150-ms 3PSC at PCC1.

As seen in the resulting plots, the generic RMS model provides a good approximation of the fault when compared to the averaged EMT model. It should be noted that the control parameters in the EMT model have not been tuned to the test system before this analysis. Nevertheless, the identified generic RMS model is found to perform well and is able to

satisfactorily capture the transient excursions of the AC and DC waveforms during transient operation. The performance of the generic RMS model is more accurate in the post-fault period rather than during the fault. The resulting waveforms at the converter on the fault side are closer to the reference waveforms than at the healthy converter.

The generic RMS model with the identified parameters is also tested in other weaker test networks with lower short circuit capabilities (20 GVA, 10 GVA and 5 GVA), and compared with the reference EMT model with the same set-up. The transient performance of the generic RMS model with the identified parameters again sufficiently follows the one seen from the reference EMT model without retuning the parameters.

In the simulation with the generic RMS model, the model is iterated with the transient stability solution algorithm. The simulation is done with different simulation time steps. The results reveal that, a time step of 5 ms or less is required to ensure accurate performance of the generic RMS model. A larger time step is inadequate to track the response of the inner PI controller which has a relatively smaller time constant.

3.5 Dynamic performance of the generic RMS model of MMC-VSC-HVDC system

The dynamic performance of the generic RMS model of MMC-VSC is investigated in this section. The MMC-VSC, whose control parameters are identified in the previous section, is employed in a point-to-point MMC-VSC-HVDC system interconnected to a typical high-voltage transmission system. The analysis is done in both time domain and frequency domain. The performance of the generic RMS model is compared with the performance of the EMT model in the time domain analysis. For the frequency domain analysis, the eigenvalues resulting from the linearized model of the MMC-VSC-HVDC system are verified in comparison with the ones obtained using the Prony analysis of the resulting time domain simulation.

3.5.1 Test network

The test system is shown in Figure 3.7. This is a 50 Hz system with five large generators which are interconnected via long high-voltage transmission lines. The generators are modeled by a detailed sixth-order model, and are equipped with speed governors, automatic voltage regulators (AVR) and power system stabilizers (PSS). There are three load centers LOAD7, LOAD9 and LOAD12 that are represented as constant impedances. A point-to-point MMC-VSC-MTDC system is inserted between Bus 7 and Bus 9. Each converter station

(VSC1, VSC2) consists of connecting transformers, phase reactors, and MMC-VSC. The five generators are located in three different areas and supply power to three load centers via a 400-kV AC transmission system and the MMC-VSC-HVDC system. The red arrows roughly denote the power flow directions in the investigated network.

The AC system is created by modifying the 10-bus-4-generator network used in [31]. The load-flow parameters of the modeled generators, transformers, transmission line and loads can be found in Figure 3.7. The dynamic parameters of the generator models and controllers (GOV, AVR, and PSS) can be found in the Appendix A.2.

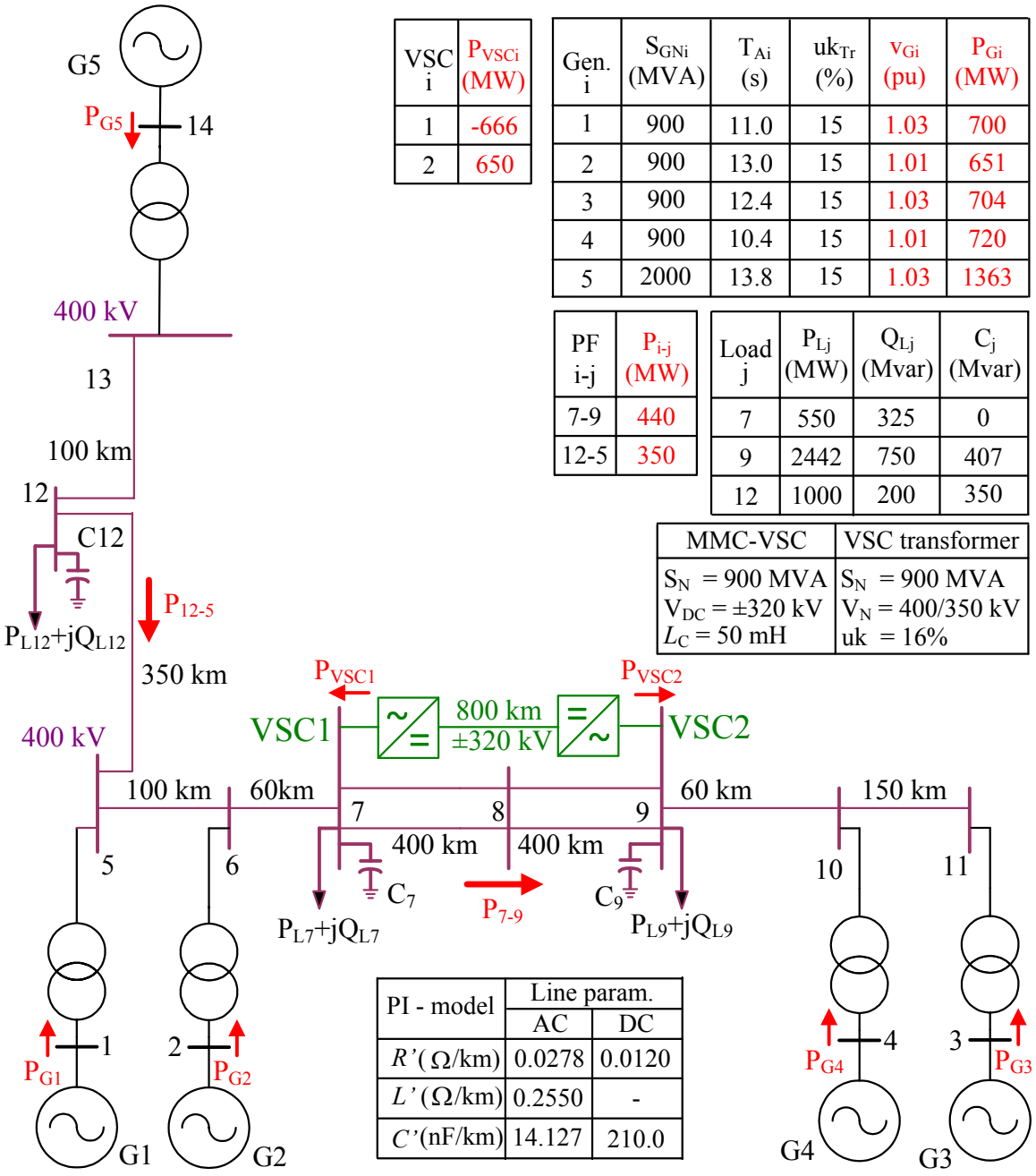

VSC i	P_{VSCi} (MW)
1	-666
2	650

Gen. i	S_{GNi} (MVA)	T_{Ai} (s)	uk_{Tr} (%)	v_{Gi} (pu)	P_{Gi} (MW)
1	900	11.0	15	1.03	700
2	900	13.0	15	1.01	651
3	900	12.4	15	1.03	704
4	900	10.4	15	1.01	720
5	2000	13.8	15	1.03	1363

PF i-j	P_{i-j} (MW)
7-9	440
12-5	350

Load j	P_{Lj} (MW)	Q_{Lj} (Mvar)	C_j (Mvar)
7	550	325	0
9	2442	750	407
12	1000	200	350

MMC-VSC	VSC transformer
S_N = 900 MVA V_{DC} = ±320 kV L_C = 50 mH	S_N = 900 MVA V_N = 400/350 kV uk = 16%

PI - model	Line param.	
	AC	DC
R' (Ω/km)	0.0278	0.0120
L' (Ω/km)	0.2550	-
C' (nF/km)	14.127	210.0

Figure 3.7: Test network for RMS model validation

3.5.2 Simulation results

To observe the dynamic performance of the generic RMS model under large disturbance conditions, a 150-ms three-phase short circuit is applied at Bus 7 at simulation time 1 s. The voltage magnitudes at Bus 7, Bus 9 and the speed deviations of generators G4 and G5 are recorded. Simulations in time domain are performed for the case with the generic RMS model and with the averaged EMT model. Figure 3.8 compares the simulation results of the two models. The dynamic response of the generic RMS model is quite the same as the performance of the averaged EMT model. They match each other especially within the first five seconds after the fault clearance. Small differences are only noticed in the generator speeds later on in the simulation time frame. The resulting speed signals possess low-frequency oscillations in two cases slightly deviating in time from each other. This shows that, the generic RMS model could not exactly represent the performance of the averaged EMT model in the lower frequency range. A detail explanation can be achieved by the analysis in the frequency domain.

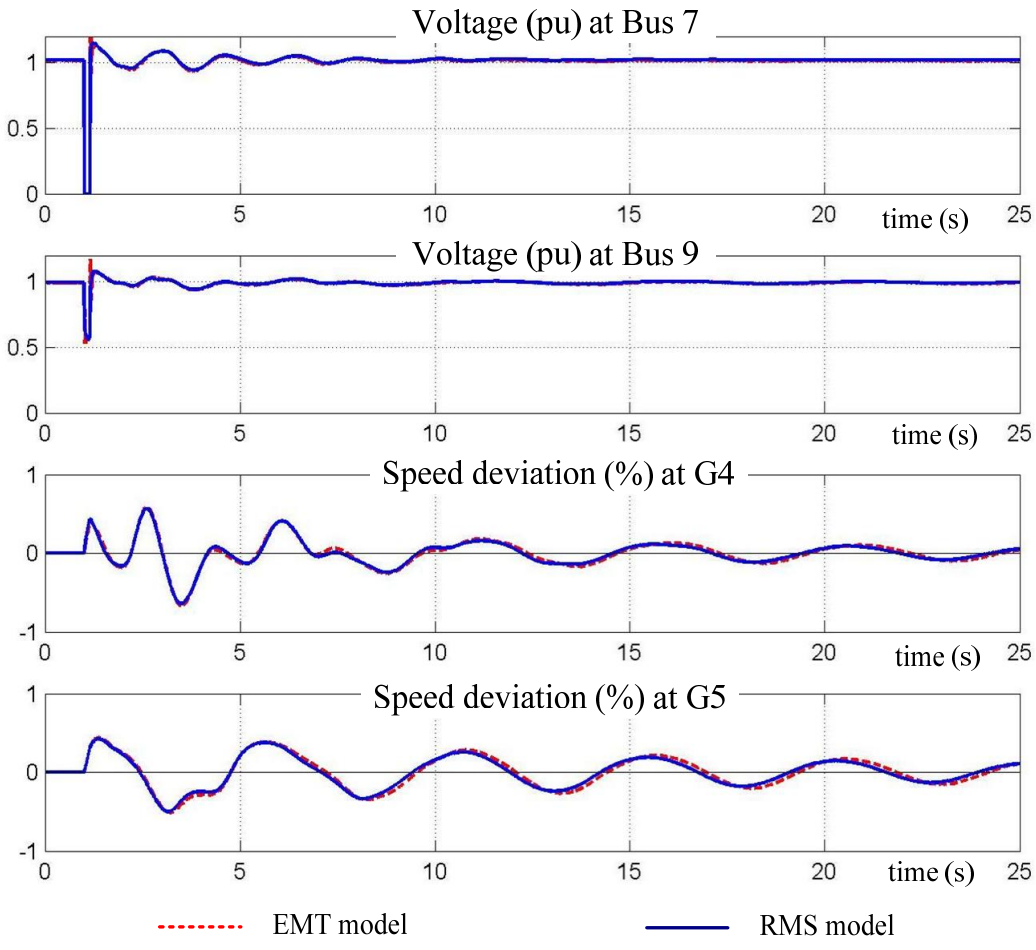

Figure 3.8: Simulation result in time domains using averaged EMT and generic RMS models

In the frequency domain analysis, an analytical modal analysis is first performed using the linearized model of the MMC-VSC-HVDC system described in the Appendix A.3. Modeling of the AC system for this analysis is described in [31]. The analytical analysis reveals four dominant low-frequency oscillatory modes, one local mode and three inter-area modes (global modes). The local mode is the oscillation mode at 1.22 Hz, 4.8% damping ratio characterizing the swinging of generator G3 against generator G4. One global mode is a weakly-damped global oscillation mode between generator group G1/G2/G5 and generator group G3/G4 at 0.85 Hz, 4.9% damping. The other global modes, associated to 0.57 Hz, 8.8% damping and 0.23 Hz, 5.4% damping, are related to swinging of generator G5 against generator group G1/G2/G3/G4.

Table 3.2: Eigen value analysis results

Mode	Analytical analysis Linearized model		Prony analysis RMS model		Prony analysis EMT model	
	Freq. (Hz)	Damp. (%)	Freq. (Hz)	Damp. (%)	Freq. (Hz)	Damp. (%)
1	1.22	4.8	1.20	5.4	1.20	4.2
2	0.85	4.9	0.86	4.4	0.85	4.3
3	0.57	8.8	0.57	8.9	0.57	9.7
4	0.23	5.4	0.22	4.7	0.20	4.9

To validate the findings of the analytical modal analysis, Prony analysis is also utilized to extract dominant oscillation modes from a given oscillatory response in time domain simulation [32]. The speed signal of generator G4, which involves all four modes of interest, is chosen for the Prony analysis. To minimize nonlinearities in the chosen speed signal, a weaker disturbance, a 40-ms three-phase short circuit at Bus 7 is applied instead. Prony analysis is carried out for both simulations with the generic RMS model and with the averaged EMT model. The resulting eigenvalues of the four modes of interest are shown in Table 3.2. The estimated oscillatory frequencies of each mode from the Prony analysis with the generic RMS model are almost identical to the one resulting from the analytical analysis. The dampings of mode 1&3 are slightly higher while the dampings of mode 2&4 are slightly lower. The maximum deviation is less than 13% of the damping found by the analytical model analysis. This small mismatch lies within the inaccuracy range due to the linearization

process and the Prony analysis. Therefore, it is in good conformity with the linearized model for the analytical model analysis.

The comparison of the results with generic RMS model and with the averaged EMT model reveals that there is a moderate difference in the low-frequency oscillatory mode at 0.2 Hz. This is the reason why there is a notable difference in the time domain simulation. There are also small mismatches in the damping. The mismatch results in a small increase in damping of one mode with slight reduction in the damping of other modes.

The generic RMS model is developed for transient stability analysis, such as AC-side faults and set point changes, with a large time-step simulation. Thereby, the model can be used to investigate dynamic influences of the MMC-VSC-HVDC system on interconnected large power systems. The linearized model of the proposed RMS model is applicable for investigating the MMC-VSC-HVDC for low-frequency electromechanical oscillation studies. However, the proposed generic RMS model considers only the fundamental frequency controlled Voltage-Source on the AC side. As a result, it is not intended for harmonic analysis purposes. For this type of study, the detailed EMT model should be employed.

4 Power oscillation damping controller

This chapter discusses the capability of MMC-VSC-MTDC systems equipped with POD controllers in improving the damping of inter-area oscillations. POD controllers have been in use in power systems for a long time. The most cost-effective POD solution is the use of the Power System Stabilizer (PSS), which provide supplementary control actions through the excitation systems of generators [33-35]. The POD control functions can be also integrated into FACTS devices, such as Static Var Compensators (SVCs). The POD controller introduces a supplementary signal to the voltage regulator loop [36-38]. The beneficial impacts of POD controllers applied on classical HVDC systems based on thyristor technology are reported in [39-40].

Recently, the VSC-based HVDC systems equipped with POD controllers have been reported in several studies. Generally, they improve the damping of inter-area oscillations [41-44, 50-52]. Different analysis methods have been used. In [43-44], the investigation has been done in time-domain simulation. References [43-44] explored the capability of damping enhancement using small-signal stability technique. In [43], a conventional approach of a PSS-based POD design incorporating washout, phase lead-lag blocks, and gain is used. The investigation focused on the selection of input signals for the POD controller. However, details about the employed VSC-HVDC system model were not provided. Reference [44] proposed a modal linear quadratic Gaussian (MLQG) controller as an example of an advanced POD controller, which was applied to the active power channel of the VSC-HVDC system control. The MLQG controller has demonstrated a greater robustness to varying operation conditions. In this investigation, a simplified model of the VSC-HVDC system was used. The VSC-HVDC system was modeled as coupled injection of active and reactive power including common control scheme controllers and a simple DC line model. Reference [42] looked into another POD controller design using Fuzzy logic technique to improve the oscillation damping by increasing the deceleration energy of oscillations. In [51], a model predictive control (MPC) scheme using relative frequency errors between generators is applied to damp the system oscillations.

Most studies in literature deal with POD controllers equipped onto the active power modulation channel of the VSC-HVDC system control. Further studies looked into the capability of POD controllers equipped onto the reactive power modulation channel. Reference [41] showed considerable contributions to damping of system oscillations through the reactive power channel, whereas the investigation in reference [50] revealed some

damping benefits achieved with the POD controller on the reactive power channel. The use of the POD controller on both the modulation channels can also effectively damp system oscillations as reported in [51, 52].

The thesis analyzes the damping support capability of a MMC-VSC-MTDC system equipped with PSS-based POD controllers onto both the active and reactive power channels. The analysis explores the damping benefits from various combinations in using the modulation channels at different VSC stations as well as local and remote signals from wide area measurement signals (WAMS). To maximize the POD controller performance, the geometric approach for input/output selection and the MVMO parameter optimization method are applied. The capability of MMC-VSC-MTDC systems in enhancing the damping of inter-area oscillations is assessed on a typical high-voltage transmission test system. The study is carried out using small-signal stability technique in which the MMC-VSC-MTDC system is represented by a linearized model. Several influencing factors to the damping support capability are as well studied, such as active power loading level, communication delay, and sensitivity to random delay variation.

The chapter is structured as follows: sections 4.1 and 4.2 illustrate the linearized model of a MMC-VSC-MTDC system and of the employed test system. This is followed by the description of the PSS-based POD controller. In this section, the POD controller structure, input/output selection method and the parameter optimization method are described. The test network is introduced in section 4.3. In the final section, the performances of the POD controllers are investigated considering various influencing aspects, such as voltage characteristics of the system loads, active power loading level, communication delay and sensitivity to the random delay variation.

4.1 Linearized model of an embedded MMC-VSC-MTDC power system

The complete state-space representation of the entire system can be obtained by combining the AC network and the state-space models of individual devices, such as MMC-VSC-MTDC system, generators and their controllers. The linearized model of the MMC-VSC-MTDC system described in (3.26) is represented as a current source. In this study, synchronous generators including AVR and GOV are modeled in the same form as derived following the description in [31]. Therefore, the state equation for a MMC-VSC-MTDC system and synchronous generators in the system may be combined into the form:

$$\begin{bmatrix} \dot{\mathbf{x}} \\ \Delta\mathbf{i} \end{bmatrix} = \begin{bmatrix} \mathbf{A}_D & \mathbf{B}_D \\ \mathbf{C}_D & \mathbf{D}_D \end{bmatrix} \begin{bmatrix} \mathbf{x} \\ \Delta\mathbf{v} \end{bmatrix} \tag{4.1}$$

where $\mathbf{x}$ is the state vector of the complete system; $\mathbf{i}$ is the current injection into the network from the devices; $\mathbf{v}$ is the vector of the system bus voltage; $\mathbf{A}_D$ and $\mathbf{C}_D$ are the block diagonal matrices composed of $\mathbf{A}_i$ and $\mathbf{C}_i$ associated with individual generators and MMC-VSC-MTDC systems.

In this work, the AC network is represented by the node equation with the admittance matrix $\mathbf{Y}_N$:

$$\Delta\mathbf{i} = \mathbf{Y}_N \Delta\mathbf{v} \tag{4.2}$$

Substituting equation (4.2) in Equation (4.1) yields the overall system state equation:

$$\dot{\mathbf{x}} = (\mathbf{A}_D + \mathbf{B}_D(\mathbf{Y}_N - \mathbf{D}_D)^{-1}\mathbf{C}_D)\mathbf{x} = \mathbf{A}\mathbf{x} \tag{4.3}$$

where $\mathbf{A}$ is the state matrix of the complete system give by:

$$\mathbf{A} = \mathbf{A}_D + \mathbf{B}_D(\mathbf{Y}_N - \mathbf{D}_D)^{-1}\mathbf{C}_D \tag{4.4}$$

4.2 POD controller for a MMC-VSC-MTDC system

In this study, the PSS-based POD controller is employed. This controller includes a washout block, a gain block and lead-lag blocks as shown in Figure 4.1. The washout block is to make sure that the controller has no interference in the steady-state operation but only works in the dynamic state.

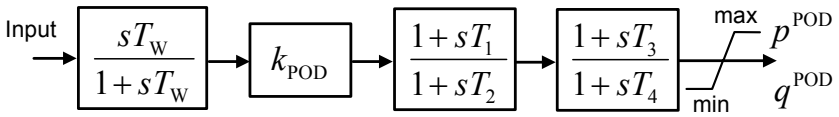

Figure 4.1: PSS-based POD controller for a MMC-VSC-MTDC system

As MMC-VSC-MTDC systems are often designed for the main power flow corridors of power systems as backbone transmission lines or inter-area connections, the MMC-VSC controls significantly influence the main power flows. Any critical inter-area oscillations across or associated to the main power corridors can be manipulated through MMC-VSC control by POD controllers. Thanks to the capability of MMC-VSC in controlling independently real and reactive powers, POD controllers can be implemented on both active and reactive power modulation channels (P and Q channels). When MMC-VSC-MTDC systems are built and work as the backbone transmission lines, critical inter-area oscillations can also be sufficiently observed from their VSC stations. The local measurements at MMC-VSC stations provide local signals such as voltage phase angles at the MMC-VSC station AC

terminals, active powers, or currents on the adjacent lines. They can be used as the local input for the POD controller. The observability of the inter-area oscillations can be improved with measurements from remote parts of the power system. Recent developments of wide-area measurement systems have made it feasible to use remote signals as inputs for the POD controller. However, using remote signals also poses a new challenge as time delays, caused by the use of communication networks for transmitting remote signals. The time delay ranges typically from tens to several hundreds of milliseconds, depending on distance, communication network, and transmission protocol [47]. The time delay is an important aspect and should be incorporated into any power system analysis. In this analysis, delays of remote signals used at POD controllers are modeled as first-order Padé approximations [48].

The capability of POD controllers in improving system oscillation damping depends on many influencing factors: locations, input/output signals and setting parameters of the POD controller are among the most important. Whereas the location is mainly related to the controllability of inter-area modes, the selected input signals are associated to the observability of inter-area modes. Location here means the modulation channels of the MMC-VSC station in which the POD controller is incorporated. Methods for input and location selection as well as parameter optimization are essential aspects of this investigation and are hence described in the next section.

4.2.1 Input/output selection algorithm

For input/output signal selection, two different approaches have been used: the geometric and the residue approaches. The analysis in [45] showed that the geometric approach was more reliable than the residue approach. In this work, the geometric approach is used. Using this approach, a joint controllability/observability measure will be defined according to the geometric measures of the controllability and observability coupled with each mode.

Let us consider a power system in which a POD controller is to be applied. The linearized model of the entire system is described by:

$$\begin{cases} \dot{\mathbf{x}} = \mathbf{A}\mathbf{x} + \mathbf{B}\mathbf{u} \\ \mathbf{y} = \mathbf{C}\mathbf{x} \end{cases} \tag{4.5}$$

where $\mathbf{x}$ is the state vector; $\mathbf{y}$ is the output vector; $\mathbf{u}$ is the input vector; $\mathbf{A}$, $\mathbf{B}$, $\mathbf{C}$ are the state, input, and output matrices, respectively. Let the eigenvalues λ_i, i = 1, 2,…, n, of $\mathbf{A}$ assumed to be distinct.

Let $\mathbf{e}_i$ and $\mathbf{f}_i$ be, respectively, the right and left eigenvectors associated with the distinct eigenvalue λ_i, i.e., $\mathbf{A}\mathbf{e}_i = \lambda_i\mathbf{e}_i$, $\mathbf{f}_i^*\mathrm{A} = \lambda_i\mathbf{f}_i^*$ where $\mathbf{f}_i^*$ is the conjugate transpose of $\mathbf{f}_i$ and the pairs

($\mathbf{e}_i$, $\mathbf{f}_i^*$) have been scaled so that $\mathbf{f}_i^*\mathbf{e}_i = 1$. The right and left eigenvectors $\mathbf{e}_i$ and $\mathbf{f}_i$ are orthogonal and normalized.

The controllability and observability measures m_{ci} and m_{oi} associated with *i-th* mode following the geometric approach are defined, respectively, as follows [46]:

$$m_{ci}(k) = \cos(\theta(\mathbf{f}_i, \mathbf{b}_k)) = \frac{\left|\mathbf{b}_k^T \cdot \mathbf{f}_i\right|}{\left\|\mathbf{b}_k^T\right\| \cdot \left\|\mathbf{f}_i\right\|} \tag{4.6}$$

$$m_{oi}(l) = \cos(\theta(\mathbf{c}_l^T, \mathbf{e}_i)) = \frac{\left|\mathbf{c}_l \cdot \mathbf{e}_i\right|}{\left\|\mathbf{c}_l\right\| \cdot \left\|\mathbf{e}_i\right\|} \tag{4.7}$$

where $\mathbf{b}_k$ is the *k-th* column of **B**; $\mathbf{c}_l$ is the *l-th* row of **C**; the superscript T denotes the transposition; $|\mathbf{z}|$ and $\|\mathbf{z}\|$ are respectively, the modulus and the Euclidian norm of **z**; $\theta(\mathbf{f}_i, \mathbf{b}_k)$ is the acute angle between the input vector $\mathbf{b}_k$ and the left eigenvector $\mathbf{f}_i$, $\theta(\mathbf{c}_l^T, \mathbf{e}_i)$ is the acute angle between the output vector $\mathbf{c}_l$ and the right eigenvector $\mathbf{e}_i$.

Using the afore-mentioned controllability measure m_{ci} and observability measure m_{oi} the joint controllability/observability measure of the *i-th* mode is defined as:

$$m_{coi}(k,l) = m_{ci}(k) \cdot m_{oi}(l) \tag{4.8}$$

4.2.2 Parameter optimization

For a PSS-based POD controller, it is important to have parameter settings tuned so that the maximum damping capability is achieved. The parameter optimization problem can be defined as follows:

$$\begin{aligned} &\text{Minimize} \qquad OF = \max\{(1-\zeta_i) : i = 1,...,n\} \\ &\text{subject to} \qquad \mathbf{x}_{min} \le \mathbf{x} \le \mathbf{x}_{max} \end{aligned} \tag{4.9}$$

where OF is objective function. $\xi_i = -\sigma_i / \sqrt{\sigma_i^2 + w_i^2}$ is the relative damping of mode $\lambda_i = \sigma_i + j\omega_i$ and vector **x** constitutes the solution to the problem, that is, the set of POD controller parameters (gains and time constants). Vectors $\mathbf{x}_{min}$ and $\mathbf{x}_{max}$ are given to define the search space for the optimal parameters. The constraint (4.9) imposes minimum and maximum limits to the gains and time constants.

The parameter optimization task is done using a heuristic optimization algorithm called Mean-Variance Mapping Optimization (MVMO) described in Section 3.5.1.

4.3 Test system

The AC test system used in the previous chapter is used once again in the present chapter. A three-terminal MMC-VSC-MTDC system is inserted between Bus 7, Bus 9 and Bus 13. In the test system without the VSC-MTDC system, the five generators located in three areas supply power to three load centers via a 400-kV double-circuit AC transmission lines between Bus 7 and Bus 9.

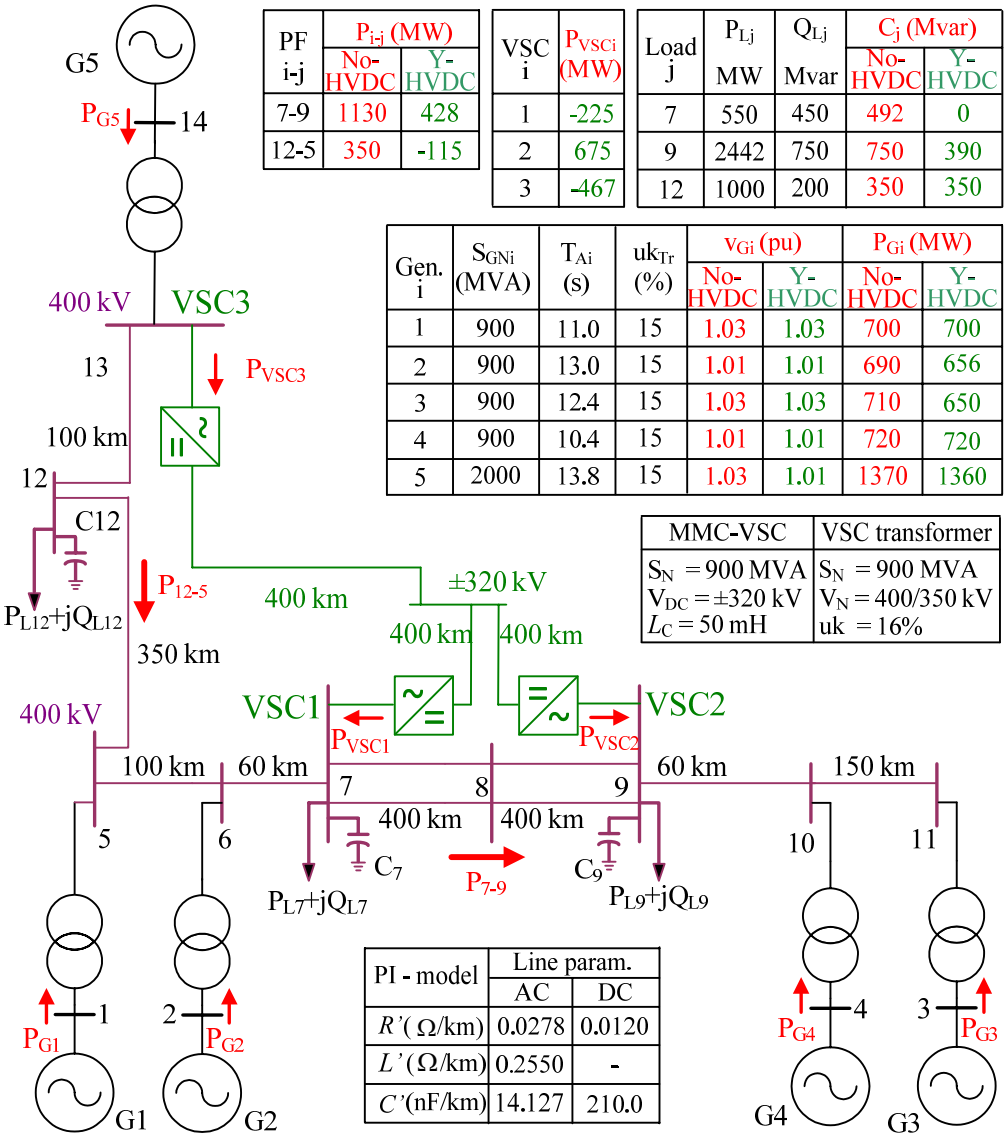

PF i-j	$P_{i\text{-}j}$ (MW) No-HVDC	Y-HVDC
7-9	1130	428
12-5	350	-115

VSC i	P_{VSCi} (MW)
1	-225
2	675
3	-467

Load j	P_{Lj} MW	Q_{Lj} Mvar	C_j (Mvar) No-HVDC	Y-HVDC
7	550	450	492	0
9	2442	750	750	390
12	1000	200	350	350

Gen. i	S_{GNi} (MVA)	T_{Ai} (s)	uk_{Tr} (%)	v_{Gi} (pu) No-HVDC	Y-HVDC	P_{Gi} (MW) No-HVDC	Y-HVDC
1	900	11.0	15	1.03	1.03	700	700
2	900	13.0	15	1.01	1.01	690	656
3	900	12.4	15	1.03	1.03	710	650
4	900	10.4	15	1.01	1.01	720	720
5	2000	13.8	15	1.03	1.01	1370	1360

MMC-VSC	VSC transformer
S_N = 900 MVA	S_N = 900 MVA
V_{DC} = ±320 kV	V_N = 400/350 kV
L_C = 50 mH	uk = 16%

PI - model	Line param. AC	DC
R' (Ω/km)	0.0278	0.0120
L' (Ω/km)	0.2550	-
C' (nF/km)	14.127	210.0

Figure 4.2: Test network for the POD analysis.

The power demands at LOAD7 and LOAD9 are partly covered by the generator G5 through a very long AC transmission link. With the presence of the VSC-MTDC system, the power loading of the AC double circuit transmission lines is reduced from 1130 MW down to 440 MW. The introduced VSC-MTDC system makes it possible to transfer power directly from the generating center at G5 to the load center LOAD9. More economical load-flow dispatches

are facilitated to reduce the transmission losses. In terms of stability, the VSC-MTDC system operated in parallel with the two main AC power transmission corridors can potentially strengthen the dynamic stability of the whole system. The power flow results with and without VSC-MTDC system can be found in Figure 4.2.

4.3.1 Modal analysis

Small-signal analysis of the test system with and without MMC-VSC-MTDC system reveals some interesting low frequency oscillation modes (see Table 4.1).

Table 4.1: Eigenvalue analysis results without POD controller

Mode	Eigenvalue analysis result				Oscillating generator group
	No HVDC		With HVDC		
	Freq. (Hz)	Damp. (%)	Freq. (Hz)	Damp. (%)	
1	1.15	+4.8	1.14	+4.9	G3 vs. G4
2	0.80	-0.6	0.89	+5.4	G1/G2/G5 vs. G3/G4
3	0.59	+16.6	0.58	+2.6	G5 vs. G1/G2/G3/G4
4	0.21	+5.3	0.21	+14.1	G5 vs. G1/G2/G3/G4

The test system without VSC-MTDC system contains mode with oscillatory instability at 0.8 Hz. The instability is caused by the inter-area oscillation between generator group G1/G2 and generator group G3/G4. There is also one weakly damped mode at 1.15 Hz relating to the local oscillation between G3 and G4. With MMC-VSC-MTDC system, the system stability is improved and the whole system becomes more stable. The oscillatory instability at 0.8 Hz is eliminated by the control action of the VSC-MTDC system. However, the weakly damped inter-area oscillations are still present in the test networks. The analysis reveals three weakly damped oscillation modes (two inter-area modes and one local mode). The first oscillation mode at 1.14 Hz is a local mode characterizing the swinging of G3 against G4. The second mode is a weakly damped global oscillation mode between generator group G1/G2 and generator group G3/G4 at 0.89 Hz. The third and fourth modes, the global modes associating at 0.58 Hz and 0.21 Hz, respectively, represent the swinging of G5 against G1, G2, G3 and G4. The damping related to the third mode is very low. The weakly damped inter-area oscillation problem in the test networks will be mitigated by POD controllers included in the

MMC-VSC-MTDC control. For each weakly damped inter-area oscillation mode, one PSS-based POD controller will be incorporated. The input, output (location) of each POD controller will be determined by the analysis in the next section.

4.3.2 POD input/output selection

At first, a controllability/observability analysis is carried out. For the input selection, voltage phase angles of buses 5 to 13 (B5,…, B13) are considered. The voltage angles of buses 7, 9 and 13 (B7, B9 and B13) are considered as local signals. The other signals are considered as global signals. For output selection, modulation channels (P and Q channels) and VSC stations (1, 2, and 3) are considered. The geometric approach is applied to calculate the controllability/observability measures for input/location selection. Figure 4.3 and Figure 4.4 show controllability and observability measure results, in which different colors are used to denote mode-corresponding measures. It can be seen that, the first mode (local mode) can be best observed at bus 10 and best controlled at VSC 2 on both modulation channels. The second mode (inter-area mode) can be best observed at bus 6 and best controlled at VSC 1 on both modulation channels. The third oscillation mode (inter-area mode) can be best observed at bus 11 and best controlled at VSC 3 on P channel or at VSC2 on Q channel. It is important to mention that a numerical comparison of controllability measures between POD on P and Q channels is not possible.

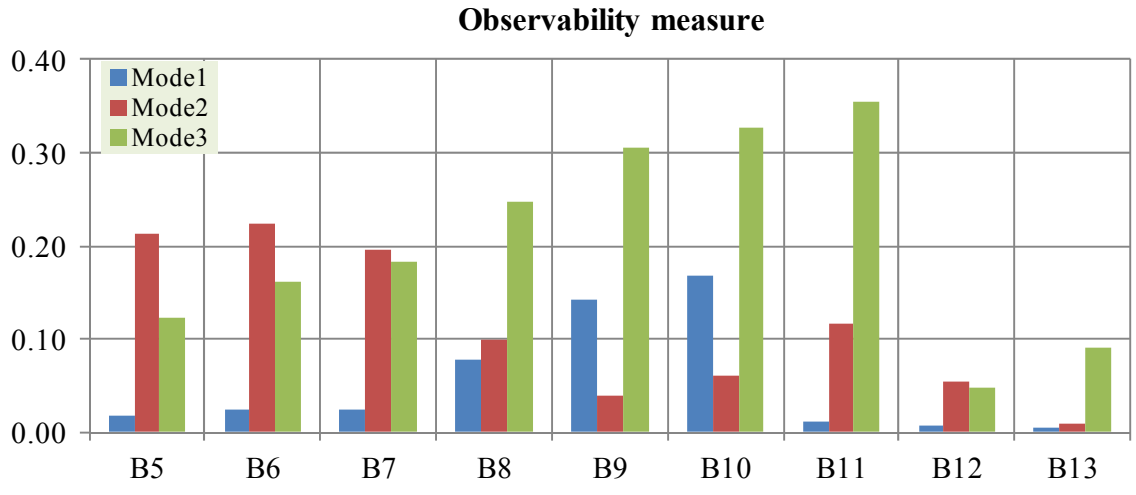

Figure 4.3: Observability measure results

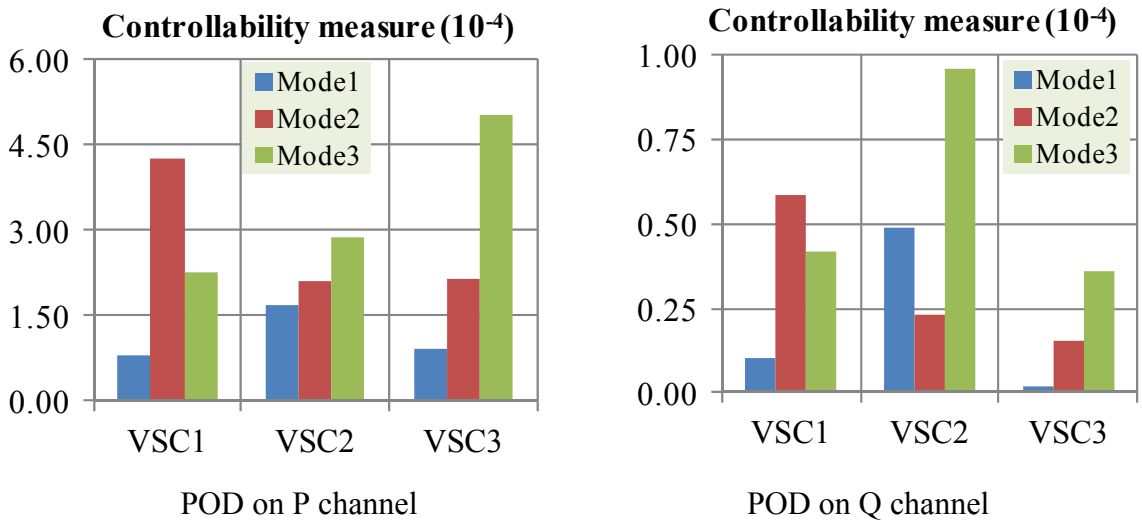

Figure 4.4: Controllability measure results (x10-4)

The joint controllability/observability measures of several best combinations of input/output concerning the local/global input and modulation channels are given in Figure 4.5. Detailed descriptions of the best combinations (POD options) are given in Table 4.2. In this table, two more combinations, which include POD controller on both modulation channels at the same time using best local and best global inputs, are added for further analysis and comparison.

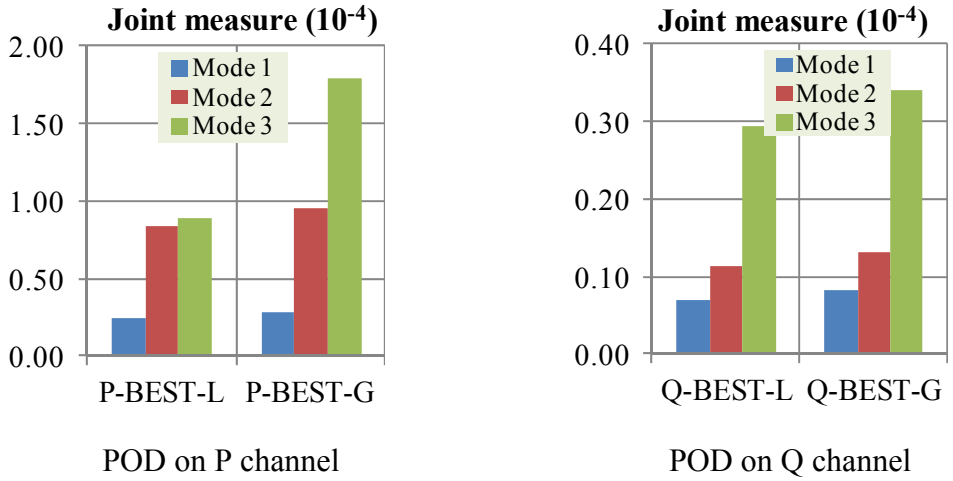

Figure 4.5: Joint Controllability/Observability measure results (x10-4): BEST-L and BEST-G are the best combination of input/output using local and global bus angle inputs, respectively, described in Table 4.2

Table 4.2: The best input-output combination for POD controller by applying the geometric approach

POD option	Best input/output combination					
	Mode 1		Mode 2		Mode 3	
	Channel-VSC	Bus angle	Channel-VSC	Bus angle	Channel-VSC	Bus angle
P-BEST-L Best local	P-VSC2	B9	P-VSC1	B7	P-VSC2	B9
Q-BEST-L Best local	Q-VSC2	B9	Q-VSC1	B7	Q-VSC2	B9
P-BEST-G Best global	P-VSC2	B10	P-VSC1	B6	P-VSC3	B11
Q-BEST-G Best global	Q-VSC2	B10	Q-VSC1	B6	Q-VSC2	B11
PQ-BEST-L Best local	Q-VSC2	B9	P-VSC1	B7	P-VSC2	B9
PQ-BEST-G Best global	Q-VSC2	B10	P-VSC1	B6	P-VSC3	B11

4.4 Damping support capability of MMC-VSC-MTDC systems equipped with POD controllers

For each POD option listed in Table 4.2, the suggested POD controllers are implemented. The parameters of the POD controllers are then optimized using the method describes in section 4.2.2 to obtain the best damping support to the system. The setting parameters for the optimal POD options can be found in the Appendix A.3. The modal analysis results are given in Figure 4.6. Significant damping is achieved with all chosen POD options. The results also confirm the effectiveness of the geometric approach to calculate the controllability/observability measures for input/location selection.

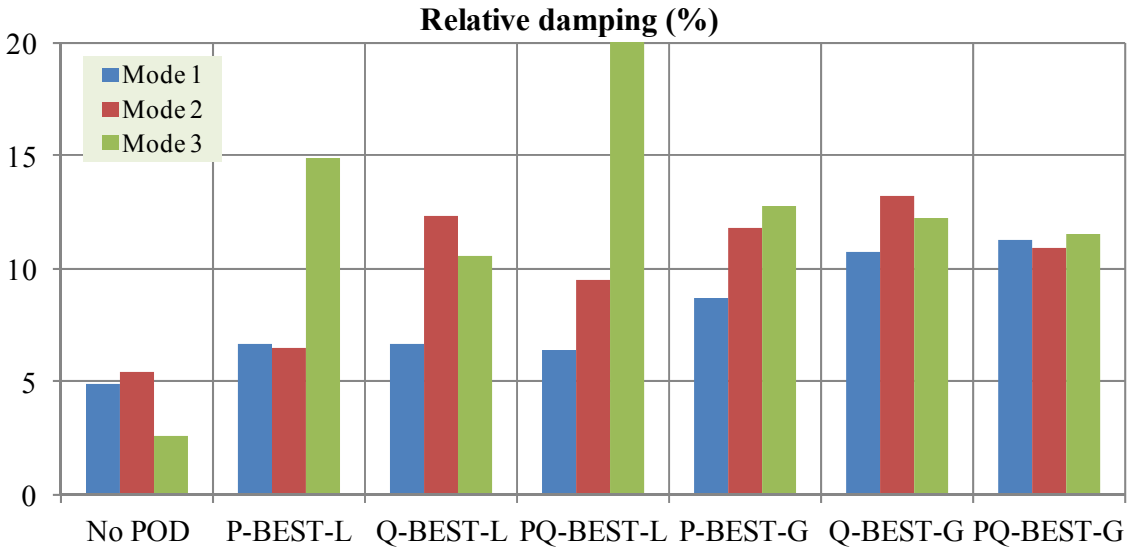

Figure 4.6: Modal analysis results of different POD options

Time domain simulations of these cases were performed to confirm the results of the modal analyses. In these tests, a 40-ms three-phase fault was applied at bus 9 with the objective of exciting all the system modes. The simulation results are plotted in Figure 4.7.

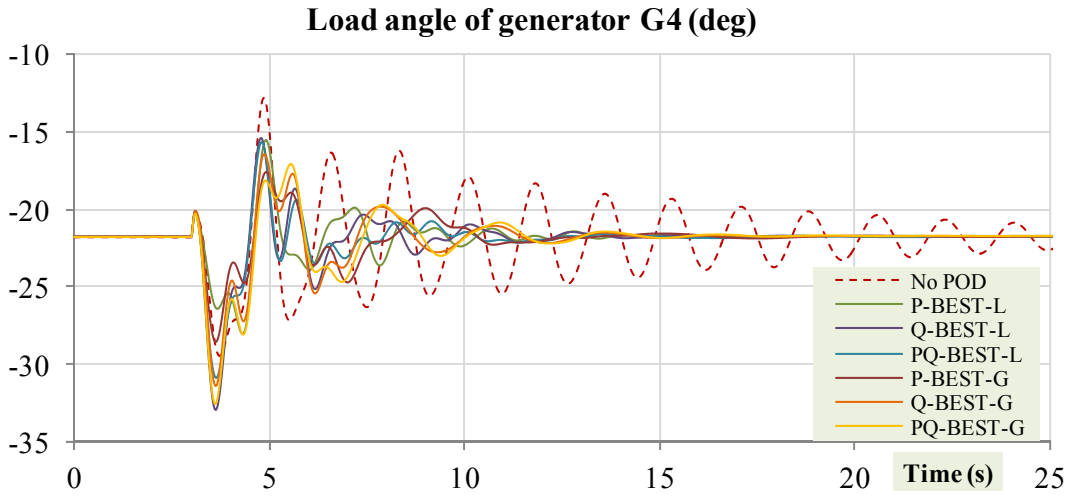

Figure 4.7: Time domain simulation results of different POD options

It is evident from the simulation results that the POD options are able to significantly contribute to damping the oscillation modes when operating on either the active or the reactive power modulation channels. The results also indicate possibilities to combine POD controllers on both channels at the same time. These combinations can bring uniform solutions to add evenly damping to all three oscillation modes.

4.4.1 Effect of system load characteristics

The simulation results show that the contribution from the POD controller on Q channel to the damping of the first two modes is better than the POD controller on P channel. The observation can be explained by the location of MMC-VSC MTDC system and the characteristic of the system loads. In this study, VSC 1 and 2 are located close to the large load centers LOAD07, LOAD09 that are characterized by a quadratic relationship with voltage (modeled as constant impedance load, const. Z). Therefore, control actions of VSC 1 and 2 through Q channel have great influences on modulating the system loads (here means the influence on the active and reactive powers drawn by the system loads). The capability in modulating the system loads at the VSC station through an appropriately tuned POD controller on Q channel is the decisive factor for damping support to inter-area modes. This observation is compatible with the findings in [49].

To investigate the effect of the load characteristics on the damping support capability of the POD controller, the load model will be changed to the constant current model (const. I) and the constant active/reactive power model (const. PQ). With these load models, the controllability measures of the best option for each mode are shown in Figure 4.8. As Figure 4.8 shows, the controllability of the POD controller on Q channel decreases with the reduction of the voltage-dependent level of the system loads. In contrast to the POD option on Q channel, the controllability of the POD option on P channel either reduces slightly or increases when the voltage-dependency of the system load decreases.

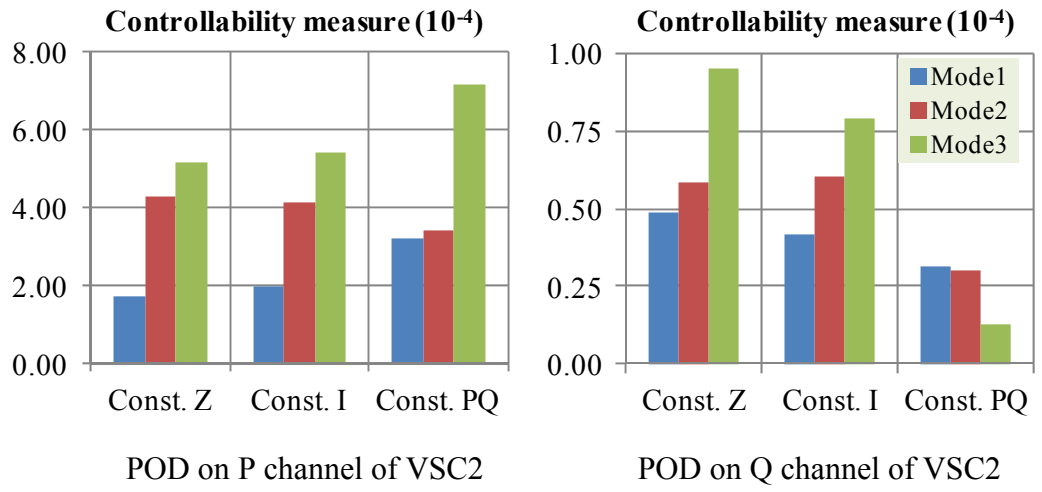

Figure 4.8: Effect of load characteristic on controllability measures of POD controllers on P and Q channels of VSC2 (x10^{-4})

4.4.2 Effect of using global signals

As Figure 4.6 shows, the POD options using global signals provide more damping to oscillation modes 1 and 2 than the options using local signals. This fact comes from the better observability of the modes in the global signals in comparison to the one in local signals. However, the damping improvement in mode 3 is lower. This phenomenon originates from the fact that the inputs and outputs of the POD controllers for modes 1 and 2 (M1-POD and M2-POD) also possess considerable observability and controllability, respectively, to mode 3. Therefore, the POD controllers can also influence the damping of the oscillation mode 3 while providing significant damping to the modes 1 and 2. Particularly in this case they moderately reduce the damping provided by the third POD controller to the mode 3.

The optimal setting parameters for the POD options using global signals shown in Figure 4.6 are not always the optimal setting for all three modes individually. In practice, a compromise option is to ensure that the most damping is provided to the lowest damping mode, as defined in the objective function of the optimization problem. However, the use of global signals enables to provide more damping to oscillation modes which cannot be locally well observed and controlled.

4.4.3 Effect of communication delay

The use of global signals from wide area measurements is shown as enabling a better damping contribution as a whole. However, these remote signals are often associated with delays initiated by the use of communication systems. The delays reduce the observability of the global signal to the system oscillations. As Figure 4.9 shows, the higher the delay is, the lower the observability is. To assure the POD controller performance, the adverse effect due to signal delays should be mitigated. In this study, the undesired effect caused by signal delays will be compensated through a parameter optimization step. To examine the damping support capability when considering delays evenly added to the input signals, the analysis of the POD options using the best global signals on both P and Q channels (PQ-BEST-G) is repeated. The simulation results are shown in Figure 4.10. It can be seen from the simulation results that POD controller with suitably-tuned parameters keeps providing good performance at a constant communication delay.

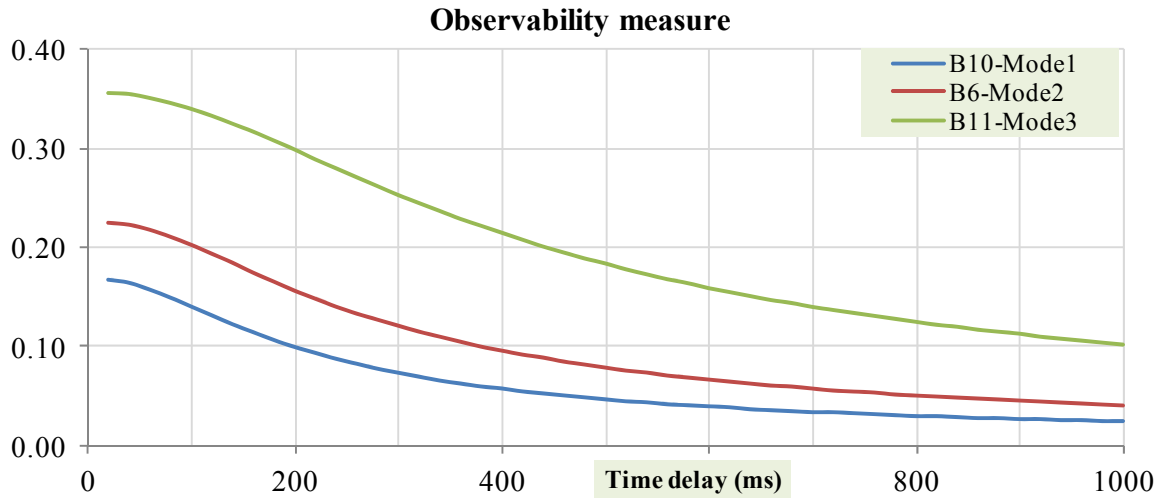

Figure 4.9: Effect of communication time delay to observability of bus angle input

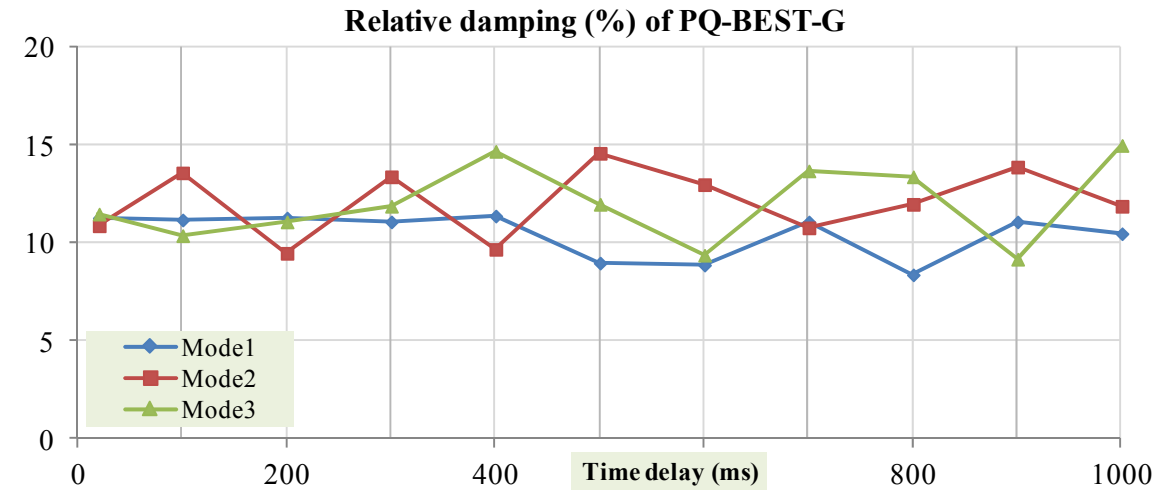

Figure 4.10: Effect of communication time delay to damping support capability of MMC-VSC-MTDC system

In fact, the communication delay varies randomly. A logical extension would be to test the time variation on the performance of the tuned POD controller. The tuned POD option PQ-BEST-G associated with 500-ms delay is further investigated considering random variations of communication time. Figure 4.11 shows the resulting relative damping of the three investigated modes as the function of the communication delay variation. For the mode 1 and 3, positive random variations of the considered 500-ms delay reduce the damping's while negative random variations of the considered delay increase the dampings. However, for the mode 2, any random variation of the considered 500-ms delay results in a reduction of the oscillation damping. To clarify the phenomenon, let us take a close look into the tuned POD option PQ-BEST-G associated with the 500-ms delay. The tuned POD parameters are optimal

for proving the maximum damping contribution for the mode 2. Consequently, any additional phase shift due to random variations of the delay will lead to reductions of the dampings of this mode. For the mode 1 and 3, the tuned POD parameters results in considerable damping contributions, but are not the optimal ones. For that reason, random variations of the delay can either improve or decrease the damping.

This study observed that proper damping to oscillations can be achieved when the random variations are between -60 ms and 150 ms. The damping to mode 2 drops dramatically if the actual communication delay deviates negatively more than 60 ms from the considered delay (500 ms).

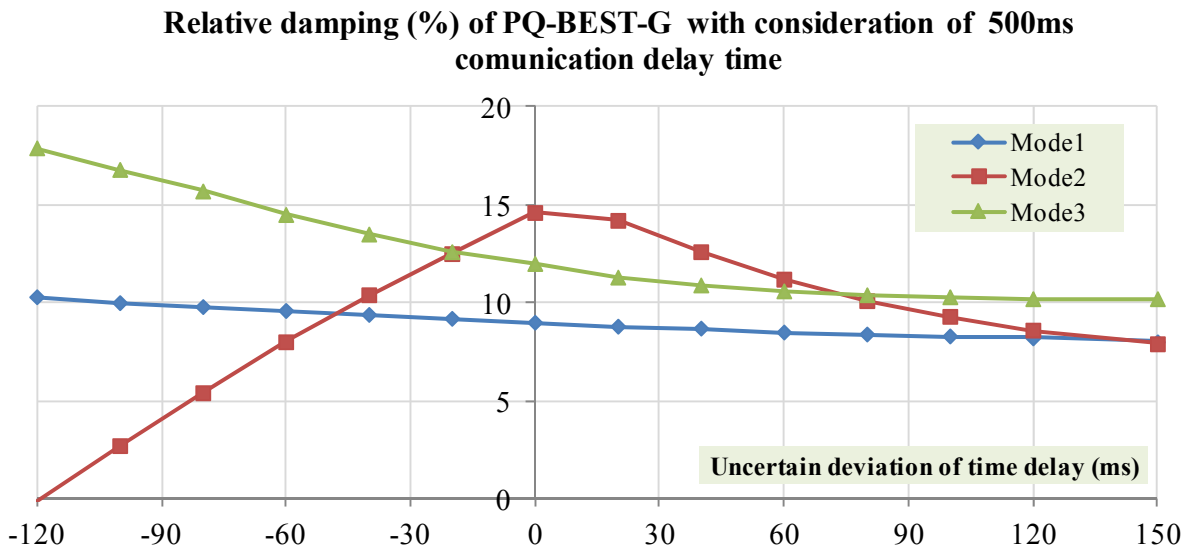

Figure 4.11: Effect of random deviation of communication time delay to damping support capability of MMC-VSC-MTDC system

4.4.4 Effect of active power loading levels

Thus far, the limitation of MMC-VSC modulation capability has not been mentioned. The simulation results shown in Figure 4.7 are achieved with the consideration of 75% active power loading at VSC 2. To assess the effect of loading level to the effectiveness of POD options, the power rating of VSC 2 is reduced so that the loading level increases to 95% with the same MW loading of VSC2. By doing this, the power flow stays unchanged. Time domain simulations of two POD options: P-BEST-G and Q-BEST-G are carried out once more and the results are plotted in Figure 4.12. It can be observed in Figure 4.12a that due to the limited availability of modulation capability (about 5% on P channel in the high loading case), the effectiveness of POD controller on P channel decreases. Hence, the power system oscillation in the high VSC-loading case lasts longer than in the lower VSC-loading case. In contrast to

the P-BEST-G option, the damping effectiveness of Q-BEST-G option in the two VSC-loading cases stays unchanged (see Figure 4.12b). It can be explained by the available modulation capability on Q channel as high as 30% even in case of 95% loading on P channel. The investigation here highlights an advantage of applying the POD controller on Q channel in case of high loading levels on the P channel.

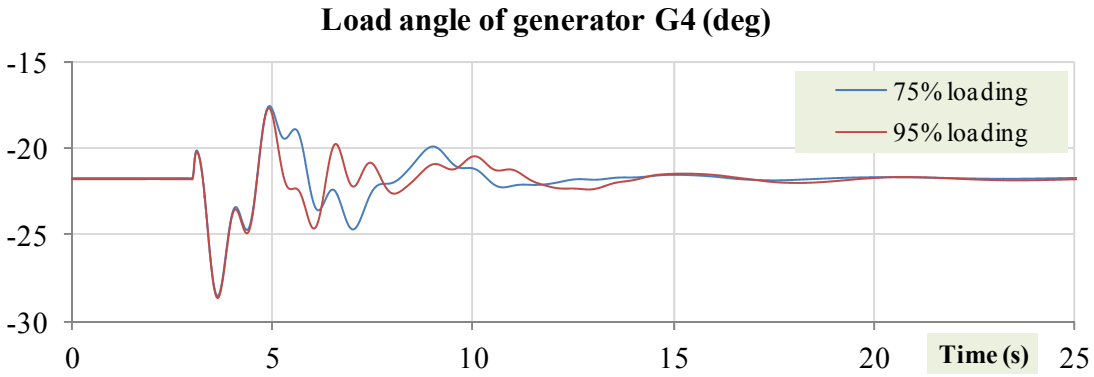

a) The best POD option using global inputs on P channel (P-BEST-G option)

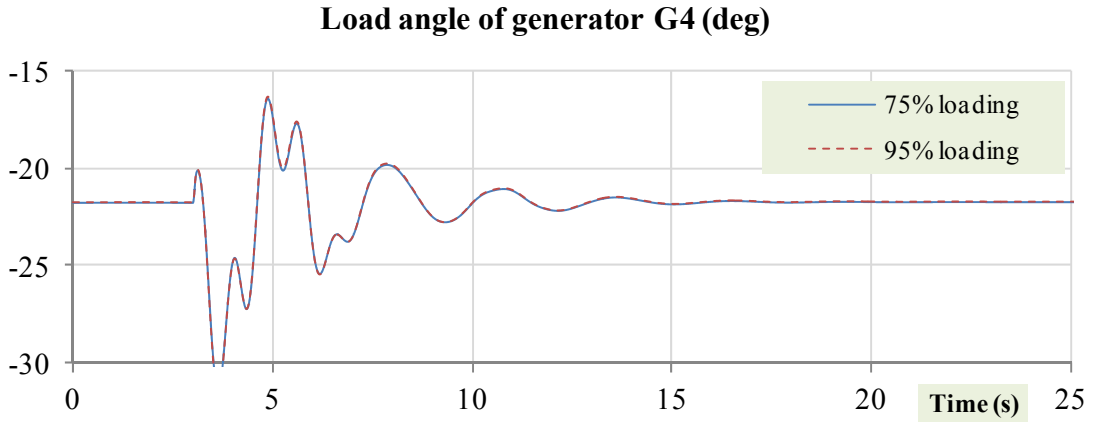

b) The best POD option using global inputs on P channel (Q-BEST-G option)

Figure 4.12: Effect of active power VSC-loading on damping support capability of POD equipped on: a) active power channel (P-BEST-G option) b) reactive power channel (Q-BEST-G option)

4.5 Summary

The simulation results presented in this chapter reveal the considerable capability to incorporate the POD controller into both channels of the MMC-VSC-MTDC system to enhance damping of inter-area oscillations. The damping capability on Q channel is observed to possess a greater potential to improve the damping of inter-area oscillations in several circumstances, such as when the system loads are excessively sensitive to voltage; or when the VSC station is located near load centers. However, the damping capability on Q channel

reduces with reduction of the voltage-dependent level of the system loads. This is not the case for the damping support capability of the POD option on P channel. When the P channel is loaded near to its maximum, the POD controller on the Q channel can be more effective than the one on the P channel. Furthermore, the use of global inputs has been investigated with the consideration of communication delay. The applied optimization method ensures good performances of the POD controller including global inputs with various communication delays.

Based on the results obtained from the simulations and analyses done in the present chapter, it is recommended to study the damping capacity of both the modulation channels with consideration of the influencing factors such as voltage characteristics of the system loads, active power loading level, communication delay and sensitivity to the random delay variation to identify the best installation of POD controller for VSC-MTDC systems.

5 Primary frequency support controller

This chapter discusses the capability of the VSC-MTDC system equipped with frequency controllers in supporting the primary frequency control of the AC interconnected systems. The frequency controller has been utilized in several thyristor-based HVDC systems [53-55]. The use of a frequency controller has offered a number of advantages, such as improving the generator stability [53] and enabling isolated operation [55].

The frequency control feature of VSC-HVDC systems has been the focus of several studies [56–61]. The investigation for the point-to-point connections between two asynchronous areas was discussed in [56–68]. In [56], the frequency controller was found to provide frequency support between the grids, and thus increase significantly the power transit capability between the two grids. Reference [57] explored the utilization of a VSC–HVDC system as the main provider for frequency regulation to an AC network with high penetration of renewable (e.g. wind), and nuclear generation. Reference [58] looked into the frequency support of a VSC–HVDC-supplied industrial system with onsite generation. The analysis also focused on the frequency control cooperation between the VSC–HVDC connection and the onsite generator.

Different frequency-control strategies for VSC station control have been investigated. Reference [59] has investigated the frequency control support of a VSC-HVDC link operated in parallel with an existing HVAC link between two interconnected areas. With properly tuned gains of the applied frequency controller, the VSC-HVDC connection has been reported to provide an adequate power exchange, and thus reduce frequency deviations in the tested system.

Research results on the possibility of exchanging primary reserves between asynchronous AC grids connected through a MTDC system for supporting frequency control have been reported in [60-61]. Reference [60] proposed a control scheme which involved all AC grids connected to the DC grid in frequency support at the point of common coupling. The control scheme combined a frequency droop control of AC grids with that of the DC voltage droop control in the DC grid. Simulation results of this study on a four-terminal HVDC system have shown the robust performance of the proposed control method during frequency variations in different terminals. Reference [61] presented two different control schemes with communication and without communication (relying on the physical quantities in the DC grid). The frequency controller regulated the power injection at each VSC station as a function of either the frequency deviation in all asynchronous areas or only the local frequency. The simulation results show that the primary reserve can be shared as in an AC network.

Most studies in literature deal with primary frequency control of asynchronous areas interconnected via VSC-HVDC systems equipped with frequency controllers. There is not much work performed on VSC-MTDC systems embedded in a synchronous area and operating in parallel with HVAC connections to interconnect the synchronous areas. As part of an integrated transmission corridor, VSC-MTDC systems should take part in helping the exchange of primary reserves between synchronous areas as a result of primary frequency control actions. With the frequency not being sensed in the VSC control, the VSC-MTDC system will not provide any additional active power support, which might drive some heavily-loaded HVAC lines to exceed thermal limits or lead to system instability. By means of frequency controllers augmented to the VSC control, the VSC-MTDC system can actively take part into this task.

In this chapter, a novel frequency controller which enables the embedded VSC-MTDC system to involve itself effectively in the primary frequency control is proposed. A feed-forward control technique is applied to build up the transient component of the proposed controller by using the inversion of a simplified power-frequency characteristic of the power system. The frequency controller gain defines the primary reserve exchanged power through the VSC-MTDC system according to the residual transferable margin of the parallel HVAC lines. In this chapter, a method to determine the frequency controller gain employing the dynamic characteristic of the VSC-MTDC system and the power-frequency characteristic of the AC system is also described. The proposed frequency controller is hereby named primary frequency support (PFS) controller in this thesis.

The chapter is structured as follows: section 5.1 deals with the power and voltage controls in a VSC-MTDC system. This is followed by section 5.2 which discusses the exchanged power between areas of an AC power system. The proposed frequency controller is described in section 5.3 and a test network is introduced in section 5.4. Finally in the section 5.5, the performance of the proposed frequency controller is investigated.

5.1 Dynamic response of MTDC systems following power reference change

In a DC grid, the active power controls of VSC stations in VSC-MTDC systems are responsibility to maintain the DC voltage and the active power exchanges with interconnected AC power systems. The active power controls continuous operating equilibrium in the DC grid with well-defined operating points for all converter stations. It should also enable to establish a new equilibrium following a stable transition under small load or topology

changes, following large disturbances. Therefore, active power control in one converter station has to work in coordination with those in other converter stations within a DC grid. Several control strategies can be applied, such as constant DC voltage control, constant DC power control and voltage – power droop control strategies [23].

The afore-mentioned active power control strategy can be formulated as follows:

$$v_{\mathrm{DC,i}} - v_{\mathrm{DC,i}}^{\mathrm{ref}} = k_{\mathrm{VP,i}}(p_{\mathrm{DC,i}} - p_{\mathrm{DC,i}}^{\mathrm{ref}}) \tag{5.1}$$

where $v_{\mathrm{DC,i}}, p_{\mathrm{DC,i}}, v_{\mathrm{DC,i}}^{\mathrm{ref}}$ and $p_{\mathrm{DC,i}}^{\mathrm{ref}}$ are the DC voltage and DC power signals and their corresponding reference values in the i-th converter station. $k_{\mathrm{VP,i}}$ is the voltage–power gain. $k_{\mathrm{VP,i}} = 0$: implies constant DC voltage control, and $k_{\mathrm{VP,i}} = \infty$: constant DC power control. All variables and parameters are in a per unit in basic of the base voltage $V_{\mathrm{DC}}^{\mathrm{base}}$ and the base power $P_{\mathrm{DC}}^{\mathrm{base}}$ of the DC grid.

Assume now that in the z-th converter station a small change $\Delta p_{\mathrm{DC,z}}^{\mathrm{ref}}$ of the reference power is applied. The z-th converter station is here named the exciting SVC and the other converter stations (where no reference power is applied) are here named the following VSC. After the transient process has ended, the system moves to a new quasi-stationary operating point, signified by "qs". The resulting relationship between the DC voltage and power at the exciting VSC and the following VSCs can be expressed in the following form:

$$\begin{cases} v_{\mathrm{DC,z}}^{\mathrm{qs}} - v_{\mathrm{DC,z}}^{\mathrm{ref}} = k_{\mathrm{VP,z}}(p_{\mathrm{DC,z}}^{\mathrm{qs}} - (p_{\mathrm{DC,z}}^{\mathrm{ref}} + \Delta p_{\mathrm{DC,z}}^{\mathrm{ref}})) \\ v_{\mathrm{DC,i}}^{\mathrm{qs}} - v_{\mathrm{DC,i}}^{\mathrm{ref}} = k_{\mathrm{VP,i}}(p_{\mathrm{DC,i}}^{\mathrm{qs}} - p_{\mathrm{DC,i}}^{\mathrm{ref}}) \quad with\ i = 1,...,S \mid i \neq z \end{cases} \tag{5.2}$$

where S is the number of the VSC stations in the DC grid.

The above equation can be rewritten as:

$$\begin{cases} \dfrac{1}{k_{\mathrm{VP,z}}} \Delta v_{\mathrm{DC,z}}^{\mathrm{qs}} = (p_{\mathrm{DC,z}}^{\mathrm{qs}} - p_{\mathrm{DC,z}}^{\mathrm{ref}} - \Delta p_{\mathrm{DC,z}}^{\mathrm{ref}}) \\ \dfrac{1}{k_{\mathrm{VP,i}}} \Delta v_{\mathrm{DC,i}}^{\mathrm{qs}} = (p_{\mathrm{DC,i}}^{\mathrm{qs}} - p_{\mathrm{DC,i}}^{\mathrm{ref}}) \qquad with\ \ i = 1,...,S \mid i \neq z \end{cases} \tag{5.3}$$

where $\Delta v_{\mathrm{DC,i}}^{\mathrm{qs}} = v_{\mathrm{DC,i}}^{\mathrm{qs}} - v_{\mathrm{DC,i}}^{\mathrm{ref}}$ with i =[1,S].

Summing all S stations leads to:

$$\sum_{i=1}^{S} \frac{1}{k_{\mathrm{VP,i}}} \Delta v_{\mathrm{DC,i}}^{qs} = (\sum_{i=1}^{S} p_{\mathrm{DC,i}}^{qs} - \sum_{i=1}^{S} p_{\mathrm{DC,i}}^{ref} - \Delta p_{\mathrm{DC,z}}^{ref}) \tag{5.4}$$

Neglecting the losses in the DC grid, we have for the sum of DC powers and DC voltage deviation across all stations:

$$\begin{cases} \sum_{i=1}^{S} p_{\mathrm{DC,i}}^{\mathrm{qs}} = 0 \\ \sum_{i=1}^{S} p_{\mathrm{DC,i}}^{\mathrm{ref}} = 0 \\ \Delta v_{\mathrm{DC,i}}^{\mathrm{qs}} = \Delta v_{\mathrm{DC,j}}^{\mathrm{qs}} = \Delta v_{\mathrm{DCO}}^{\mathrm{qs}} \ \ with\ i, j = 1,...,S \end{cases} \tag{5.5}$$

Substituting (5.5) into (5.4) gives:

$$\Delta v_{\mathrm{DCO}}^{\mathrm{qs}} \sum_{i=1}^{S} \frac{1}{k_{\mathrm{VP,i}}} = -\Delta p_{\mathrm{DC,z}}^{\mathrm{ref}} \tag{5.6}$$

The power in the i-th VSC station with i ≠ z in response can be calculated by substituting (5.6) into (5.3) as follows:

$$\Delta p_{\mathrm{DC,i}}^{\mathrm{qs}} = p_{\mathrm{DC,i}}^{\mathrm{qs}} - p_{\mathrm{DC,i}}^{\mathrm{ref}} = -\frac{1/k_{\mathrm{VP,i}}}{\sum_{i=1}^{S} \frac{1}{k_{\mathrm{VP,i}}}} \Delta p_{\mathrm{DC,z}}^{\mathrm{ref}} \tag{5.7}$$

As shown in (5.7), the power deviation in the following VSCs is proportional to the droop of the voltage-power characteristic. If a VSC uses constant DC power control strategy, then it has no sensitivity for the step change from other terminals in the DC grids. If a VSC employs constant DC voltage control strategy (slack VSC), it will mobilize additional power to cover all requested additional power from other converter stations.

The power $\Delta p_{\mathrm{DC,z}}^{\mathrm{qs}} = p_{\mathrm{DC,z}}^{\mathrm{qs}} - p_{\mathrm{DC,z}}^{\mathrm{ref}}$ at the exciting VSC (z-th VSC) can be calculated by replacing (5.6) into (5.3) as follows:

$$\Delta p_{\mathrm{DC,z}}^{\mathrm{qs}} = \left(1 - \frac{1/k_{\mathrm{VP,j}}}{\sum_{i=1}^{S} \frac{1}{k_{\mathrm{VP,i}}}}\right) \Delta p_{\mathrm{DC,z}}^{\mathrm{ref}} = k_{\mathrm{VSC,z}} \Delta p_{\mathrm{DC,z}}^{\mathrm{ref}} \tag{5.8}$$

where $k_{\mathrm{VSC,z}}$ is defined as power-response factor of the exciting VSC:

$$k_{\mathrm{VSC,z}} = \left(1 - \frac{1/k_{\mathrm{VP,z}}}{\sum_{i=1}^{S} \frac{1}{k_{\mathrm{VP,i}}}}\right) \tag{5.9}$$

The power-response factor $k_{\mathrm{VSC,z}}$ lies within [0, 1]. $k_{\mathrm{VSC,z}}$ is equal to 1 only if there is a slack VSC among the following VSCs. Equation (5.8) shows that, the actual response power of the exciting VSC can be smaller than its desired reference power change.

5.2 Exchanged powers between areas in AC grids in primary frequency control

Consider an AC grid in which N areas are interconnected to each other. From a steady-state operation point, assume a generation outage with the value P_{ZG} occurs in z-th area (here noted as the outage area). After the outage, each i-th area (i = 1,..,N) is characterized by available generating power $P_{G,i}$, load $P_{L,i}$, droop characteristic of primary frequency control $R_{P,i}$ and a frequency-dependent load droop $R_{L,i}$ (The power losses are here neglected). The generation droop $R_{P,i}$ and load droop $R_{L,i}$ are in a per unit in basic of the fundamental frequency f_0 and the available generating power $P_{G,i}$.

The frequency droop $R_{N,i}$ of the i-th area can be formulated as:

$$\frac{1}{R_{N,i}} = \frac{1}{R_{P,i}} + \frac{1}{R_{L,i}} \tag{5.10}$$

Hence, the grid-frequency droop R_N of the whole grid is given as:

$$\frac{1}{R_N} = \frac{\sum_{i=1}^{N} \frac{1}{R_{N,i}} P_{G,i}}{\sum_{i=1}^{N} P_{G,i}} \tag{5.11}$$

Based on the grid-frequency droop, the steady-state frequency deviation Δf_S can be calculated as [31, 62]:

$$\frac{\Delta f_S}{f_0} = -R_N \frac{P_{ZG}}{P_G} \tag{5.12}$$

where, $P_G = \sum_{i=1}^{N} P_{G,i}$

The exchanged power of the i-th area (i≠z) into the other areas is determined as follows:

$$\Delta P_{EX,i} = -\frac{\Delta f_S}{f_0} \frac{P_{G,i}}{R_{N,i}} \tag{5.13}$$

The expression for the exchanged power $\Delta P_{EX,z}$ of the outage area z into other areas is given by:

$$\Delta P_{EX,z} = -\frac{\Delta f_S}{f_0} \left(\frac{P_{G,z}}{R_{N,z}} - \frac{P_G}{R_N}\right) = -K_{EX,z} \Delta f_S \tag{5.14}$$

where, $K_{EX,z}$ is the power-exchange factor of the outage area (MW/Hz):

$$K_{\mathrm{EX,z}} = \frac{1}{f_0}\left(\frac{P_{\mathrm{G,z}}}{R_{\mathrm{N,z}}} - \frac{P_{\mathrm{G}}}{R_{\mathrm{N}}}\right) \tag{5.15}$$

According to the current practice, the exchanged power between areas is transferred automatically only through the AC transmission lines. With a supplementary frequency controller, VSC-MTDC systems will also share this duty with the parallel AC transmission lines. The proposed frequency controller equipped to the VSC-MTDC system control will be described in the next section.

5.3 Primary frequency support controller in VSC-MTDC-embedded network

In this section, the proposed PFS controller to incorporate a VSC-MTDC system operated in parallel with HVAC tie lines into an overall primary frequency control will be described. The proposed PFS controller uses the frequency deviation as input. The controller structure comprises a dead-band element, a static gain and a transient component (see Figure 5.1). The static gain defines the primary reserve power exchanged through the VSC-MTDC system according to the residual transferable margin of the parallel HVAC lines. The transient component (described by the transfer function $G_{\mathrm{PFS}}(s)$) is derived by inversing the simplified power-frequency characteristic of the VSC-MTDC-embedded system.

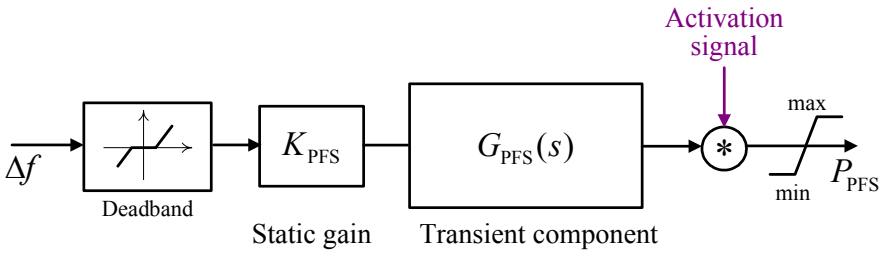

Figure 5.1: Schematic structure of the proposed PFS controller

5.3.1 PFS gain determination

From the power-frequency characteristic analysis in section 5.3, the exchanged power of the outage area can be estimated using (5.14). The exchanged power to the outage area is assumed to be done through both MTDC connection and parallel AC transmission lines. The additional transferred power through MTDC system can be determined according to residual transferable margins of the AC lines. If the pre-outage loading of the AC line is close to its transmission limit, the residual transferable margin is low. Then, the MTDC system should exchange more power. According to the residual transferable margin of the parallel AC lines,

the power exchanged through VSC-MTDC system at the exciting VSC can be defined by a participation factor α_{DC} of the total exchanged power. (The value of the introduced participation factor ranges between zero, i.e. no power, and one, i.e. all the additional power).
When a sudden power imbalance due to an outage in the z-th area is detected, the PFS controller equipped to the z-th VSC station is activated. The controller adds a reference change $\Delta p_{DC,z}^{ref}$ (controller output) to the z-th VSC station control. The dynamic characteristic analysis of the VSC-MTDC system in section 5.1 provides the actual power response at this VSC station, given by (5.8), due to a reference change $\Delta p_{DC,z}^{ref}$. Linking these two relationships described by (5.8) and (5.14), the gain of the PFS controller can be expressed as:

$$K_{PFS} = -\alpha_{DC} \frac{K_{EX,z}}{k_{VSC,z}} = -\alpha_{DC} K_{PFS0} \tag{5.16}$$

The additional power transferred into the outage area through the exciting VSC station is mobilized from the other AC areas through the interconnected VSC stations. It is reasonable to presume that the power response at the following VSC station is proportional to the additional power exchange generated in the corresponding interconnected AC area. With this assumption, the power exchange can be directly transmitted to the outage area via the MTDC system, without causing extra power circulating through the AC transmission lines.
The power response at the following i-th VSC station is defined by (5.7) while the additional power exchange generated by the corresponding i-th interconnected AC area is defined by (5.13). Connecting these two relationships gives the proposed settings so that the voltage-power droops fulfill the primary frequency control objective:

$$\frac{\Delta p_{DC,i}^{qs}}{\Delta P_{EX,i}} = \frac{\Delta p_{DC,j}}{\Delta P_{EX,j}} \quad \text{with i, j = 1,…,S | i, j} \neq z \tag{5.17}$$

The proposed droop setting is therefore expressed as follows:

$$\frac{k_{VP,i}}{k_{VP,j}} = \frac{R_{N,i}/P_{G,i}}{R_{N,j}/P_{G,j}} \quad \text{with i, j = 1,…,S | i, j} \neq z \tag{5.18}$$

5.3.2 Transient component

The proposed PFS controller uses the system frequency to sense the generation outage. In fact, the quasi-steady-state frequency deviation reflects the amount of the power outage. Nevertheless, the frequency excursions following generation outages may include a large frequency deviation occurring right after the outage incident. This frequency deviation can be much larger than the quasi-steady-state frequency deviation, which is the reference for

determining the gain in the previous section. Consequently, during the transient process, the frequency support controller may mobilize more exchanged power through MTDC system than scheduled. This surplus in power then circulates through the AC transmission lines and this could lead to prolonging power oscillation on the AC transmission system. To avoid this undesired effect due to transient frequency input on the system, a feed-forward control technique is applied. The feed-forward control is known as an effective way to reject controlled system disturbances [63-64]. This technique has been considered for load-frequency control in deregulated power system under high stress conditions [65]. Using this control technique, the disturbances are measured and can be compensated or minimized before they can influence the system.

Applying the feed-forward control technique, a new transient component is included the proposed PFS controller. The transient component is derived from the power-frequency model of the embedded VSC-MTDC grids.

In a embedded VSC-MTDC grid, the control action of the VSC-MTDC system control is much faster than the dynamic response of the AC grid in the primary frequency control such that the desired power exchanges with AC grid are quickly achieved. Neglecting the power losses in the VSC-MTDC system, the sum of the power exchange from the VSC-MTDC system to the AC power system is zero. The dynamic behavior of the embedded VSC-MTDC system can therefore be neglected in the estimation of the frequency/generation outage transfer function. The embedded VSC-MTDC grid for primary frequency control study can be simplified as shown in Figure 5.2

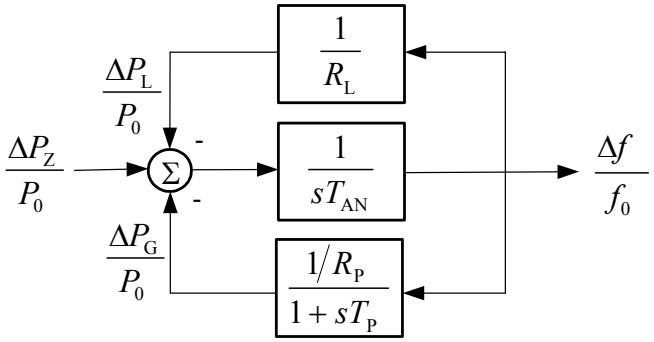

Figure 5.2: Simplified power-frequency model of embedded VSC-MTDC grid

In this simplified model, only the power-frequency characteristic of the AC grid is considered. In this model, R_L is the frequency-dependent load droop, which represents the frequency sensitive load change. R_P, T_P represents the characteristic for the primary control of the generation units. R_P and R_L are in a per unit in basic of the fundamental frequency f_0 and the total generation power P_0. T_{AN} stands for the overall inertia constant of the AC grid. The losses in the AC grid are also neglected in this simplified model.

The transfer function of the frequency deviation Δf against the generation deviation ΔP_Z is then given as:

$$G_N(s) = \frac{\Delta f(s)/f_0}{\Delta P_Z(s)/P_0} = R_N \frac{1+sT_P}{1+sR_N(T_{AN}+T_P/R_L)+s^2R_NT_{AN}T_P} \tag{5.19}$$

where, R_N is the grid-frequency droop defined as:

$$R_N = \frac{R_L R_P}{R_L + R_P} \tag{5.20}$$

According to the feed-forward controller, the design formula of the transient component of the PFS controller is then:

$$G_{PFS}(s) = G_N^{-1}(s) = \frac{1+sT_P\left(\frac{R_N}{R_L}\right)}{1+sT_P} + sR_NT_{AN} \tag{5.21}$$

This transient component is included to compensate the transient excursion of the frequency, which reflects the power-frequency characteristics of the embedded VSC-MTDC grid, within the proposed PFS controller. Figure 5.3 illustrates the block diagram of the proposed PFS controller.

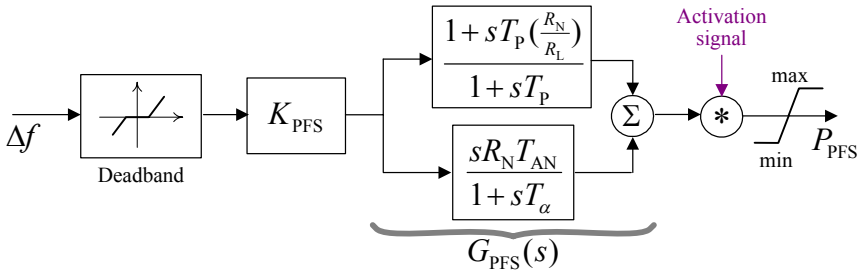

Figure 5.3: Novel PFS controller using feed-forward control technique

5.3.3 Controller activation scheme

The PFS controller is designed to support the primary frequency control in synchronous AC interconnected systems. The controller is inactive in steady state. It is activated when there is an outage of large generation units. In this case, the PFS controller at the VSC station interconnected to the area where the outage happens will be activated. The controller will mobilize the power from other interconnected area through the VSC-MTDC system to the outage area.

A suitable activation scheme is needed to detect severe outage situations and send the activation signal to the corresponding VSC station. Right after a generation outage event, the frequency measured at the VSC terminal connected to the outage area is temporarily smaller

than ones of other VSC terminals. Therefore, the increment of the bus voltage angle of this VSC terminal is temporarily less than the ones of the other VSC terminals. This observation can be used to detect the generation outage even and the corresponding outage area. Based on this observation, in this thesis, a novel activation scheme is proposed. The proposed scheme compares the increment of the bus voltage angles measured at the VSC-MTDC terminals. The VSC station which has the smallest voltage angle incremental at the terminal bus will be recognized as the VSC connected to the outage area. Then the PFS controller at this VSC station will be activated where as the other PFS controllers within the MTDC system will be blocked. The detection logic is shown in Figure 5.4.

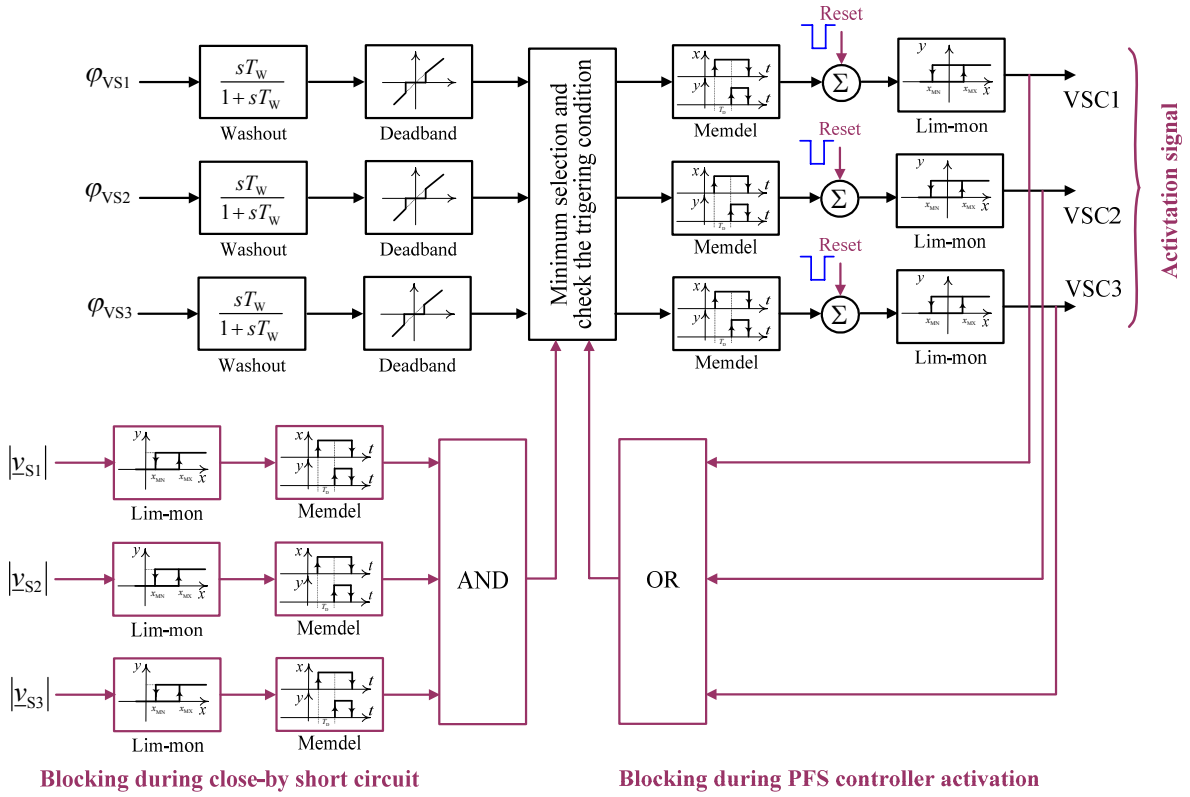

Figure 5.4: Activation scheme applied for PFS controller

The voltage angle at each VSC terminal bus is measured and sent to the control center. A washout block is used to calculate the increment of the signal. The deadband block is employed to filter out small turbulences in power systems. Then, the comparison is done between the signals. If a VSC station has the smallest voltage angle increment at the terminal bus over a certain time, a generation outage situation is defined and the control center sends an activation signal to the corresponding PFS controller while sending the blocking signal to other PFS controllers. From this moment on, the comparison process in the activation schema is blocked until a reset signal is triggered.

In the activation scheme, there is a so-called blocking scheme during close-by short circuit. This scheme will block the activation scheme during and a certain time after the incidence of a close-by short-circuit which can lead to a significant fluctuation of the voltage phase during and right after the short circuit. This phenomenon may lead to a misleading action of the activation scheme. Sometimes the close-by short-circuits initiate generation outages.
The activation scheme enables the use of the local measurement for the PFS controller. The communication system is only employed to send either the activation signal or blocking signal to the PFS controller. After that, the PFS controller uses only the local measurement, which increases the reliability of the PFS controller in the primary frequency control.

5.4 Test system

The test system described in the previous chapter is modified to be used in this primary frequency control study. The generators within each area will be combined and represented by an aggregated generator. Three generators located in three areas supply power to four load centers via 400kV AC transmission lines and a VSC-MTDC system in radial Y-configuration which is interconnected to the power system at Bus 7, Bus 9 and Bus 13. The red color roughly denotes the power flow direction in the investigated network. The single line diagram of the test system is shown in Figure 5.5, as well as the load flow parameters of the system components. The dynamic parameters of the generator model and AVR are given in the Appendix A.4. In this load-flow case, the total power losses in AC system and DC grid are 63 MW and 8 MW respectively.
Focusing on the primary frequency control study, each generator is equipped with turbine governors as depicted in Figure 5.6. The setting parameters of the governors and load models are given in Table 5.1. Based on these parameters, the frequency droop of each area is calculated using (5.20). The voltage-power droop for each VSC station can be as well defined using (5.18). These parameters can be found in Table 5.1.
To enable the VSC-MTDC system to taking part in primary frequency control, each VSC station is equipped with the proposed PFS controller. The setting parameters for each PFS controller are defined considering an outage of the biggest generation unit of the interconnected area. In this study, the outage of a 300 MVA generating unit loaded at 240 MW is considered. Table 5.2 shows the setting parameters in this study. These parameters do not change during the simulations. The VSC droop and the parameters for PFS controller are updated only when the given parameters in Table 5.1 change with a new dispatch scenario.

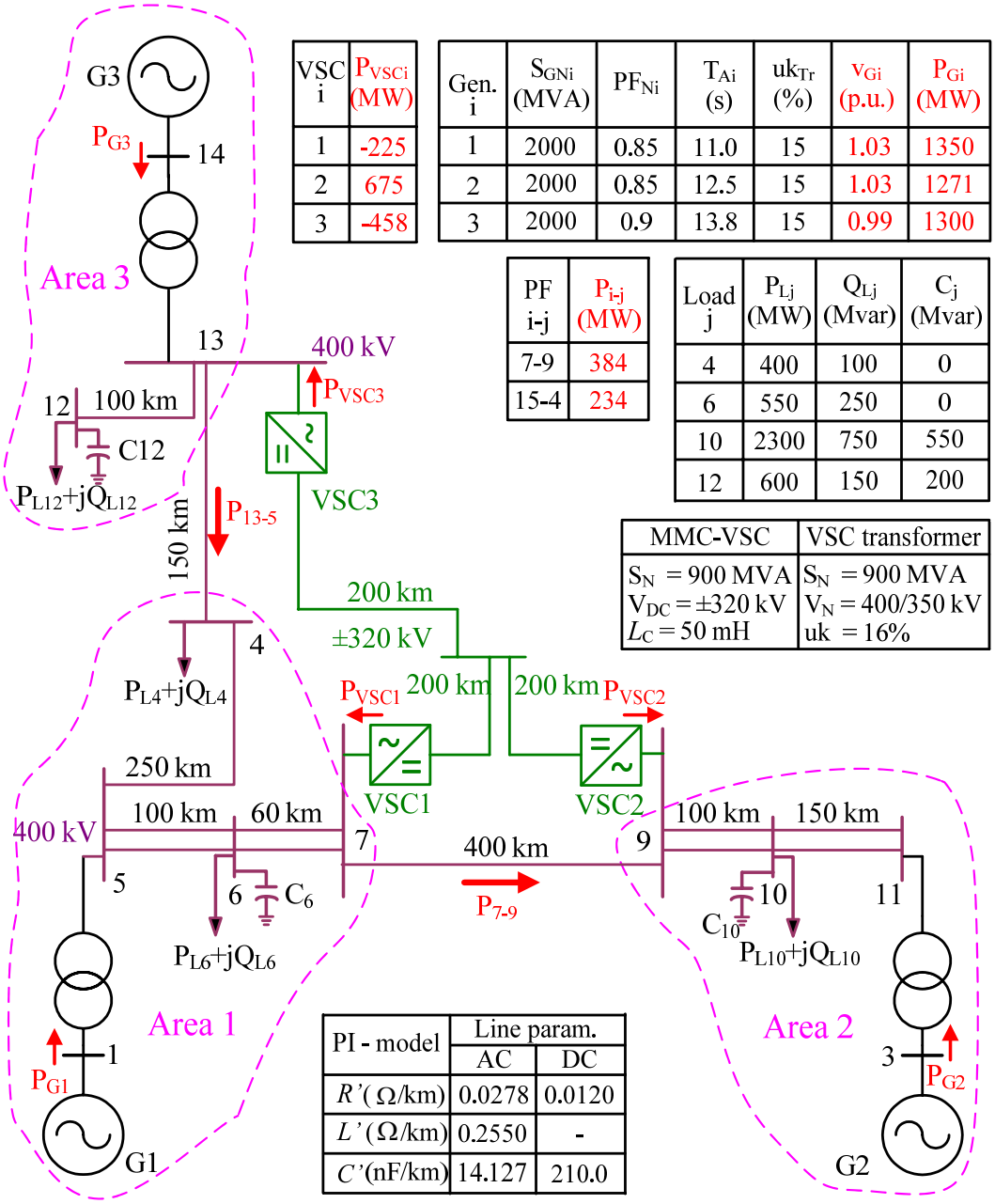

VSC i	P_{VSCi} (MW)
1	-225
2	675
3	-458

Gen. i	S_{GNi} (MVA)	PF_{Ni}	T_{Ai} (s)	uk_{Tr} (%)	v_{Gi} (p.u.)	P_{Gi} (MW)
1	2000	0.85	11.0	15	1.03	1350
2	2000	0.85	12.5	15	1.03	1271
3	2000	0.9	13.8	15	0.99	1300

PF i-j	P_{i-j} (MW)
7-9	384
15-4	234

Load j	P_{Lj} (MW)	Q_{Lj} (Mvar)	C_j (Mvar)
4	400	100	0
6	550	250	0
10	2300	750	550
12	600	150	200

MMC-VSC	VSC transformer
S_N = 900 MVA V_{DC} = ±320 kV L_C = 50 mH	S_N = 900 MVA V_N = 400/350 kV uk = 16%

PI - model	Line param.	
	AC	DC
R' (Ω/km)	0.0278	0.0120
L' (Ω/km)	0.2550	-
C' (nF/km)	14.127	210.0

Figure 5.5: Test network for the primary frequency control analysis

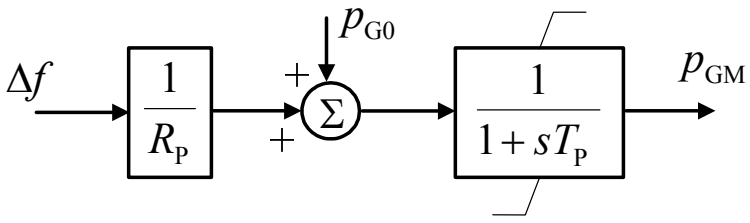

Figure 5.6: Turbine governor block diagram

Table 5.1: Parameters for governors, load model and VSC control

Area	P_G (MW)	P_L (MW)	R_P (p.u.)	R_L (p.u.)	T_P (s)	R_N (p.u.)	VSC droop k_{VP} (p.u.)
1	1700	950	0.10	1.00	10	0.0947	0.284
2	1700	2300	0.20	1.00	20	0.1574	0.472
3	1800	600	0.05	1.00	5	0.0464	0.139

Table 5.2: Control parameters for PFS controllers

VSC	K_{PFS0} (MW/Hz)	T_P (s)	T_{AN} (s)	R_N (p.u.)	R_L (p.u.)
1	1327	8.81	14.4	0.079	1.00
2	1323	8.64	14.3	0.077	1.00
3	1268	9.16	14.3	0.082	1.00

5.5 Simulation results

To investigate the dynamic performance of the proposed PFS controller, several study cases are carried out in the time domain. The study cases are defined to check the performance of the proposed static gain, the effect of the transient components with considerations of different outage locations and the values of the participation factor α_{DC}. A parameter sensitivity analysis is performed as well. Additionally, a study case where the proposed PFS control approach is applied for VSC-MTDC system connecting isolated areas is also investigated.

5.5.1 Performance of the proposed static gain

First of all, the PFS controller having only the static gain part is considered. The transient component will be taken into account in the next study case. An outage of a 300 MVA generating unit loaded at 240 MW in area 2 is applied at t = 1 s. Following the outage, the PFS controller equipped at VSC 2 is activated by the activation scheme. The simulation is carried out with three different values for the participation factor α_{DC} (0, 0.5 and 1.0). The simulation results are presented in Figure 5.7. This figure includes the results of the frequency deviation at Bus 9, the powers transferred through line 13-5, line 7-9 and the power exchanged at each VSC station. Table 5.3 summarizes the simulation results at quasi-steady state in this study case.

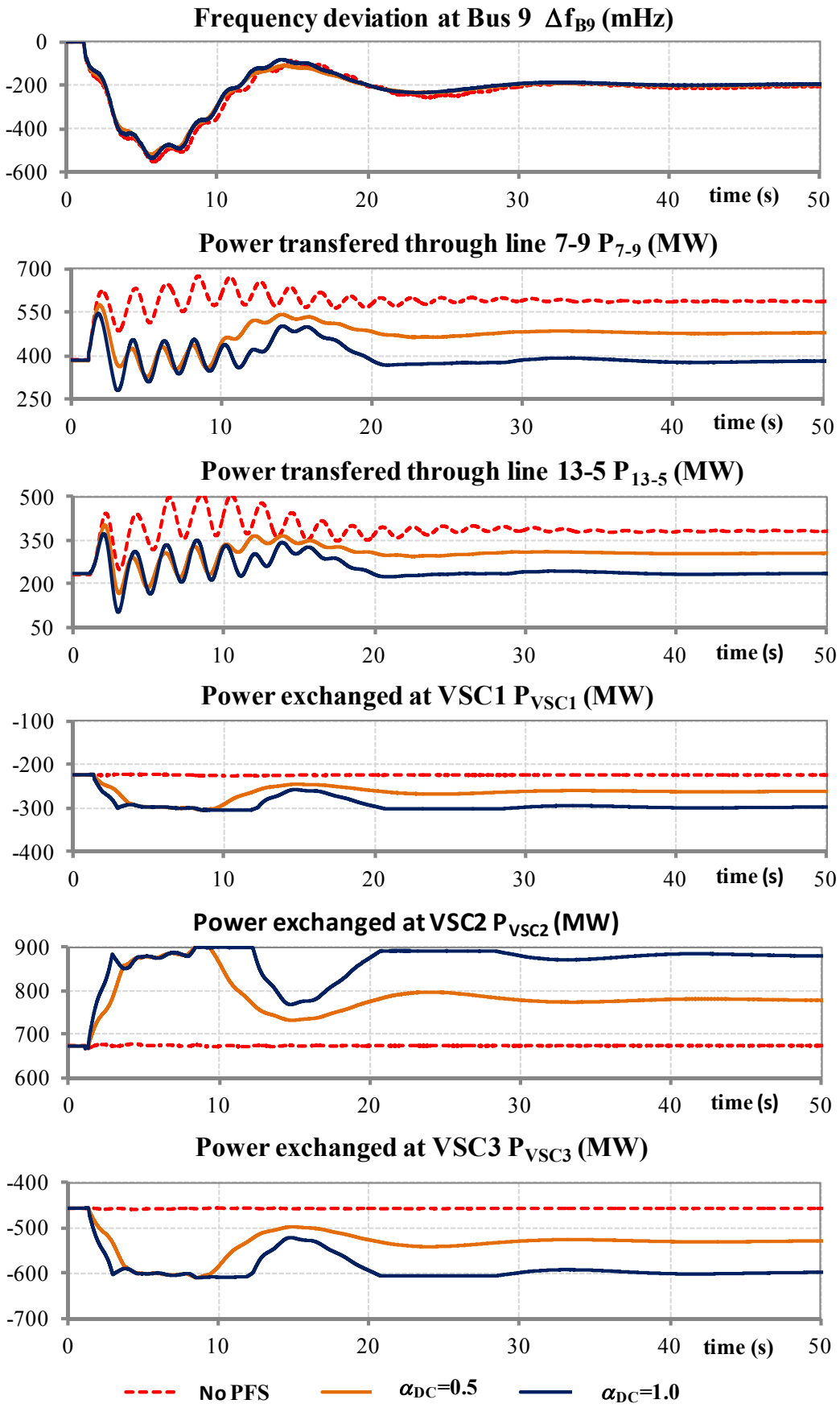

Figure 5.7: Case 1a: PFS controller without $G_{PFS}(s)$, 240 MW generation outage in area 2

Table 5.3: Simulation result of case 1a at quasi-steady state

α_{DC}	Δf_{B9} (mHz)	HVAC		HVDC		
		$\Delta P_{13\text{-}4}$ (MW)	$\Delta P_{7\text{-}9}$ (MW)	ΔP_{VSC1} (MW)	ΔP_{VSC2} (MW)	ΔP_{VSC3} (MW)
0.0	-205	147	200	0	0	0
0.5	-197	71	96	-37	105	-72
1.0	-193	0	4	-72	206	-141

It can be seen from Table 5.3, when α_{DC}=0, the powers exchanged at VSC converters stay unchanged. The additional power transferred from the areas 1 and 3 to area 2 are transmitted only through line 13-4 and line 7-9. When α_{DC}=0.5, the MTDC system takes over almost the half of the extra powers transferred from the areas 1 and 3 to area 2. It takes additionally 72 MW from area 3 and 37 MW from area 1. When α_{DC}=1.0, the MTDC system takes over almost all of the extra powers transferred from the areas 1 and 3 to area 2. The results in Table 5.3 illustrate that the actual participation of the MTDC system is nearly equal to the desired one defined by the given participation factor α_{DC}. It shows that neglecting the transmission losses and the linearization made during the mathematical development of the proposed method lead only to small divergences in the simulation results. Therefore, it is proved that the PFS gain determined by the proposed analytical method can ensure the planned amount of exchanged power transmitted through VSC-MTDC system.

Another case where there is an outage of 300 MVA generating unit loaded at 240 MW in area 1 is investigated. The simulation results are presented in Figure 5.8 and Table 5.4. The simulation result also shows an excellent performance of the proposed analytical method.

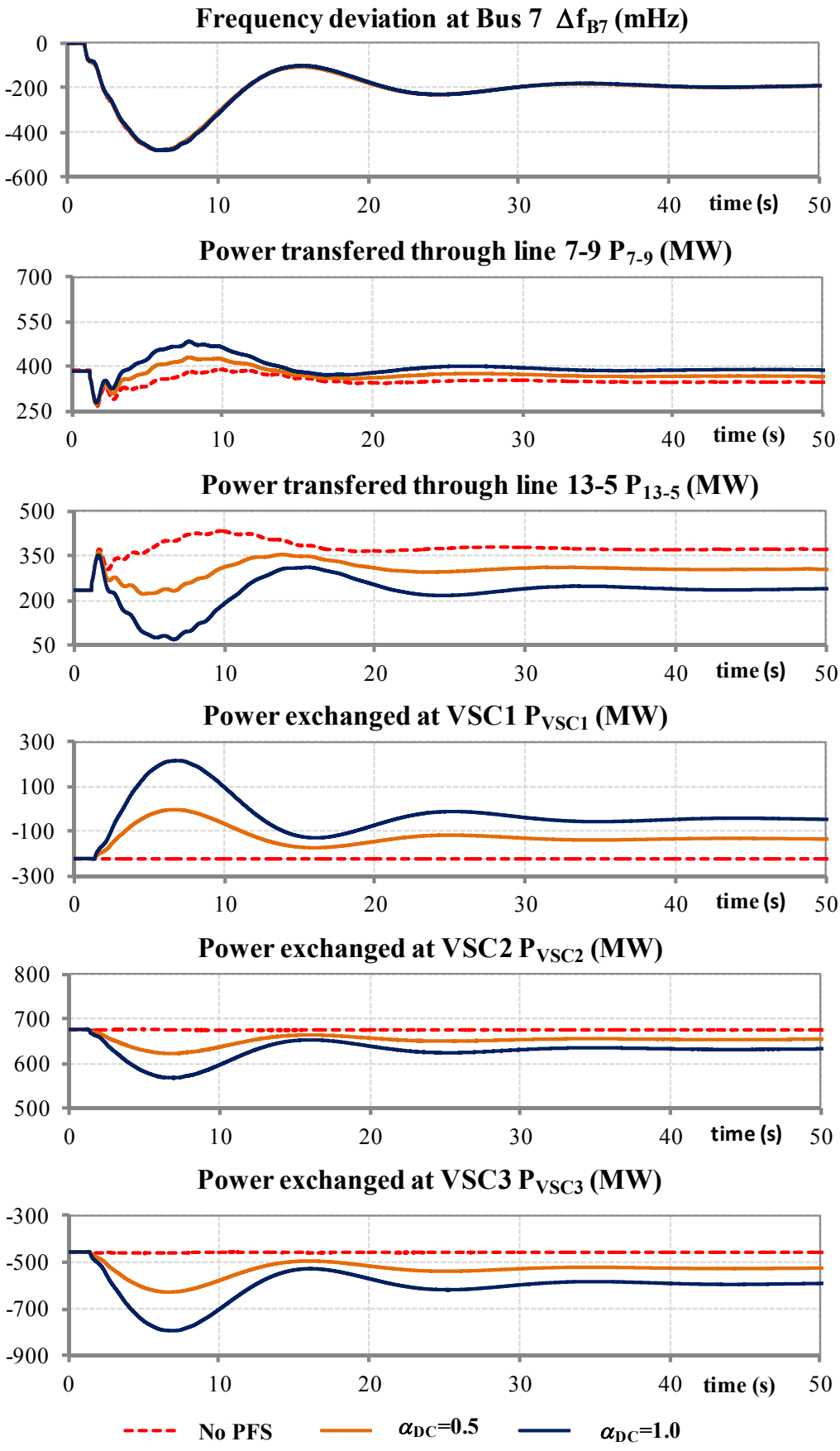

Figure 5.8: Case 1b: PFS controller without GPFS(s), 240 MW generation outage in area 1

Table 5.4: Simulation result of case 1b at quasi-steady state

α_{DC}	Δf_{B7} (mHz)	HVAC		HVDC		
		$\Delta P_{13\text{-}4}$ (MW)	$\Delta P_{7\text{-}9}$ (MW)	ΔP_{VSC1} (MW)	ΔP_{VSC2} (MW)	ΔP_{VSC3} (MW)
0.0	-191	137	-40.0	0	0	0
0.5	-190	70	-19	87	-21	-67
1.0	-189	4	2	174	-42	-134

5.5.2 Performance of transient component

In the previous study cases (1a and 1b), the PFS controller including only the static gain was applied. For the transient performance, the transition process was stable in both cases. However, in case study 1a, the oscillation provoked after the generation outage does not die out within the first 15 s. In case study 1b, over-regulation from the PFS controller at the first frequency dip resulted in stronger and longer power swings over the AC transmission systems. These concerns can be eliminated by including the transient component in the PFS controller. The study cases 1a and 1b are re-simulated with PFS controllers including the transient component and for α_{DC}=1.0.

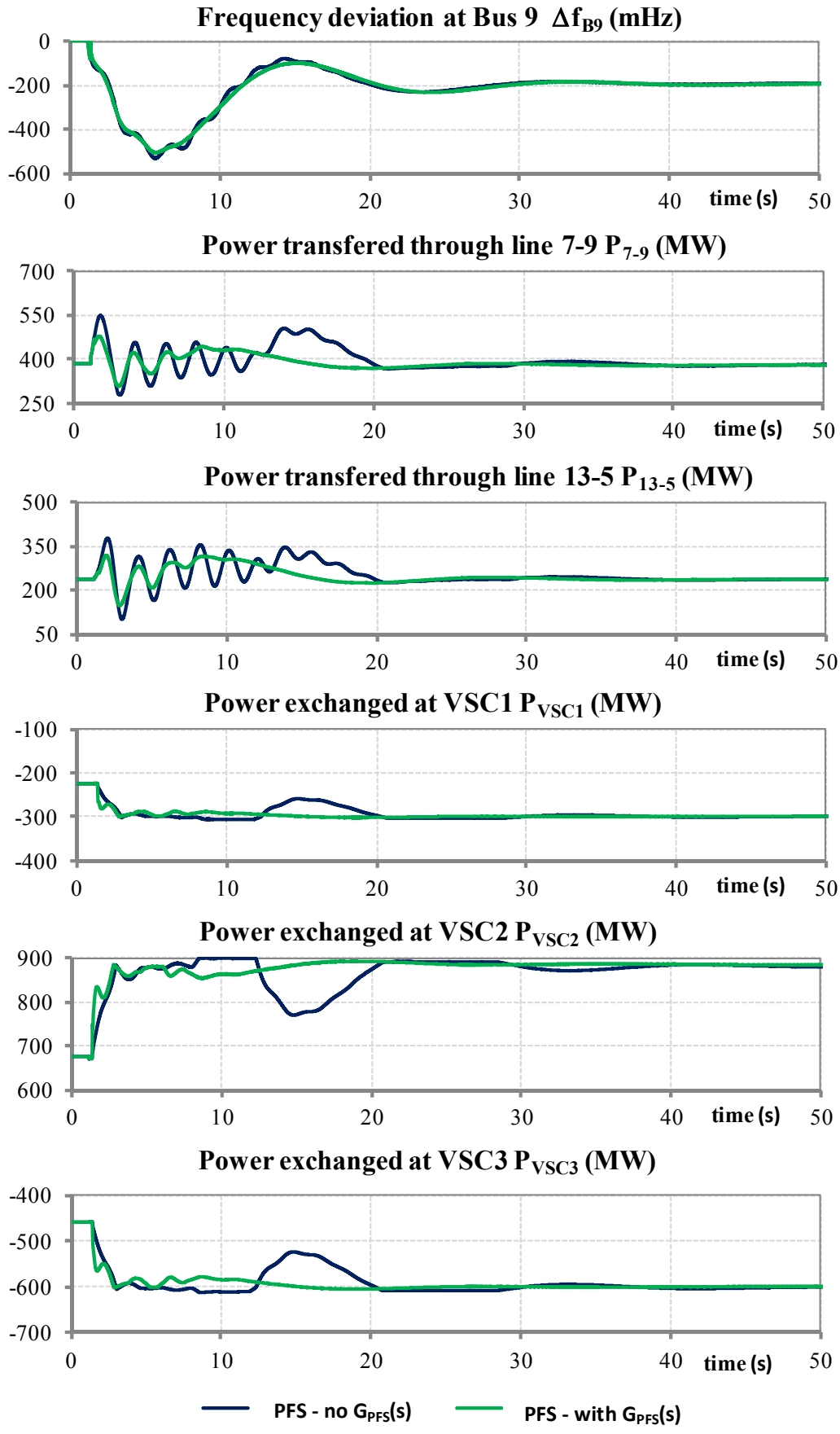

Figure 5.9: Case 2a: PFS controller with $G_{PFS}(s)$, α_{DC}=1.0, generation outage of 240 MW in area 2

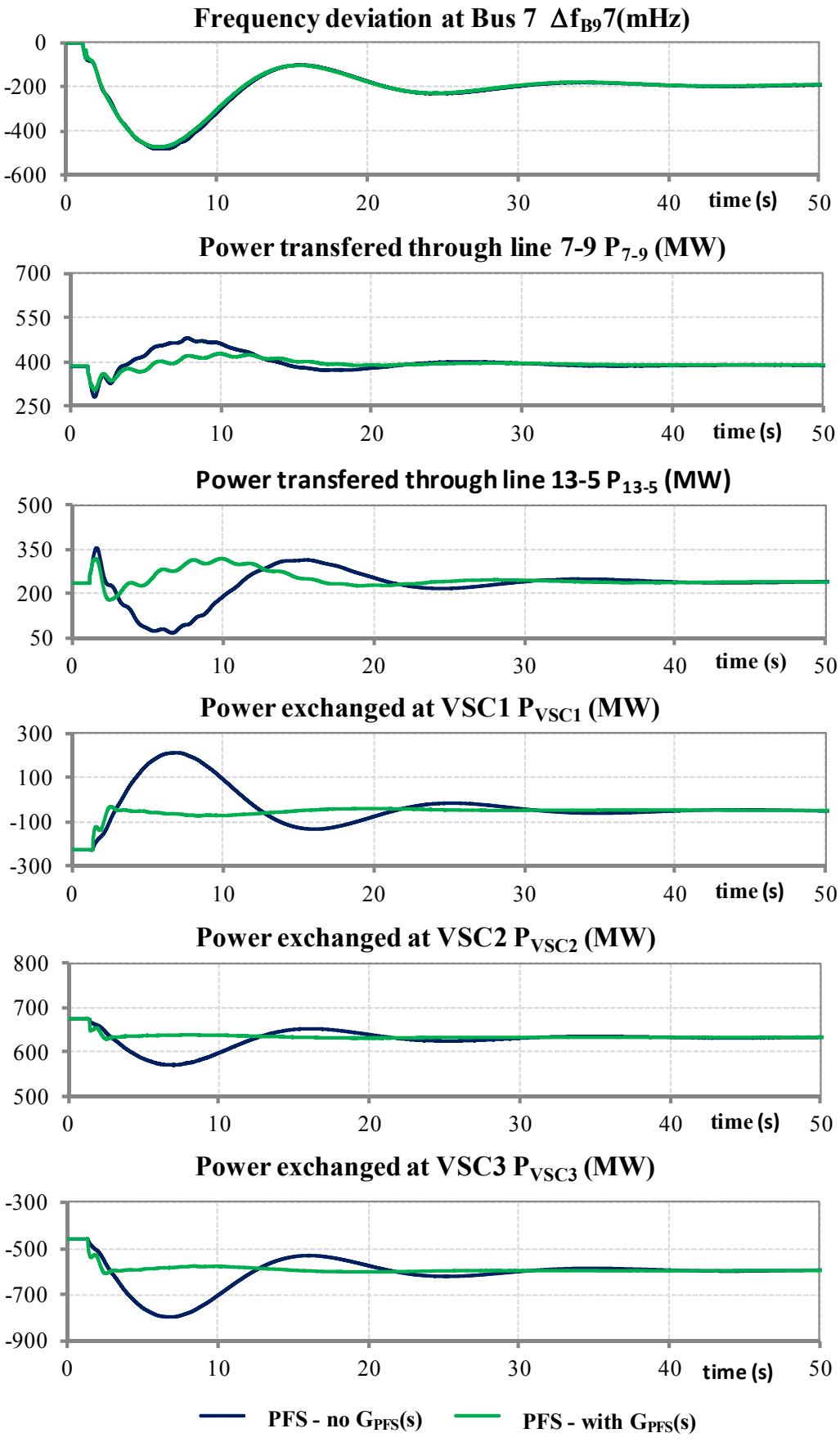

Figure 5.10: Case 2b: PFS controller with $G_{PFS}(s)$, α_{DC}=1.0, generation outage of 240 MW in area 1

Figure 5.9 and Figure 5.10 compare the simulation results of the study cases with and without the transient component. Based on the simulation results, it is obvious that the PFS controller with the proposed transient component can provide better damping of system oscillations in case 2a. It can also eliminate the large power oscillations due to the first frequency dip seen in case 1b. In summary, the transient component improves the dynamic performance of the proposed PFS controller.

5.5.3 Parameter sensitivity analysis

Thus far, only the outage of the biggest generation unit in one area is considered. This outage is actually used for estimating the setting parameters of the PFS controller. A logical extension would be to check the performance of the PFS controller under a smaller outage. So an outage of 200MVA unit loaded 160MW in area 2 is considered in this test.

Furthermore, there are practical concerns about the required system data (R_P, T_P, R_L, T_{AN}) for estimating the PFS parameters. These parameters may not be exactly estimated and they may vary as well during the transient process. To investigate the influence of the inaccuracy of the required system input data on the performance of PFS controller, two new tests are studied. Here, the setting PFS parameters are recalculated with ± 20% errors added onto the given data of R_P, T_P, R_L, T_{AN} in Table 5.2.

The simulation results of the three new tests with α_{DC}=1.0 are presented in Figure 5.11 and Table 5.5. If the provided data are accurate (0% error), the PFS controller keeps performing very well in this smaller outage. The additional powers transferred through HVAC are almost zero. The VSC-MTDC system transmits all additional transferred powers to the area 1. If there are ± 20% error associated with the provided data, the additional transferred powers that area 1 receives through VSC1 deviate 14% and 23%, respectively, from the scheduled one.

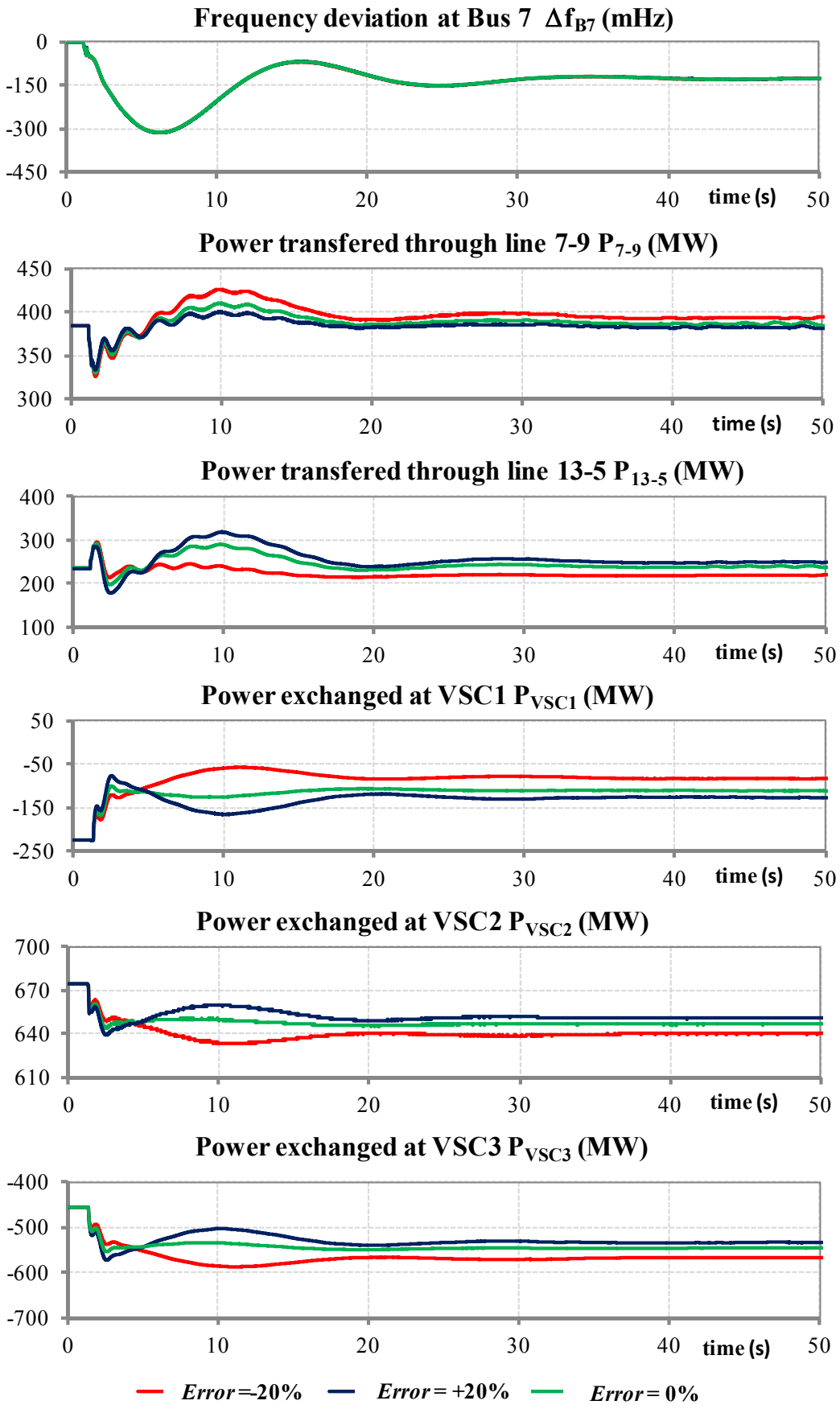

Figure 5.11: Case 3: PFS controller with $G_{PFS}(s)$, α_{DC}=1.0, generation outage of 160 MW in area 1

Table 5.5: Simulation result of case 3 at quasi-steady state

Data error (%)	Δf_{B9} (mHz)	HVAC		HVDC		
		$\Delta P_{13\text{-}4}$ (MW)	$\Delta P_{7\text{-}9}$ (MW)	ΔP_{VSC1} (MW)	ΔP_{VSC2} (MW)	ΔP_{VSC3} (MW)
0.0	-124	2	1	114	-28	-88
+20	-124	15	-3	98	-24	-76
-20	-126	-18	7	141	-34	-108

5.5.4 PFS control application on MTDC systems connecting isolated systems

The proposed PFS controller can as well be applied in case the VSC-MTDC system interconnects asynchronous areas. In this case, no AC parallel lines, the participation factor is fixed at 1.0. The frequency/generation outage transfer function is derived considering all power frequency characteristics of the asynchronous areas. The estimated gain using the proposed analytical method can result in a reasonable share of primary frequency control duty between areas according to their power-frequency characteristics. A global optimum for the quasi-steady-state frequency deviation can be achieved. By this way, the frequency deviations in all areas are equal to each other, and the whole system interconnected by the VSC-MTDC system acts similarly to the system interconnected by AC transmission lines in primary frequency control.

To demonstrate the above-mentioned statement, a new test system is created based on the present test system. Therefore, line 13-4 and line 7-9 are removed. The three areas are now interconnected only through the VSC-MTDC system. The 234 MW of LOAD4 and the 384 MW of LOAD10 are added to LOAD12 and LOAD6. The capacitors at the load centers are tuned to keep the bus voltages unchanged. An outage of a 300 MVA unit loaded at 240 MW in area 2 is considered. The simulation results are shown in Figure 5.12. It can be seen that the frequency deviations in all areas are equal to each other. The results prove that the proposed PFS controller can be applied also for VSC-MTDC system interconnecting asynchronous areas.

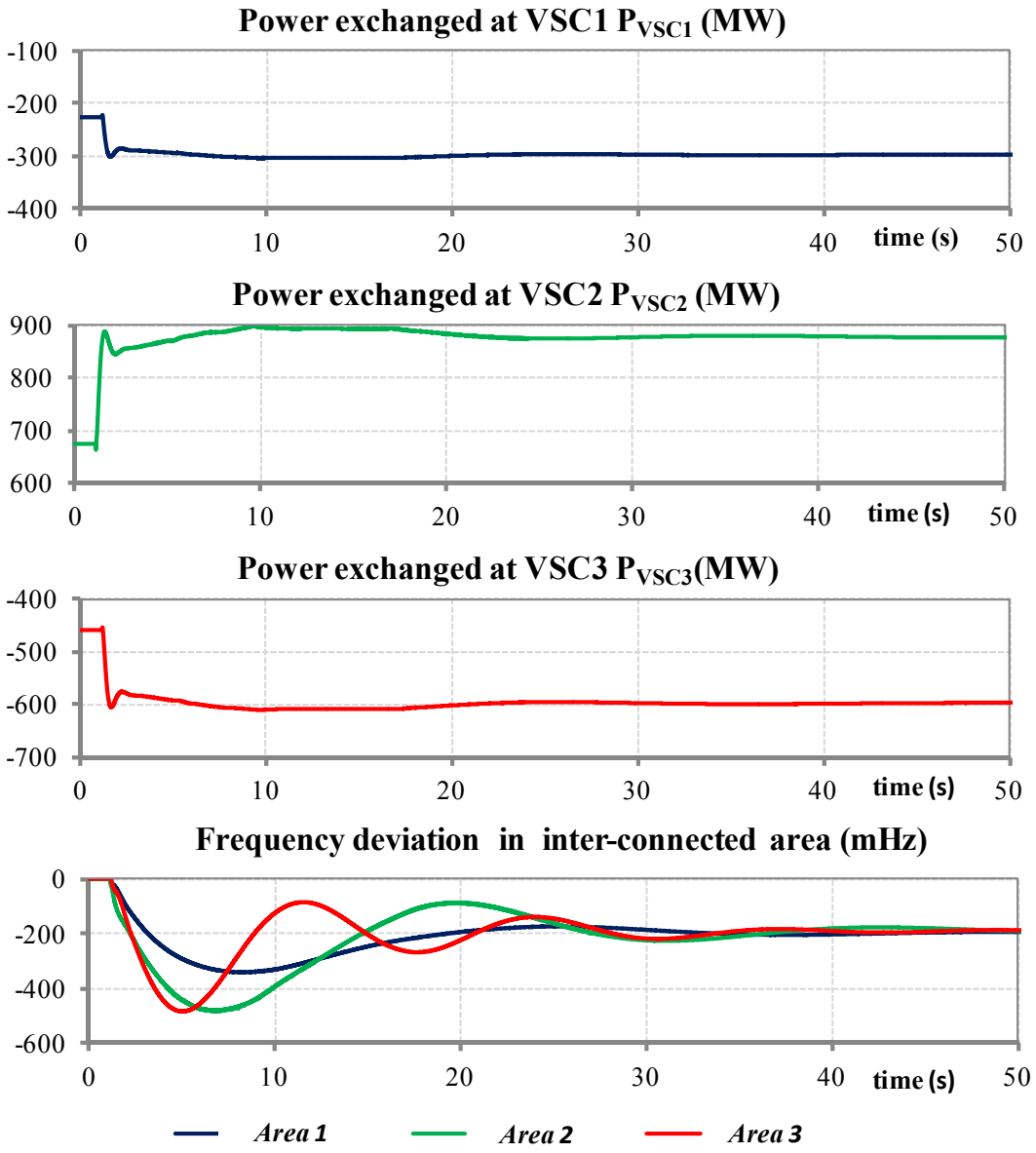

Figure 5.12: Case 4: VSC-MTDC connecting isolated areas, PFS controller with $G_{PFS}(s)$, α_{DC}=1.0, generation outage of 240MW in area 2

5.6 Summary

The proposed primary frequency support controller using feed-forward control technique including analytical gain estimation for VSC-MTDC systems has been tested in a typical transmission system. The results show that a VSC-MTDC system equipped with the proposed frequency controller shares the responsibility of transmitting power with the parallel HVAC lines. The PFS gain estimated by the proposed method assures an accurate schedule of exchanged power through VSC-MTDC system according to the residual transferable margin of the parallel HVAC lines. The problem related to circulations of exchanged power among the MTDC system and the AC lines due to unreasonable gain setting can be also avoided. The

transient component of the PFS controller is developed based on the inversion of the power-frequency characteristic of the AC power system, such that undesirable transient excursions of the frequency input are already compensated in the controller design. The PFS controller and the gain estimation method developed in this chapter can be applied not only for VSC-MTDC systems interconnecting synchronous areas within an AC power system, but also for VSC-MTDC systems interconnecting different asynchronous areas.

6 Fast voltage support controller

This chapter focuses on investigating the capability of MMC-VSC-MTDC systems to enhance the transient stability of AC systems by supporting the system voltage recovery after a three-phase short circuit in the power system. In this context, the MMC-VSC station control is equipped with a fast voltage support (FVS) controller on the reactive power control channel. The performance of the FVS controller is investigated together with the P&Q coordination control, which gives priority of using the converter current limitation for the reactive power control channel in case of high voltage drops at the point of common coupling (PCC). Furthermore, the investigation of the voltage support by the MMC-VSC-MTDC system during a line-to-line short circuit in the DC grid is also analyzed. The analysis refers only to MMC-VSC-MTDC systems with full-bridge sub-modules, which is able to block the fault current flowing into the DC grid [66]. At the same time, the full-bridge MMC can maintain the control function on the reactive power channel of the VSC station. In a special operational mode, called STATCOM mode, the full-bridge MMC-VSC control deactivates the active power channel to block the fault current but it maintains the control function on the reactive power channel.

6.1 FVS controller structure

The FVS controller acts on the reactive power control channel and has a slow reference tracking behavior. It is often implemented using a slow PI controller. In some cases, a voltage-drop compensation controller is also included. The voltage-drop compensation controller acts to compensate the voltage drop over the phase reactors due to active power exchanges with the AC systems. Normally, the reactive power control is a slow voltage support which, under a large and severe disturbance, provides a negligible support for the system voltage. The FVS controller is designed to support the system voltage in fast and large voltage fluctuation events, such as short-circuit events. The FVS controller utilizes the voltage support capability of the MMC-VSC-HVDC system to the AC power system in these cases. The controller block diagram is illustrated in Figure 6.1. Due to the washout filter, the FVS is only activated during the transient process by adding an additional reactive power request upon the given reactive power reference.

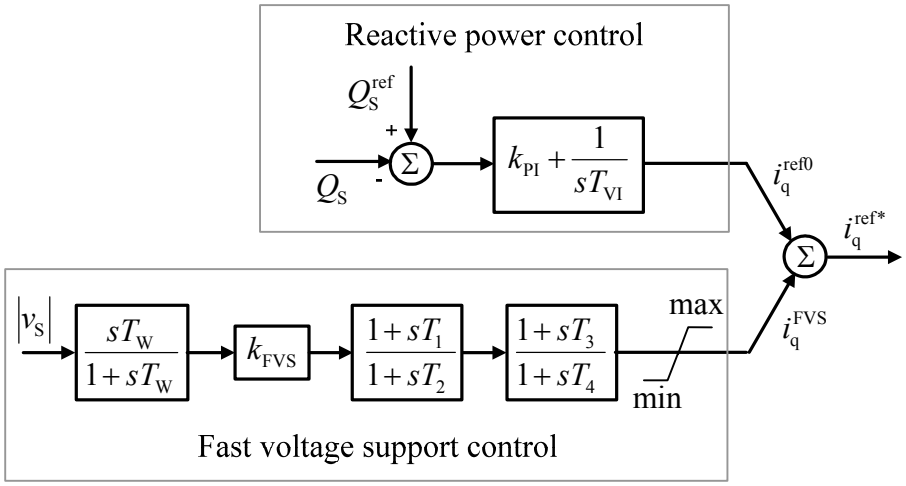

Figure 6.1: FVS controller structure

6.2 P&Q coordination control

As shown in Figure 6.2, there are several options to give the priority of using the converter current transfer capability between the active and reactive channels.

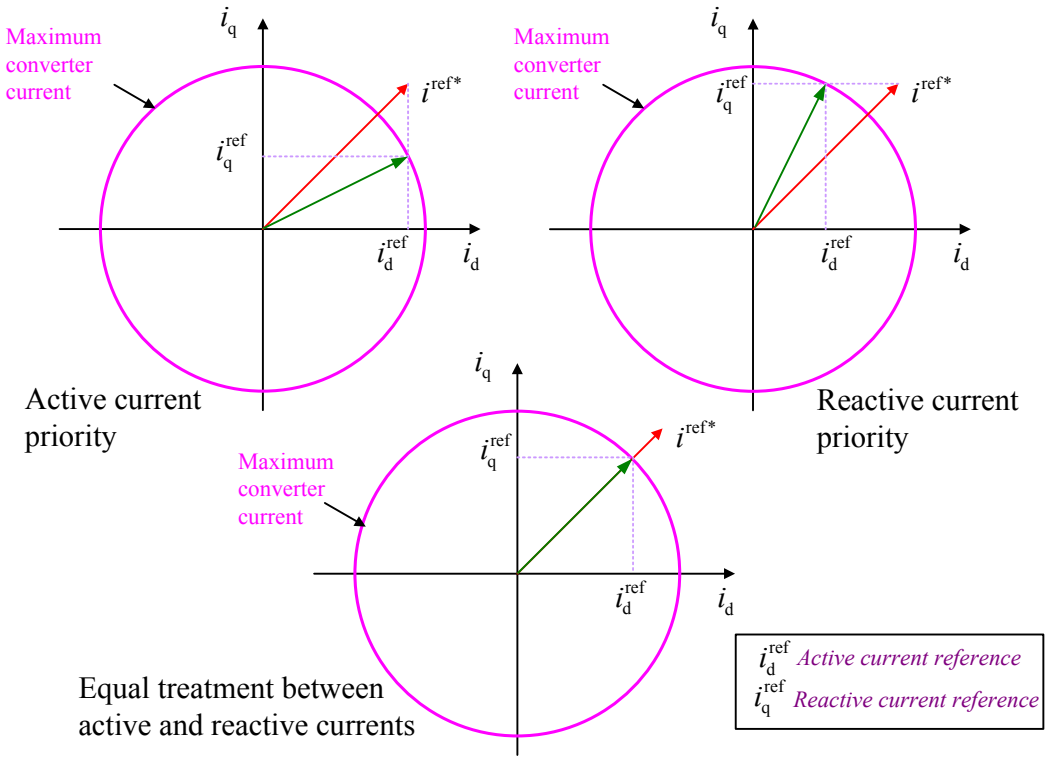

Figure 6.2: Limitation allocation options

In this figure, the red arrow denotes a reference current which is over the maximum converter current (i_{sclim}). The green arrow indicates the limited reference current associated with each priority option. In normal operation, the priority is often given to the active power channel to utilize the MTDC system for transferring active power. In severe under-voltage situations, i.e.

when the AC terminal voltage shrinks below 0.9 p.u, the voltage stability problem may arise. In most of these cases, the transient stability of power systems can be kept by additional injecting reactive power, usually at a cost of a moderate reduction of the transferred active power. In this case, the P&Q coordination control shifts the priority of using the converter current limitation from the active power control channel to the reactive power control channel. By doing so, more reactive power can be generated and injected into the power system at the PCC to support the system voltage, thus enhancing the transient stability of the power system. As a result, the P&Q coordination control improves the contribution of the FVS controller to the system voltage performance. The block diagram of the P&Q coordination control is illustrated in Figure 6.3.

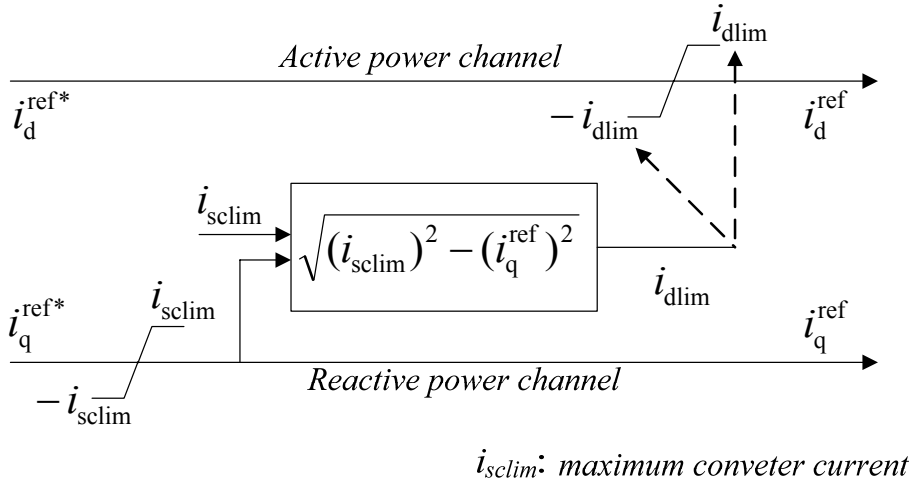

Figure 6.3: Structure of the P&Q Coordination Control

6.3 STATCOM mode

Following a pole-to-pole short circuit in DC grid there will be a high fault current flowing from the AC side of the MMC-VSC station into the DC grid. A MMC-VSC-MTDC system with full-bridge sub-modules (shown in Figure 6.4) is able to block this fault current. It can also maintain the VSC station control function on the reactive power channel. In this case, the MMC-VSC switches to function in STATCOM mode. Working in this mode, the MMC-VSC control deactivates the active power controller module to block the fault current. The reference current on the q-coordinate axis is then set only for covering the losses on connecting elements (transformer and phase reactor) between the PCC and the converter. The reference current on d-coordinate axis is still the output of the reactive power controller module. The operation of the MMC-VSC in STATCOM mode is investigated in the next section.

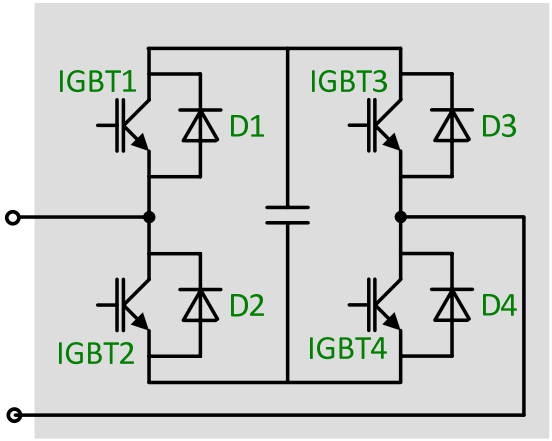

Figure 6.4: Full-bridge configuration

6.4 Test system

In general the system voltage performance highly depends on its load characteristics. Dynamic loads influence much the stability state of the system voltage. To highlight different system voltage problems, the test system used in Chapter 4 is modified in a suitable way. Two dynamic load scenarios are considered. In the first dynamic load scenario, 100% loads at Bus 7, Bus 13 and 80% load at Bus 9 are represented as constant impedance loads. The rest 20% load at Bus 9 is modeled by an asynchronous motor (ASM) model. This load scenario is employed to investigate the voltage stability problems associated with asynchronous motor reacceleration. Another dynamic load scenario, in which all loads are represented as constant power load (const. PQ load) model is introduced as well to study voltage stability problems linked with load angles of generators. The power-flow parameters of the system components can be found in Figure 6.5. All the PSS of the generators are active. POD controllers are not applied to the VSC-MTDC system. The parameters employed in the FVS controller can be found in Table 6.1.

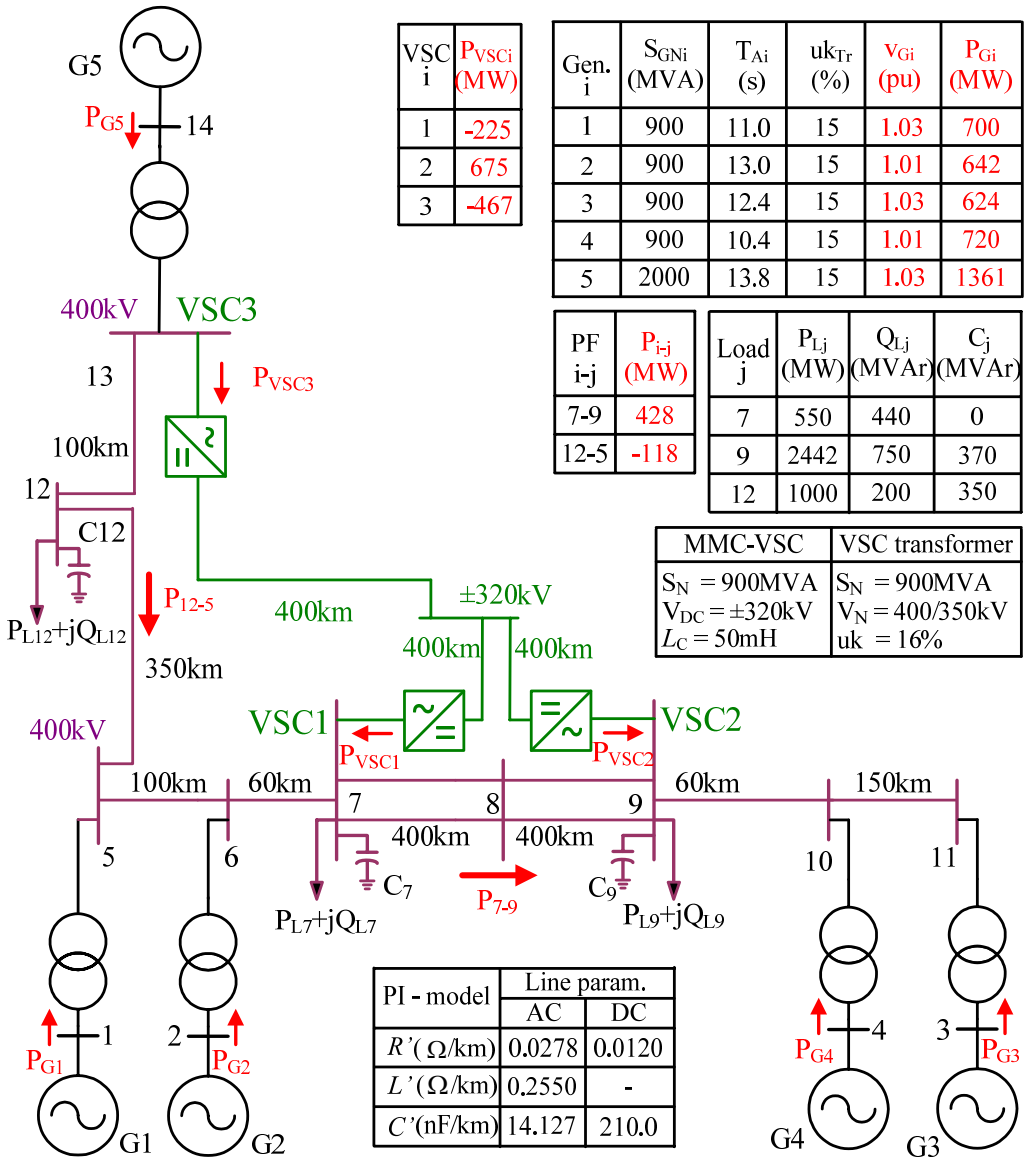

VSC i	P_{VSCi} (MW)
1	-225
2	675
3	-467

Gen. i	S_{GNi} (MVA)	T_{Ai} (s)	uk_{Tr} (%)	v_{Gi} (pu)	P_{Gi} (MW)
1	900	11.0	15	1.03	700
2	900	13.0	15	1.01	642
3	900	12.4	15	1.03	624
4	900	10.4	15	1.01	720
5	2000	13.8	15	1.03	1361

PF i-j	P_{i-j} (MW)
7-9	428
12-5	-118

Load j	P_{Lj} (MW)	Q_{Lj} (MVAr)	C_j (MVAr)
7	550	440	0
9	2442	750	370
12	1000	200	350

MMC-VSC	VSC transformer
S_N = 900MVA V_{DC} = ±320kV L_C = 50mH	S_N = 900MVA V_N = 400/350kV uk = 16%

PI - model	Line param.	
	AC	DC
R' (Ω/km)	0.0278	0.0120
L' (Ω/km)	0.2550	-
C' (nF/km)	14.127	210.0

Figure 6.5: Test system for voltage stability analysis

Table 6.1: Setting parameters for FVS controller

VSC station	Setting parameters for FVS controller					
	k_{FVS} (p.u.)	T_1 (s)	T_1 (s)	T_2 (s)	T_3 (s)	T_4 (s)
2&3	-20	30	0.5	3.5	1.2	2.5

6.5 Simulation results

In this study, three selected fault scenarios are investigated as defined in Table 6.2. The voltage magnitude at Bus 9, the reactive current at VSC 2 and 3, the speed of ASM and the load angle of generator G5 with and without the FVS controller are presented.

Table 6.2: Study cases for voltage stability analysis

No	*Fault Type*	*Fault Description*	*Load Model*	*Instability Related Issues*
1	AC fault	3PSC at Bus 9	Const. Z load and ASM load	ASM reacceleration
2	AC fault	3PSC at Bus 4	Const. P/Q load	Generator load angle
3	DC fault	Pole-to-pole SC in DC grid	Const. P/Q load	Generator load angle

In the first fault scenario, a three-phase short circuit (3PSC) with various fault durations is applied at Bus 9 of the test power system with the ASM load. After removing this AC fault, the asynchronous motor reaccelerates. The acceleration process requires reactive power from the power grid. The longer the fault duration, the more reactive power from asynchronous motor is required and the longer the voltage recovery process takes. In this study, without the FVS function equipped to the MMC-VSC control, the ASM load cannot successfully regain its pre-fault speed if the fault duration is longer than 100 ms. With the FVS controller, the MMC-VSC control increases the reactive power injection immediately to support the voltage recovery and, in turn, the ASM reacceleration. From the transient stability point of view, the FVS controller increases the transient stability of the power system. Without the FVS controller, the critical fault clearing time is 100 ms. With the FVS controller, the critical fault clearing time is increased to 180 ms. Figure 6.6 shows simulation results of the case with a fault duration of 150 ms.

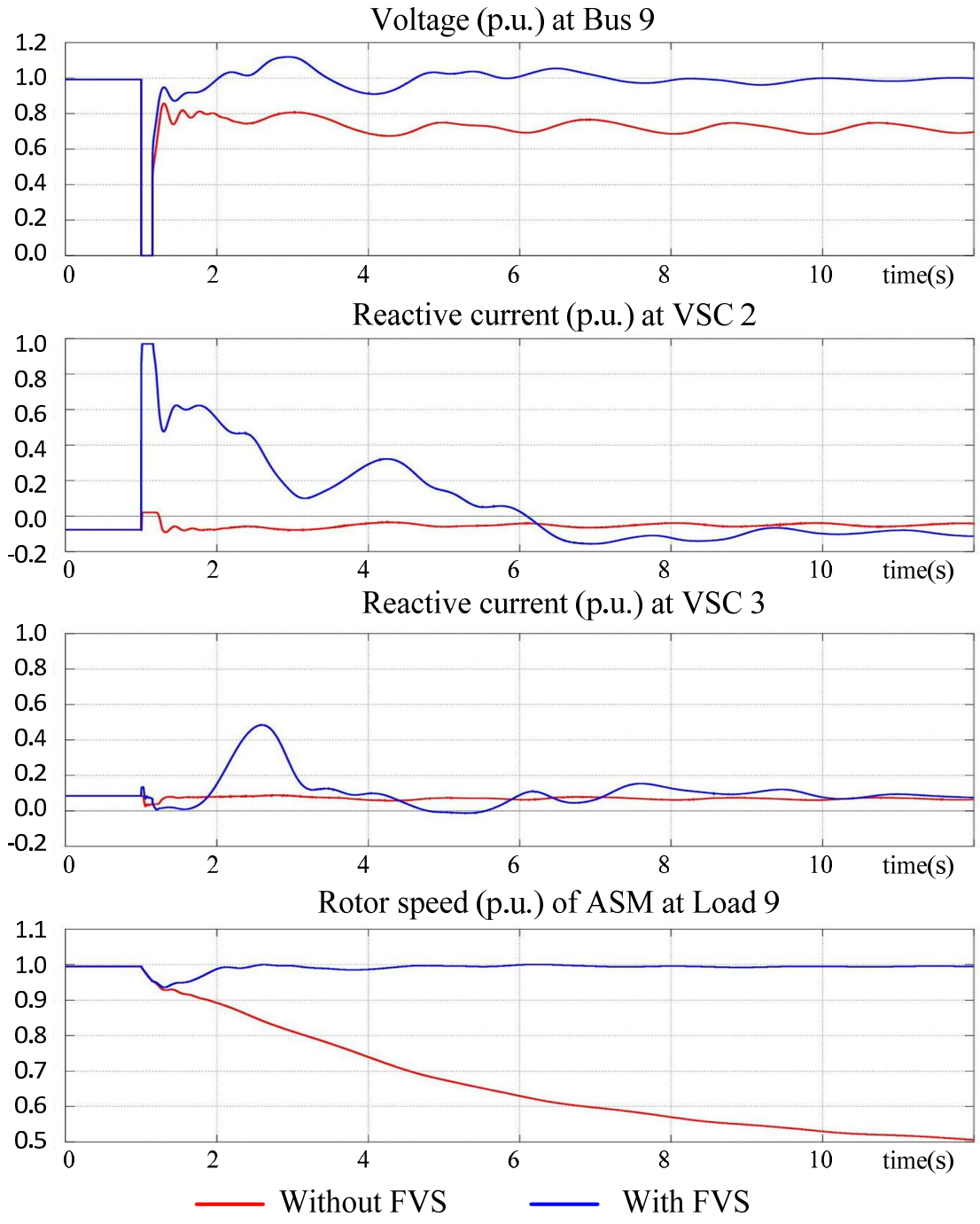

Figure 6.6: Simulation results of a 150-ms 3PSC applied at Bus 9

In the second fault scenario, a 3PSC with various fault durations is applied at Bus 4 of the test power system with const. PQ load. This AC fault excites the interacting power swing between generators. The power swing transmitted through AC transmission lines causes the voltage to drop. The longer the fault duration is, the stronger the power swing is. Together with the deeper voltage drop on the system buses, the generator load angles run further apart from each other. Without the FVS controller, load angle instability occurs in case the fault persists longer than 140 ms. The voltage support of the MMC-VSC control equipped with the FVS

controller helps the power system in keeping stable for faults lasting up to 210 ms. Figure 6.7 shows the simulation results of the case with a 150-ms fault duration.

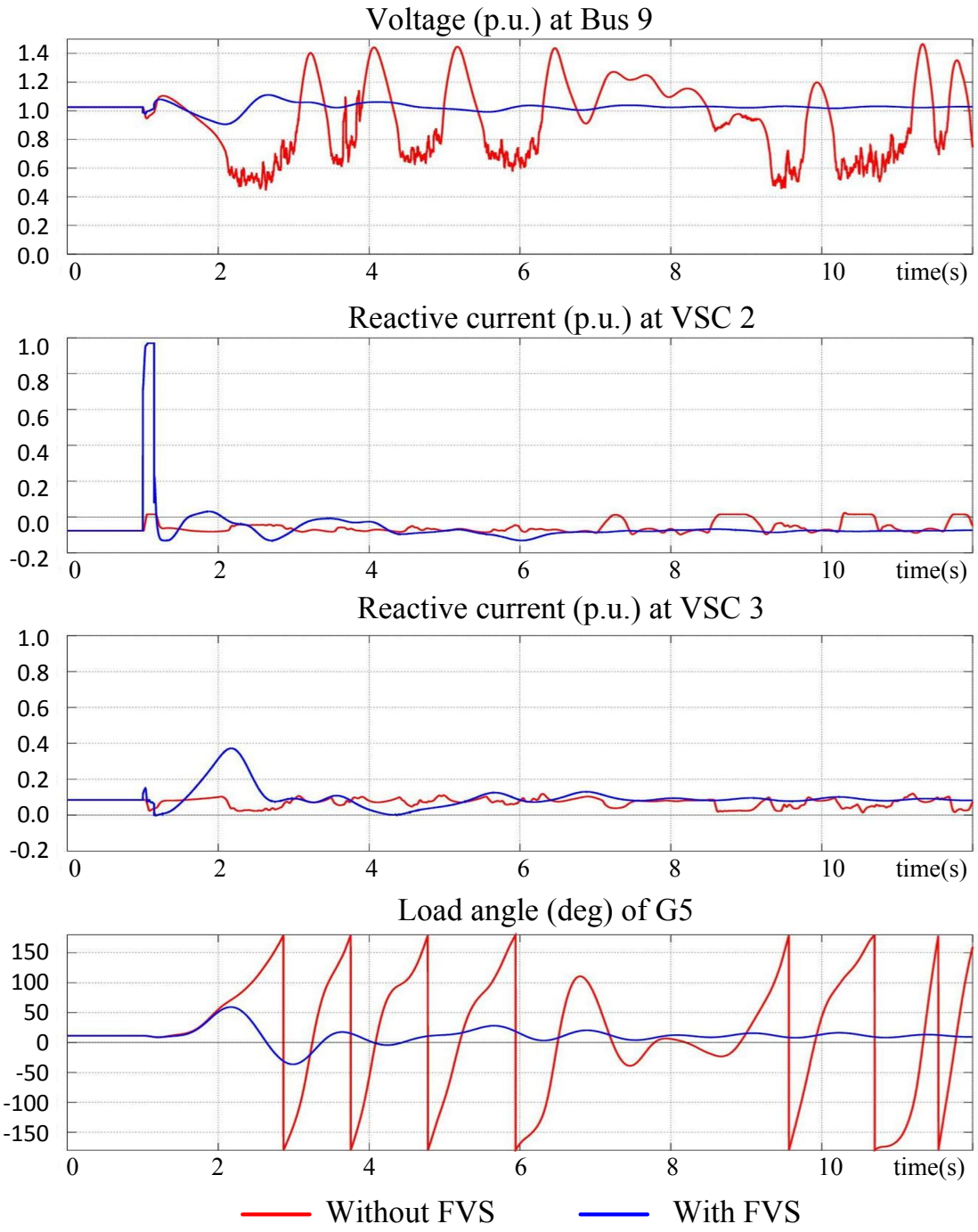

Figure 6.7: Simulation results of a 150-ms 3PSC applied at bus 4

In the third fault scenario, a permanent line-to-line short circuit is applied in the DC grid. During this DC fault, the MMC-VSC-HVDC system with the full-bridge sub-modules blocks the transferred active power. The pre-fault active power transferred through MMC-VSC-HVDC system is then redistributed among the AC transmission lines in the test system. As a consequence of the increased loading on the long AC transmission line, a deep voltage drop appears and causes a transient instability in the test power system. An out-of-step problem is

observed at the generator G5. With the FVS controller, the voltage support capability of the MMC-VSC-HVDC system operated in STATCOM mode is employed. The reactive power injection from the MMC-VSC stations is fast in time and large enough to prevent the generator out-of-step problem and maintain the stability of the test power system. The simulation results of this case are shown in Figure 6.8.

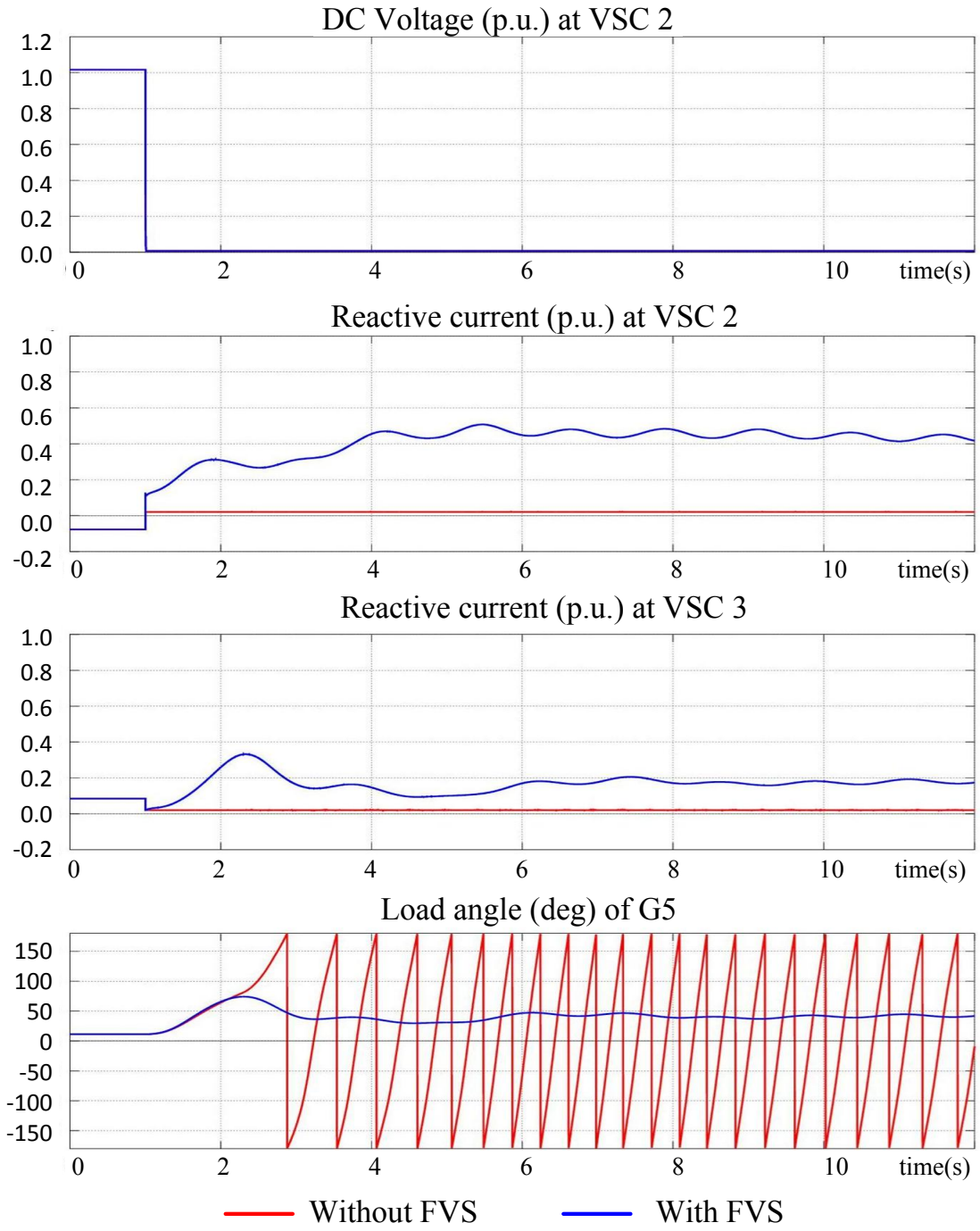

Figure 6.8: Simulation results of a line-to-line fault in DC grid

6.6 Summary

The simulation results clearly proved that the MMC-VSC-HVDC system is capable of enhancing the transient stability of power system effectively applying the FVS controllers. With the proposed FVS controller, the system voltage is strongly supported during fast and large voltage fluctuation events, such as short circuits in both the AC grid and in the DC grid. In addition to supporting the system voltage, the transient stability is also improved and the critical fault clearing time of the power system is extended.

7 Controller coordination

Thus far, this thesis has discussed the controllers individually to purely discover typical interaction between the controllers and the interconnected AC power systems. In fact, the controllers can be operated on the same channel at the same VSC station. In a severe disturbance, such as a three-phase short-circuit at the VSC terminal, various stability problems may arise at the same time. In this case, several controllers are activated at the same time. Therefore, there are inevitable interactions between them. Each controller will try to follow its designed target. Hence, the actions of the controllers may not be well coordinated. For the supplementary controllers working on the same modulation channel, one controller may act in a direction against the others. This uncoordinated reaction can reduce the effectiveness of each controller. If the controllers share the same control tendency, possible problems in sharing limited controlling bandwidths available at each VSC station may take place as well. The problems often occur in case of severe disturbances in which large amounts of current injections are highly requested from all controllers at the same time. In these cases, the priority in using the controlling bandwidth should be given to the appropriate controllers to avoid the unwanted interaction between the controllers. A study on the possible interaction between the controllers in a bigger test system is described into detail in this chapter. Through this study, possible problems are identified and several counter measures are proposed.

7.1 Test system

As a matter of a fact, the complex interactions between a large inter-connected AC network and a MMC-VSC-MTDC system, especially as a hybrid network (AC/DC coupling), cannot be fully perceived and considered in a simple test network. Therefore, the New-England test system (an IEEE test system with 10 generators, 39 buses) is used in this investigation. The New-England test system is reasonably sized to investigate the interaction of all previously developed controllers while allowing for an intuitive understanding of the power flow conditions.

The test system is described in Figure 7.1. In this test system, a three-terminal MMC-VSC-MTDC system is inserted between Bus 19, Bus 16 and Bus 22. The MTDC system takes part in transferring the power from two generation centers in area 1 and 3 into the system. This power is feed to the four load centers located at Bus 15, Bus 16, Bus 21, and Bus 24. It is assumed that 20% of each load center is induction-motor load. All other loads have a frequency-dependant load droop of 1%. Their reactive power demands are proportional to the

square of the magnitude of the bus voltage. The load-flow case and corresponding data are shown in the Figure 7.1. The dynamic data of the test network are given in the Appendix A.5. The MMC-VSC-MTDC system is equipped with the PFS and FVS controllers at all stations. The POD controllers will be equipped at both the VSC 1 and VSC 3 in two options: on either reactive power channel or on the active power channel. The setting parameters for the controllers can be found in the Appendix A.5.

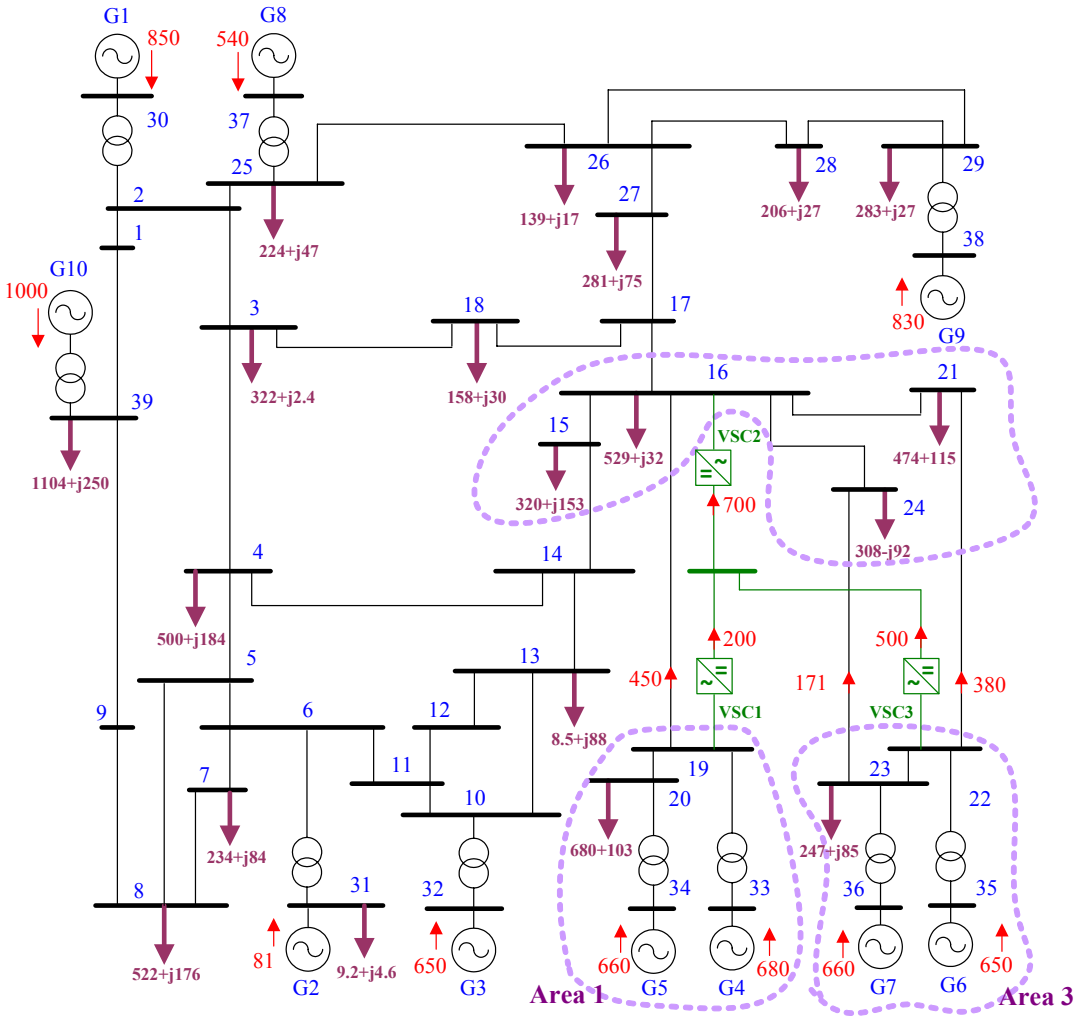

Figure 7.1: Test system for control coordination study

7.2 Small-signal stability analysis

Firstly, the small-signal stability analysis is conducted to see how the equipped controllers influence the stability of the power system. Table 7.1 shows the simulation results without the POD controllers. The table shows the three weakly-damped oscillations which can be highly influenced by the VSC-MTDC system. There are five cases investigated: No controller (none), with the FVS controllers at each VSC station (+FVS), with the FVS controllers plus

one of the PFS controllers (+PFS1, +PFS2, and PFS3). The simulation results show that the FVS and PFS controllers slightly alter the damping of the system oscillations. The controllers improve the damping of the third mode while slightly reducing the damping of the second mode.

Table 7.1: Results of modal analysis without POD controller

Mode			Relative damping (%)				
			No FVS	+FVS			
No	f(Hz)	Oscillating generator group	No PFS	No PFS	+PFS1	+PFS2	+PFS3
1	1.33	G4 vs rest	3.1	3.1	3.4	3.1	3.2
2	0.95	G4, G5 vs rest	4.4	3.8	3.7	3.9	6.1
3	0.58	G10 vs rest	5.1	6.8	7.2	6.2	6.6

The POD controllers are included in the MMC-VSC-MTDC control to improve the damping of the three modes. Two POD options are investigated. The first option (PODp) considers two three-channel POD controllers equipped in the active power modulation channel of the VSC 1 and 3. The second option (PODq) considers two three-channel POD controllers equipped in the reactive power modulation channel of the VSC 1 and 3. The setting parameters for the two POD options are tuned using the methodology described in section 4.2.2. The optimization considers all four possible operation cases: without and with one of the PFS controller in operation. The resulting setting parameters are given in the appendix A.5. The results of the small-signal stability analysis of the two POD options are shown in Figure 7.2.

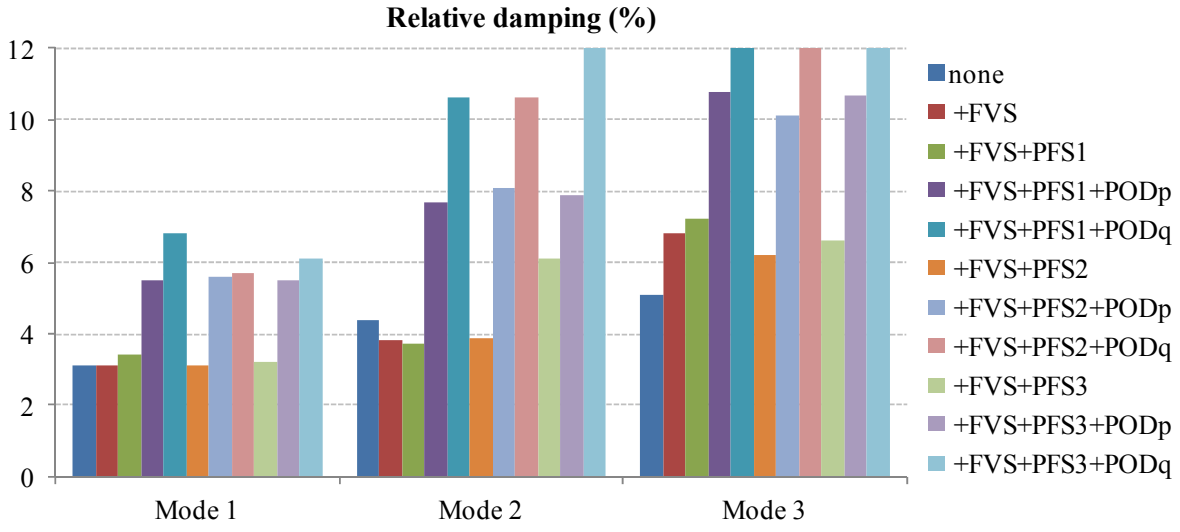

Figure 7.2: Relative damping results of control coordination study

Both POD options can contribute significantly to the improvement of the damping of all investigated modes. The small-signal stability results are confirmed by the time domain simulation shown in Figure 7.3 through the load angle of the generator G5. In this simulation, one 50-ms-three-phase short-circuit is applied at Bus 16.

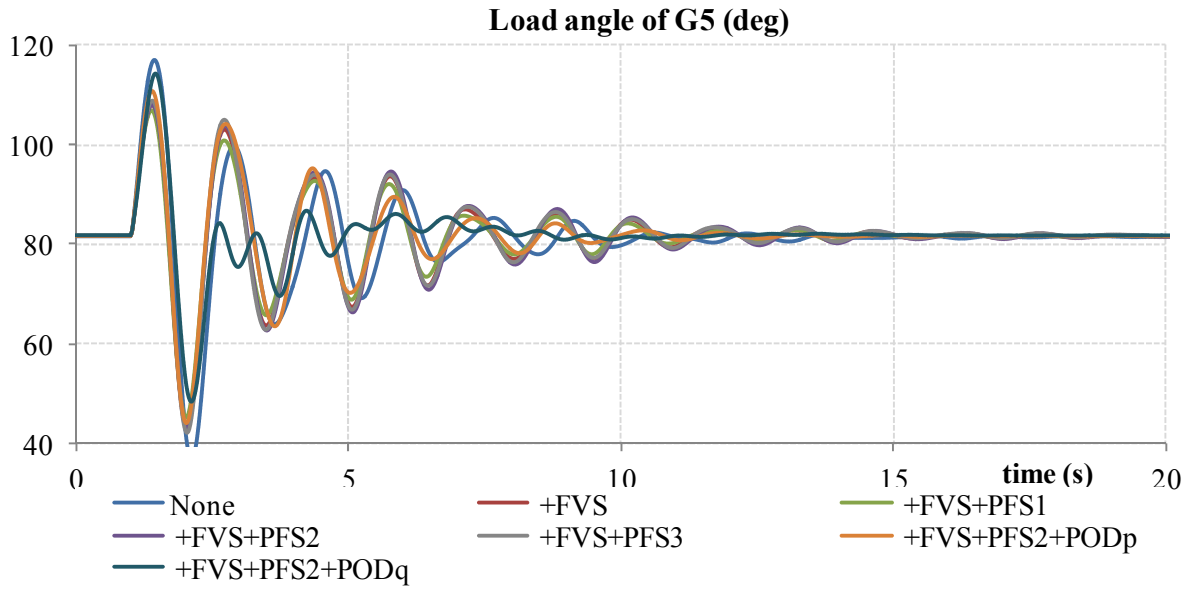

Figure 7.3: Time-domain simulation results of control coordination study

7.3 Large disturbance analysis

This analysis aims to check the interaction between controllers under large disturbances. Two fault scenarios listed in Table 7.2 are considered. In the first fault scenarios, the POD option on the reactive power modulation channel is considered. A 150-ms-three-phase short-circuit is applied at bus 16 in the load center areas where the motor loads are located. The induction motor acceleration after fault clearance may prolong the voltage recovery process. In this case, the FVS controllers intensively work on the reactive power modulation channel. In addition, the three-phase short-circuit also excite the involvement of the POD controller on this modulation channel. The interaction between the POD and FVS controllers on the Q channel can be seen through this fault case. In the second fault scenario, a 150-ms-three-phase short-circuit is applied at bus 22 followed by an outage of a 400 MVA generation unit in area 3. The fault ignites the operation of both the PFS and POD controllers on the P channel, therefore the interactions can be investigated. Figure 7.4 shows the location of the applied faults.

Table 7.2: Study cases for control coordination study

No	Fault description	Interaction related issues
1	150-ms 3PSC applied at bus 16	Interaction between the POD and FVS controllers on Q channel
2	150-ms 3PSC applied at bus 22, then trip a 400 MVA generator loading 264 MW in area 3	Interaction between the POD and PFS controllers on P channel

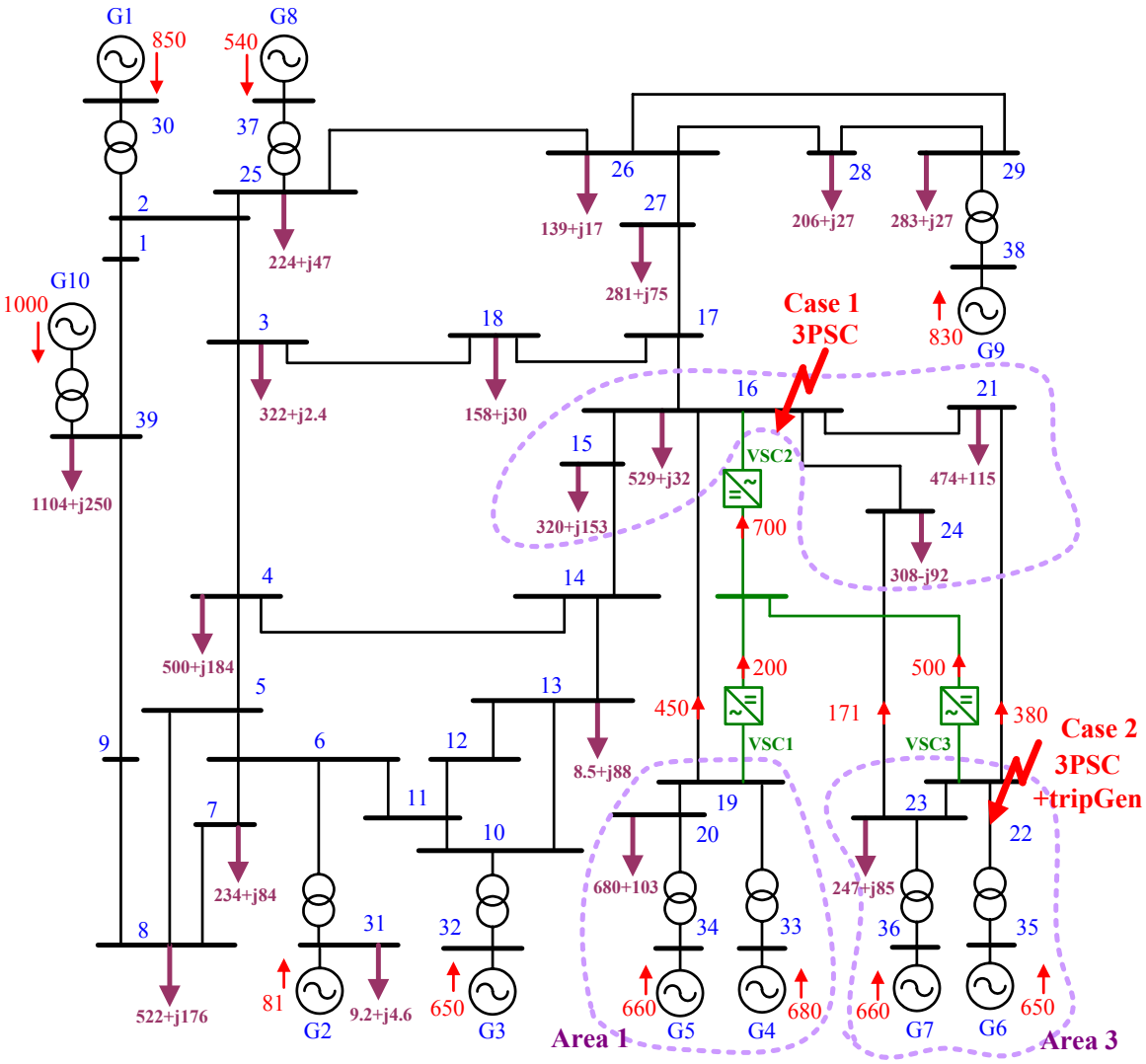

Figure 7.4: Fault scenarios considered for control coordination study

7.3.1 Control coordination on reactive power channel

The simulation results of the first fault scenario are displayed in Figure 7.5. The figure shows the voltage magnitude at the three VSC AC terminals, the reactive power outputs of the FVS and POD controllers, as well as the total reactive power measured at each VSC AC terminal.

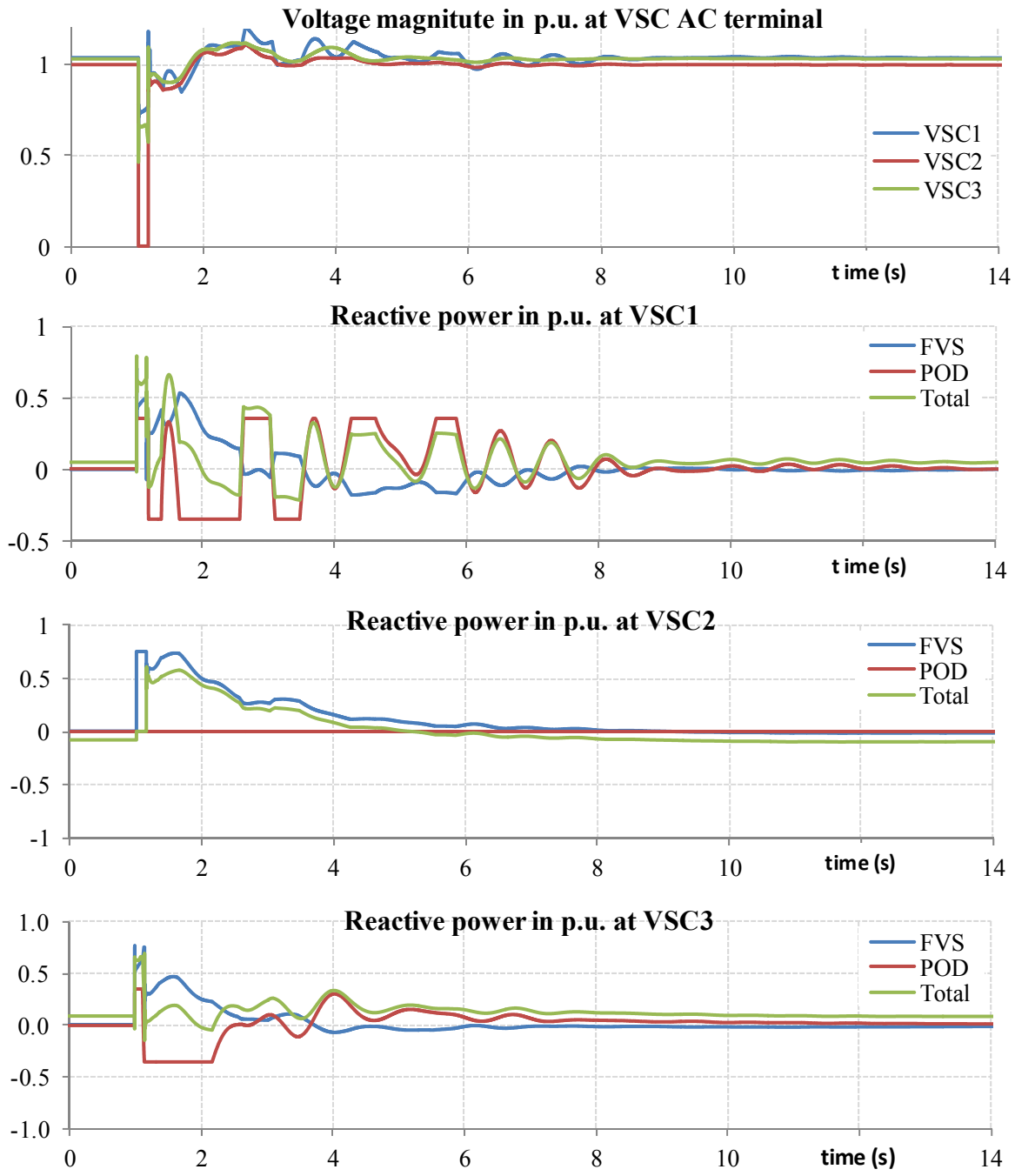

Figure 7.5: Simulation results of control coordination study on Q channel

It can be seen from the Figure 7.5 that the FVS controllers at VSC 1 and VSC 3 call for an immediate reactive power injection in the power system after the fault clearance. However, the POD controllers at VSC 1 and VSC 3 act against the FVS controllers, especially within the first 2 s after the fault clearance. The phenomenon results in a low reactive power injection which should be as high as possible to support the voltage recovery. In this thesis, the POD controller is proposed to be blocked after a certain time (here 1.5 s after removing the fault). The proposed blocking scheme is described in the Figure 7.6. The blocking scheme blocks the POD controller during the fault and 1.5 s after the fault clearance.

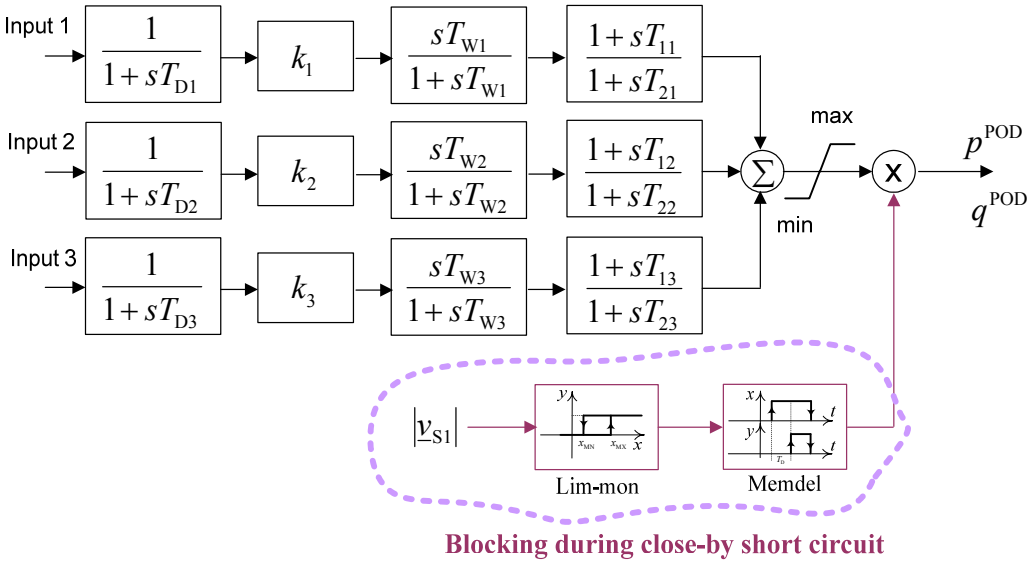

Figure 7.6: The proposed POD controller with additional blocking scheme

The simulation of the first fault scenario is repeated with the consideration of the blocking scheme. The results, given in Figure 7.7, show that the terminal voltages recover faster with the presence of the blocking scheme whereas the damping of the system oscillation stays nearly the same. The comparison between the resulting terminal voltages of the cases with and without the blocking scheme can be seen in Figure 7.8.

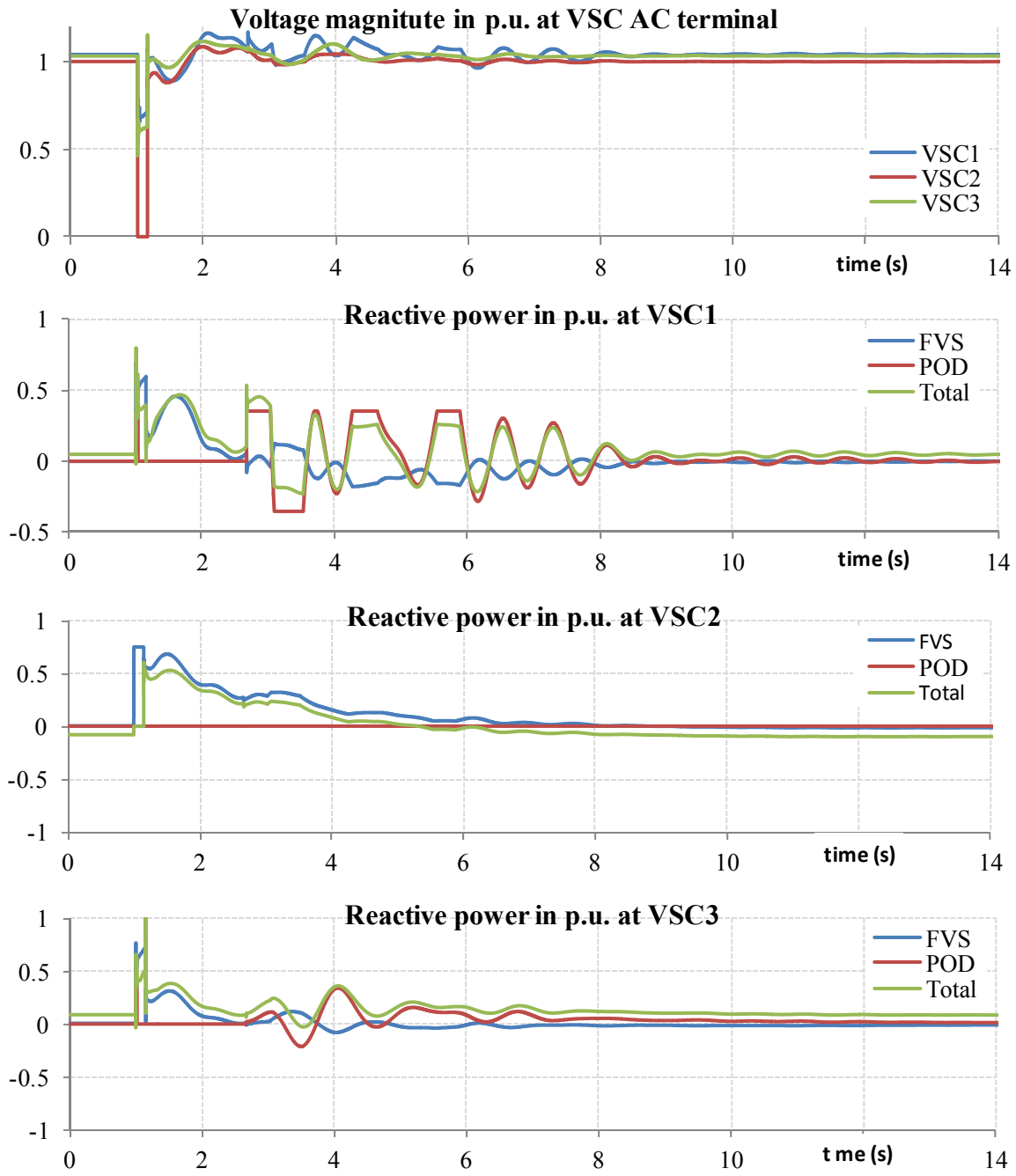

Figure 7.7: Simulation results of control coordination study on Q channel with the blocking scheme

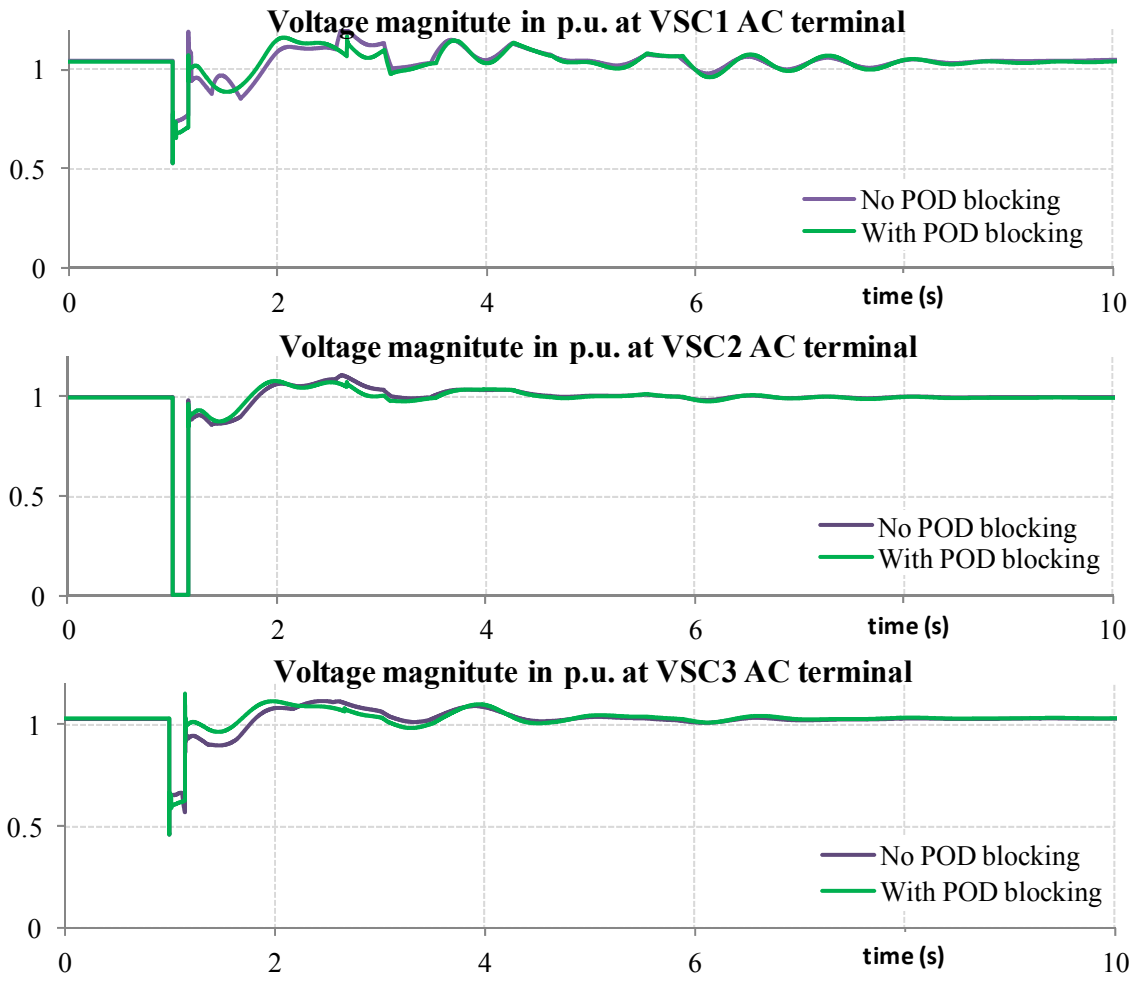

Figure 7.8: Comparison of the resulted terminal voltages of cases with and without the blocking scheme

7.3.2 Control coordination on active power channel

The simulation results of the second fault scenario are depicted in Figure 7.9. It shows the frequency deviation at the three VSC AC terminals, the active power outputs of the PFS and POD controllers, as well as the total active power measured at each VSC AC terminal.

It can be seen from the Figure 7.9 that both the PFS and POD controllers are excited by the fault scenario. The POD controllers intensively act right after the fault initiation. But this action decreases dramatically after 5 s. In contrast, the PFS controller slowly increases its control output. Therefore, there is no significant counter interaction between the controllers, but a well coordinated action resulted from the nature of the two controllers. Therefore, no counter measure is needed to ensure the coordination in this case.

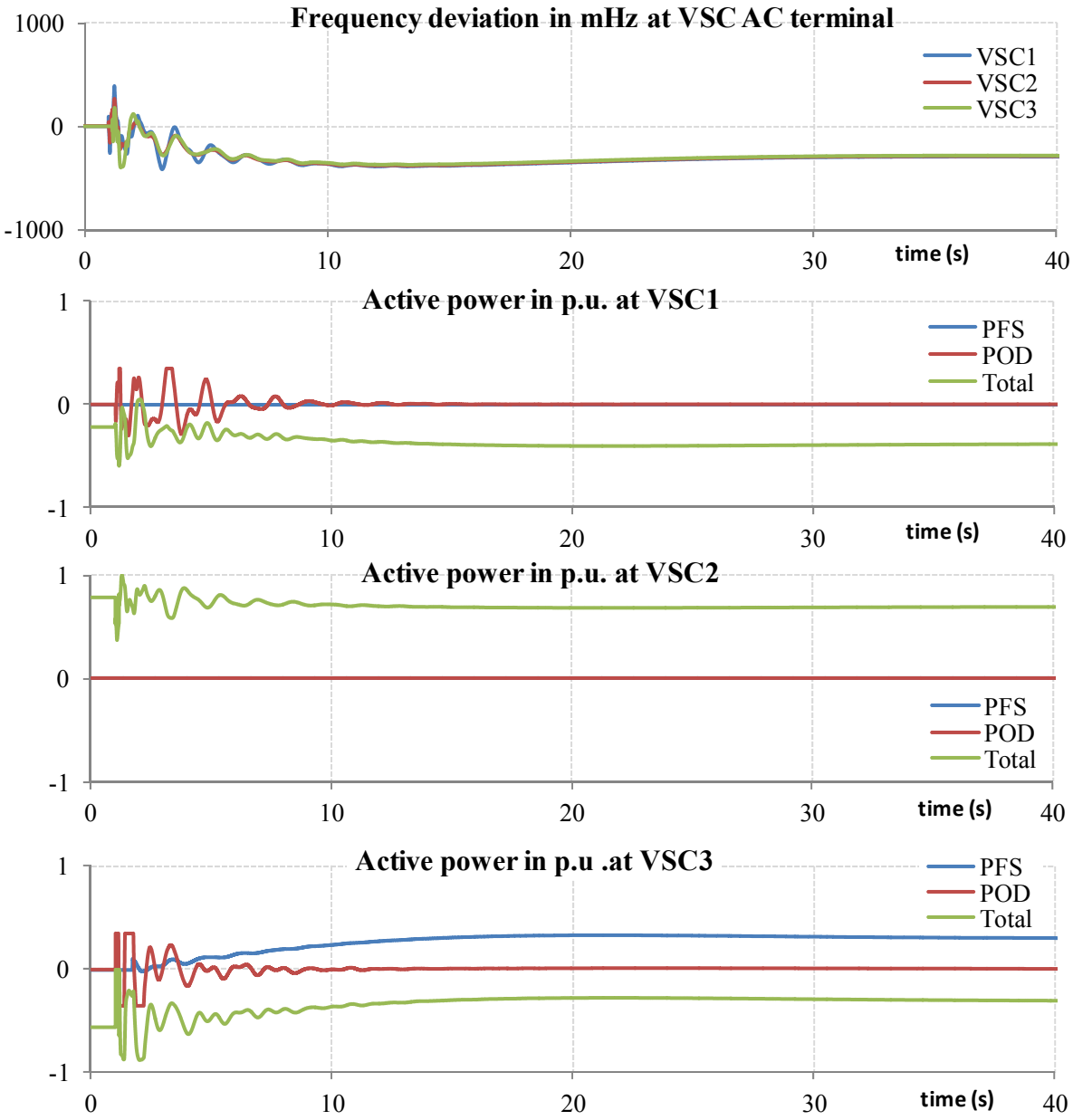

Figure 7.9: Simulation results of control coordination study on P channel

8 Conclusions and future work

8.1 Conclusions

This thesis has presented the investigations of utilizing MMC-VSC-MTDC systems to enhance the dynamic performance of AC power systems. In this context, several supplementary controllers are equipped into the standard VSC station controller to exploit its fast response and independent control of the active and reactive powers in MTDC systems. These functional controllers are the Power Oscillation Damping (POD) controller, the Primary Frequency Support (PFS) controller, and the Fast Voltage Support (FVS) controller. Each controller is designed to enhance one stability aspect of the power system.

The POD controller improves the damping of oscillations in the AC power systems. The PFS control is used to support the primary frequency control following outages of large generation units. The FVS controller is used to support the recovery of the positive sequence voltage after incidents of short circuits whereas the NSV controller is used to reduce the negative sequence voltage, thus improving the phase voltage symmetry during unbalanced faults.

First of all, the supplementary controllers were individually studied considering several influence factors to explore their main features. The controllers design and appropriate methodologies for selecting their setting parameters have been proposed. Analytical methods together with time-domain simulations were employed to validate the proposed methodologies. At last, possible interactions between the investigated supplementary controllers which may influence their effectiveness were investigated.

To facilitate the study, which focuses on slow dynamic stability phenomena and the performance analyses of the MMC-VSC-HVDC system within a large-scale AC power system, a generic RMS model for the MMC-VSC-MTDC system was developed based on an existing averaged EMT model. The developed model in this thesis, using voltage and current sources with suitable adaptations to include the MMC-VSC control structure with two separate DC and the AC control parts, is similar to the existing RMS model developed for conventional VSC-HVDC systems. A linearized model of the MMC-VSC-HVDC for low-frequency electromechanical oscillation studies was also proposed. Both models were validated in both time-domain simulation and frequency-domain analysis in a typical high-voltage transmission network.

The investigation of the capabilities of a MMC-VSC-MTDC system in improving the damping of the system oscillations were conducted in both the modal analysis and the time

domain simulation. In this framework, a PSS-based POD controller was incorporated to the MMC-VSC-MTDC system control. Established approaches for input/output selection and parameter optimization were applied. The study results revealed the considerable capability to incorporate POD controller into both channels of the MMC-VSC-MTDC system to enhance damping of inter-area oscillations. The damping capability on Q channel is observed to possess a greater potential to improve the damping of inter-area oscillations in several circumstances, such as when the system load is excessively sensitive to voltage; or when the VSC station is located near load centers. However, the damping capability on Q channel reduces with reduction of the voltage-dependent level of the system loads. This is not the case for the damping support capability of the POD option on the P channel. In case of high loading on active power channel, the POD controller on Q channel can be more effective than on the P channel. Furthermore, the use of global inputs has been investigated with the consideration of communication delay. The applied optimization method ensures good performance of the POD controller including global inputs with various communication delays.

For the primary frequency control analysis, the primary frequency support controller is equipped to the VSC-MTDC control to enable the VSC-MTDC system to share the responsibility of transmitting the exchanged power with parallel HVAC lines. The PFS controller proposed in this thesis is designed using the feed-forward control technique including an analytical method to estimate the controller gain. The PFS gain estimated by the proposed method assures an accurate schedule of exchanged power through the VSC-MTDC system according to the residual transferable margin of the parallel HVAC lines. The problem related to circulation of exchanged power among MTDC system and AC lines due to unreasonable gain settings can be also avoided. The transient component of the PFS controller was developed based on the inversion of the power-frequency characteristic of AC power system, such that undesirable transient excursions of the frequency input are already compensated in the controller design. The PFS controller and the gain estimation method developed in this thesis can be applied not only for the VSC-MTDC system interconnected synchronous areas within an AC power system, but also for the VSC-MTDC system interconnecting different asynchronous areas.

The capability of the MMC-VSC-HVDC in enhancing the transient stability of the power system was investigated with the consideration of the fast voltage support controller. The simulation results prove that the system voltage is strongly supported in fast and large voltage fluctuation events, such as short circuit events in both AC grid and DC grid. By supporting

the system voltage through the FVS controller, the transient stability is improved and the critical fault clearing time of the power system is extended. The coordination between the FVS controller and the P&Q coordination control increases the contribution of the FVS controller to the system voltage performance.

In the last chapter of the thesis, a study on the interaction between the supplementary controllers in a larger test system was conducted. The results of the small-signal stability analysis reveal that the FVS and PFS controllers slightly alter the damping of the system oscillations. The setting parameters, defined by the proposed analytical method, were appropriate for the controllers in the small-signal stability extent. The POD controllers tuning using the proposed methodology can significantly improve the damping of the system oscillations.

The large disturbance analysis shows that there are possible incorporated interactions between the FVS controller and the POD controller on the reactive power channel within the first few second after removing a closed-by fault. This phenomenon results in a low reactive power injection which should be as high as possible to support the voltage recovery. The counter measure proposed in this thesis is to block the POD controller during this time. The results showed that the terminal voltages recovered faster with the presence of the blocking scheme whereas the damping of the system oscillation stays nearly the same.

In contrast to the interaction on the reactive power channel, there is no significant counter interaction between the PFS and POD controllers on the active power channel, but a well coordinated action resulted from the nature of the two controllers. Both the PFS and POD controllers are excited by the fault scenario. The POD controllers act intensively right after the fault initiation. The action of the POD controllers decrease dramatically after 5 s while the PFS controller slowly increases its control output. No counter measure was then needed in this case.

8.2 Future work

The following is a list of possible future work to thoroughly validate the effects of the MMC-VSC-HVDC system on AC power systems due to the supplementary controller whose designs and the methodologies for setting the parameters were proposed in this thesis:

1. Further investigation on the capability of the POD controllers on the active and reactive power channels with consideration of high penetration of electronic- based loads, reduced inertia AC systems and reduced short-circuit power systems.

2. Verify the operation of the activating scheme proposed for the PFS controllers in different power system configurations under the consideration of further fault cases.
3. Validate the methodologies for setting parameters of the controllers proposed in this thesis in a realistic power system where the various interactions between the controllers can be seen, since these cannot be observed from the small test system. Furthermore, the complexity of the stability problem in the system might excite the difficulties in applying the method.

Another possible future work constitute developing a RMS model which can directly use all setting parameters from an existing EMT model, without the need for parameter tuning. This model might include controlled voltage sources on both the AC and DC sides.

References

[1] S. Cole, R. Belmans, “Transmission of Bulk Power: The History and Applications of Voltage-Source Converter High-Voltage Direct Current Systems,” IEEE Ind. Electron. Mag (2009).

[2] D. Retzmann, "Global Prospects of Bulk Power Transmission", in Utility Automation & Engineering T&D, United States of America, 2008.

[3] J. Dorn, H. Huang, D. Retzmann, “A new Multilevel Voltage-Sourced Converter Topology for HVDC Applications,” CIGRE, August 24-29, 2008, Paris, pp. 1-8.

[4] K. Friedrich, “Modern HVDC PLUS application of VSC in Modular-Multilevel Converter topology,” in Proc. IEEE International Symposium on Industrial Electronics, 2010, pp. 3807 – 3810.

[5] H.-J. Knaak, “Modular-Multilevel converters and HVDC/FACTS: A success story,” in Proc. 14th European Conference on Power Electronics and Applications, 2011, pp. 1 - 6.

[6] N. Ahmed, S. Norrga, H.-P. Nee, A. Haider, D. Van Hertem, Zhang Lidong L. Harnefors, “HVDC SuperGrids with Modular-Multilevel converters — The power transmission backbone of the future,” International Multi-Conference on Systems, Sygnals&Devices (2012), p. 1 – 7.

[7] Feng Wang, L. Bertling, T. Le, A. Mannikoff, A. Bergman, “ An Overview Introduction of VSC-HVDC: State-of-art and Potential Applications in Electric Power Systems,” Cigrè International Symposium, Bologna, Italy, Sept. 2011

[8] D. Van Hertem and M. Ghandhari, “Multi-terminal VSC-HVDC for the European supergrid: Obstacles,” Renewable and Sustainable Energy Reviews, vol. 14, no. 9, pp. 3156–3163, Dec. 2010.

[9] S. Cole, T. K. Vrana, O. B. Fosso, J.-B. Curtis, A.-M. Denis, C.-C. Liu, "A European Supergrid: Present State and Future Challenges," in Proceedings of the 17th PSCC 2011, Stockholm, Sweden, 22-26 August 2011.

[10] de Oliveira, A.L.P.; Tiburcio, C.E.; Lemes, M.N.; Retzmann, D., “Prospects of Voltage-Sourced Converters (VSC) applications in DC transmission systems”, 2010 IEEE/PES Transmission and Distribution Conference and Exposition: Latin America (T&D-LA)(2010) p. 491 – 495, ISBN 978-1-4577-0488-8, Journal Paper (English).

[11] U. N. Gnanarathna, A. M. Gole, and R. P. Jayasinghe, “Efficient modeling of Modular-Multilevel HVDC converters (MMC) on electromagnetic transient simulation programs,” IEEE Trans. Power Del., vol. 26, no. 1, pp. 316–324, Jan. 2011.

[12] E.N. Abildgaard, M. Molinas, "Modelling and Control of the Modular-Multilevel Converter (MMC)," Energy Procedia, vol. 20 issue (Technoport 2012 - Sharing Possibilities and 2nd Renewable Energy Research Conference), RERC2012, pp. 227-236.

[13] J. Peralta, H. Saad, S. Dennetière, J. Mahseredjian, and S. Nguefeu, “Detailed and averaged models for a 401-level MMC-HVDC system,” IEEE Trans. Power Del., vol. 27, no. 3, pp. 1501–1508, Jul. 2012.

[14] S. Cole, J. Beerten, R. Belmans, "Generalized Dynamic VSC MTDC Model for Power System Stability Studies," IEEE Transactions on Power Systems, vol. 25, issue 3, pp. 1655 – 1662, 2010.

[15] B. Berggren, R. Majumder, N. Johansson, "A Generic VSC HVDC Primary Control Structure Suitable for Stability Studies," 2013 EPRI HVDC and FACTS Conference, August 2013, Palo Alto, USA, pp. 1-8.

[16] W. Yao, J. Wen, S. Cheng, H. He, "Modeling and simulation of VSC-HVDC with dynamic phasors," 2008 Third International Conference on Electric Utility Deregulation and Restructuring and Power Technologies, 2008, vol., p.1416 – 1421.

[17] Zheng Chao, Zhou Xiaoxin, Li Ruomei, "Dynamic Modeling and Transient Simulation for VSC based HVDC in Multi-Machine System," 2006 International Conference on Power System Technology, 2006, pp. 1 – 7.

[18] S. P. Teeuwsen, "Simplified dynamic model of a voltage-sourced converter with Modular-Multilevel converter design," in Proc. IEEE Power Eng. Soc., Power Syst. Conf. Expo., Seattle, WA, Mar. 2009, pp. 1–6.

[19] M. Saeedifard and R. Iravani, "Dynamic performance of a Modular-Multilevel back-to-back HVDC system," IEEE Trans. Power Del., vol. 25, no. 4, pp. 2903–2912, Oct. 2010.

[20] M. P. Kazmierkowski and L. Malesani, "Current control techniques for three-phase voltage-source PWM converters: A survey," IEEE Trans. Ind. Electron., vol. 45, no. 5, pp. 691–703, Oct. 1998.

[21] J. Svensson, "Voltage angle control of a Voltage-Source inverter, application to a grid-connected wind turbine," in Proc. 6th Eur. Conf. Power Electronics and Applications, Sevilla, Spain, 1995, Vol. 3, pp. 539-544.

[22] H. Saad, J. Peralta, S. Dennetiere, J. Mahseredjian, J. Jatskevich, J.A. Martinez, A. Davoudi, M. Saeedifard, V. Sood, X. Wang, J. Cano, A. Mehrizi-Sani, "Dynamic Averaged and Simplified Models for MMC-Based HVDC Transmission Systems," IEEE Transactions on Power Delivery, vol. 28, issue 3, pp. 1723 – 1730, 2013.

[23] C. Dierckxsens, K. Srivastava, M. Reza, S. Cole, J. Beerten, R. Belmans, "A distributed dc voltage control method for VSC MTDC systems," Electric Power Systems Research, 2012, vol. 82 issue 1, pp. 54-58.

[24] D. Jovcic, L.A. Lamont, L. Xu, "VSC transmission model for analytical studies," 2003 IEEE Power Engineering Society General Meeting, 2003, vol. 3, pp. 1737 – 1742.

[25] C. Karawita, U.D. Annakkage, "Multi-Infeed HVDC Interaction Studies Using Small-Signal Stability Assessment," IEEE Transactions on Power Delivery, vol. 24, issue 2, pp. 910 – 918, 2009.

[26] G.O. Kalcon, G.P. Adam, O. Anaya-Lara, S. Lo, K. Uhlen, "Small-Signal Stability Analysis of Multi-Terminal VSC-Based dc Transmission Systems," IEEE Transactions on Power Systems, vol. 27, issue 4, pp. 1818 – 1830, 2012.

[27] I. Erlich, G. K. Venayagamoorthy, and W. Nakawiro, "A mean-variance optimization algorithm", in WCCI IEEE World Congress on Computational Intelligence Barcelona, Spain, 2010, pp. 1–6.

[28] I. Erlich, "MVMO background," 2010 [Online]. Available: http://www.uni-due.de/mvmo/

[29] I. Erlich, W. Nakawiro, and M. Martinez, "Optimal Dispatch of Reactive Sources in Wind Farms," in IEEE PES General Meeting Detroit, USA, 2011, pp. 1–7.

[30] C. Cepeda, J. L. Rueda, and I. Erlich, "Identification of Dynamic Equivalents based on Heuristic Optimization for Smart Grid Applications", in WCCI IEEE World Congress on Computational Intelligence Brisbane, Australia, 2012, pp. 1–8.

[31] P. Kundur, "Power system stability and control," New York: McGraw-Hill, 1994, ch. 12, pp. 835.

[32] S. Singh, “Prony Toolbox,” Sep. 2003 [Online]. Available: http://www.mathworks.com/matlabcentral/fileexchange/3955-prony-toolbox

[33] P. Kundur, M. Klein, G.J. Rogers, M.S. Zywno, "Application of power system stabilizers for enhancement of overall system stability," IEEE Transactions on Power Systems, vol. 4, issue 2, pp. 614 – 626, 1989.

[34] A.R. Messina, J.M. Ramirez, J.M. Canedo C., "An investigation on the use of power system stabilizers for damping inter-area oscillations in longitudinal power systems," IEEE Transactions on Power Systems, vol. 13, issue 2, pp. 552 – 559, 1998.

[35] Yuanzhang Sun, Lixin Wang, Guojie Li, Jin Lin, “A review on analysis and control of small-signal stability of power systems with large scale integration of wind power,” 2010 International Conference on Power System Technology, 2010, pp. 1 – 6.

[36] N. Noroozian, G. Andersson, "Damping of inter-area and local modes by use of controllable components," IEEE Transactions on Power Delivery, vol. 10, issue 4, pp. 2007 – 2012, 1995.

[37] A.R. Messina, O. Begovich M, M. Nayebzadeh, "Analytical investigation of the use of static VAR compensators to aid damping of inter-area oscillations," International Journal of Electrical Power and Energy Systems, vol. 21 issue 3, pp. 199-210.

[38] N. Mithulananthan, C. A. Ca˜nizares, J. Reeve and G. J. Rogers, “Comparison of PSS, SVC and STATCOM Controllers for Damping Power System Oscillations,” IEEE Transactions on Power Systems Vol. 18 No. 2, May 2003, pp 786-792.

[39] T. Smed, G. Andersson, "Utilising HVDC to damp power oscillations," IEEE Transactions on Power Delivery, vol. 8, issue 2, pp. 620 - 627. ,1993

[40] S. P. Teeuwsen, R. Rössel, “Dynamic performance of the 1000 MW BritNed HVDC interconnector project,” in Proc. 2010 IEEE PES General Meeting, Minneapolis, USA, July 25-29, 2010.

[41] N.T. Trinh, I. Erlich, S. P. Teeuwsen, "Methods for Utilization of MMC-VSC-HVDC for Power Oscillation Damping," IEEE PES General Meeting, Washington DC, 27-31 July 2014.

[42] Chunye Li, Sheng Li, Fuchun Han, Jingfu Shang, Ermin Qiao, "A VSC-HVDC fuzzy controller to damp oscillation of AC/DC power system," 2008 IEEE International Conference on Sustainable Energy Technologies, pp.816 – 819.

[43] H.F. Latorre, M. Ghandhari, L. Soder, "Use of local and remote information in POD control of a VSC-HVdc," 2009 IEEE Bucharest PowerTech, vol., pp.1 - 6

[44] R. Preece, A.M. Almutairi, O. Marjanovic, J.V. Milanovic, "Damping of electromechanical oscillations by VSC-HVDC active power modulation with supplementary wams based modal LQG controller," 2011 IEEE Power and Energy Society General Meeting, 2011, pp. 1 – 7.

[45] A. Heniche, I. Kamwa, "Assessment of Two Methods to Select Wide-Area Signals for Power System Damping Control," IEEE Transactions on Power Systems, vol. 23, issue 2, pp. 572 – 581, 2008.

[46] H. M. A. Hamdan and A. M. A. Hamdan, “On the coupling measures between modes and state variables and subsynchronous resonance,” Elect. Power Syst. Res., vol. 13, pp. 165–171, 1987.

[47] B. Naduvathuparambil, M. C. Valenti, and A. Feliachi, “Communication delays in wide area measurement systems, ” in Proc. 34th Southeast. Symp. Syst. Theory, 2002, pp. 118 – 122.

[48] J. Lam, “Model reduction of delay systems using Pade approximants,” Int. J. Control, vol. 57, pp. 377–391, 1993.

[49] M. Klein, G.J. Rogers, S. Moorty, P. Kundur, "Analytical investigation of factors influencing power system stabilizers performance," IEEE Transactions on Energy Conversion, vol. 7, issue 3, p. 382 – 390, 1991.

[50] R. Preece, J.V. Milanovic, A.M. Almutairi, O. Marjanovic, "Damping of inter-area oscillations in mixed AC/DC networks using WAMS based supplementary controller," IEEE Transactions on Power Systems, 2013, vol. 28, issue 2, pp. 1160 – 1169.

[51] A. Fuchs, M., Imhof, T. Demiray, M. Morari, "Stabilization of Large Power Systems Using VSC–HVDC and Model Predictive Control," IEEE Transactions on Power Delivery, vol. 29, issue 1, p. 480 – 488.

[52] L. Zeni, R. Eriksson, S. Goumalatsos, M. Altin, P. Sorensen, A. Hansen, P. Kjaer, B. Hesselbaek, "Power Oscillation Damping from VSC-HVDC connected Offshore Wind Power Plants," IEEE Transactions on Power Delivery, published on30 April 2015 (DOI: 10.1109/TPWRD.2015.2427878)

[53] J. Chand, “Auxiliary power controls on the Nelson river HVDC scheme,” IEEE Trans. Power Syst., vol. 7, no. 1, pp. 398–402, Feb. 1992.

[54] M. Davies, A. Kolz, M. Kuhn, D. Monkhouse, and J. Strauss, “Latest control and protection innovations applied to the basslink HVDC interconnector,” in Proc. Inst. Elect. Eng., 8th Int. Conf. ac dc Power Transmission, Mar. 2006, pp. 30–35.

[55] N. Rostamkolai, C. Wegner, R. Piwko, H. Elahi, M. Eitzmann, G. Garzi, and pp. Tietz, “Control design of Santo Tome’ back-to-back HVDC link,” IEEE Trans. Power Syst., vol. 8, no. 3, pp. 1250–1256, Aug. 1993.

[56] C.E. Spallarossa, Y. Pipelzadeh, T.C. Green, "Influence of frequency-droop supplementary control on disturbance propagation through VSC HVDC links," IEEE Power & Energy Society General Meeting, 2013, pp. 1 – 5.

[57] O.A. Giddani, Abdelaziz Y.M. Abbas, Grain P. Adam, O. Anaya-Lara, K.L. Lo, "Multi-task control for VSC–HVDC power and frequency control," International Journal of Electrical Power and Energy Systems, vol. 53, pp. 684-690.

[58] Cuiqing Du, E. Agneholm, G. Olsson, "Use of VSC-HVDC for Industrial Systems Having Onsite Generation With Frequency Control," IEEE Transactions on Power Delivery, vol.23, p.2233 – 2240.

[59] E. Rakhshani, A. Luna, K. Rouzbehi, P. Rodriguez, I. Etxeberria-Otadui, "Effect of VSC-HVDC on load frequency control in multi-area power system," IEEE Energy Conversion Congress and Exposition (ECCE), 2012, pp. 4432–4436.

[60] T.M. Haileselassie, K. Uhlen, "Primary frequency control of remote grids connected by multi-terminal HVDC," IEEE PES General Meeting, 2010, pp. 1 – 6.

[61] A. Sarlette, J. Dai, Y. Phulpin, D. Ernst, "Cooperative frequency control with a multi-terminal high-voltage dc network," Automatica, vol. 48 issue 12, pp. 3128-3134.

[62] A. J. Wood, B. F. Wollenberg, “Power Generation, Operation and Control, ” 2nd Edition, John Wiley & Sons, 2012.

[63] E. J. Adam, J. L Marchetti, “Designing and Tuning Robust Feedforward Controllers,” Computers & Chemical Engineering, 2004, Vol. 28. – Iss. 9. – pp. 1899–1911.

[64] P. C. Badavas, “Feedforward Methods for Process Control Systems,” Chemical Engineering, 1984, pp. 103–108.

[65] A. Morattab, Q. Shafiee, H. Bevrani, "Decentralized Model Predictive load-frequency control for deregulated power systems in a tough situation," 2011 IEEE Trondheim PowerTech, 2011, pp. 1 – 5.

[66] J. Dorn, H. Gambach, J. Strauss, T. Westerweller, and J. Alligan, "Trans Bay Cable – A Breakthrough of VSC Multilevel Converters in HVDC Transmission," in Proc. Cigre Colloquium on HVDC and Power Electronic Systems Including overhead line and insulated cable application, San Francisco, 2012, B4-8.

Publications

[1] N.T. Trinh, I. Erlich, S. P. Teeuwsen, "Methods for Utilization of MMC-VSC-HVDC for Power Oscillation Damping," *IEEE PES General Meeting, Washington DC*, 27-31 July 2014.

[2] N.T. Trinh, I. Erlich, M. Zeller, K. Wuerflinger, "Enhancement of Grid Transient Stability Using MMC-VSC-HVDC Control," *IET International Conference on AC and DC Power Transmission, Birmingham UK*, 09-12 Feb. 2015., p. 1 – 6.

[3] N.T. Trinh, I. Erlich, M. Zeller, K. Wuerflinger, "Generic Model of MMC-VSC-HVDC for Interaction Study with AC Power System," IEEE Transactions on Power Systems, vol. 31, no. 1, pp. 27-34, Jan. 2016

[4] N.T. Trinh, I. Erlich, M. Zeller, K. Wuerflinger, "Utilization of Embedded VSC-MTDC System for Supporting Power Flow during Primary Frequency Control," *19th Power Systems Computation Conference (PSCC 2016), Genoa (Italy)*, 20-24 June 2016.

[5] N.T. Trinh, I. Erlich, "Analytical Investigation of Factors Influencing Controllability of MMC-VSC-HVDC on Inter-area and Local Oscillations in Interconnected Power Systems," *IEEE PES General Meeting, Boston, MA*, 17-21 July 2016.

Appendixes

A.1 Proposed RMS equivalent model

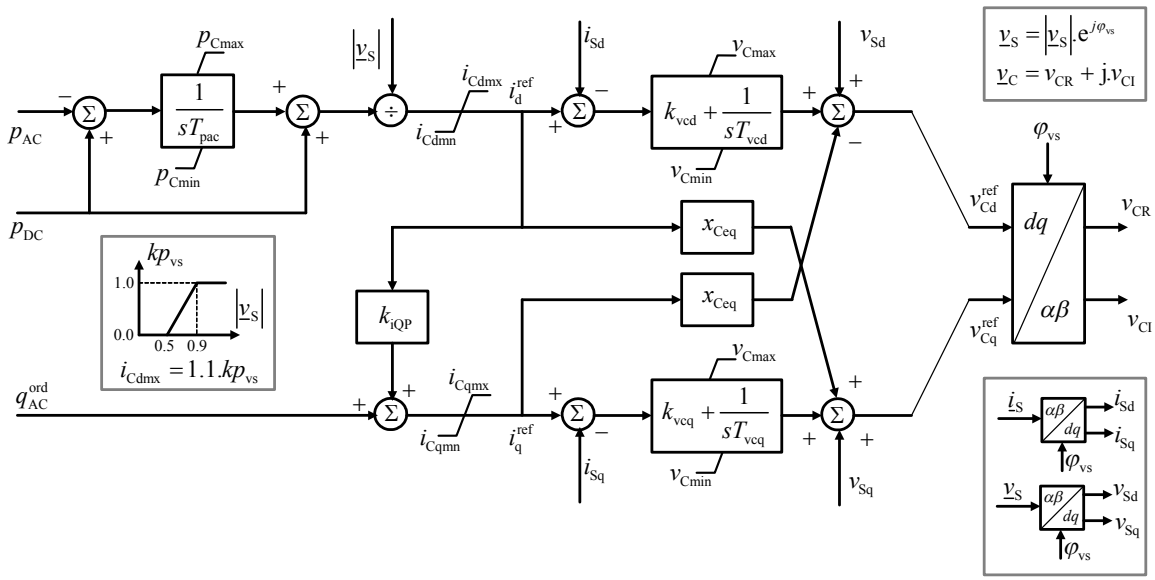

Parameter	*Value*	*Unit*	*Parameter*	*Value*	*Unit*
T_{pac}	1.00	s	k_{vcd}	0.10	pu
p_{Cmax}	1.10	pu	T_{vcd}	0.20	s
p_{Cmin}	-1.10	pu	k_{vcq}	0.10	pu
i_{Cdmx}	$1.1.kp_{vs}$	pu	T_{vcq}	0.20	s
i_{Cdmn}	$-1.1.kp_{vs}$	pu	v_{Cmax}	1.00	pu
i_{Cqmx}	1.00	pu	v_{Cmin}	-1.00	pu
i_{Cqmn}	-1.00	pu	k_{iQP}	-0.129	pu

Figure A.1. 1 Proposed generic RMS model/ AC quantity control loop

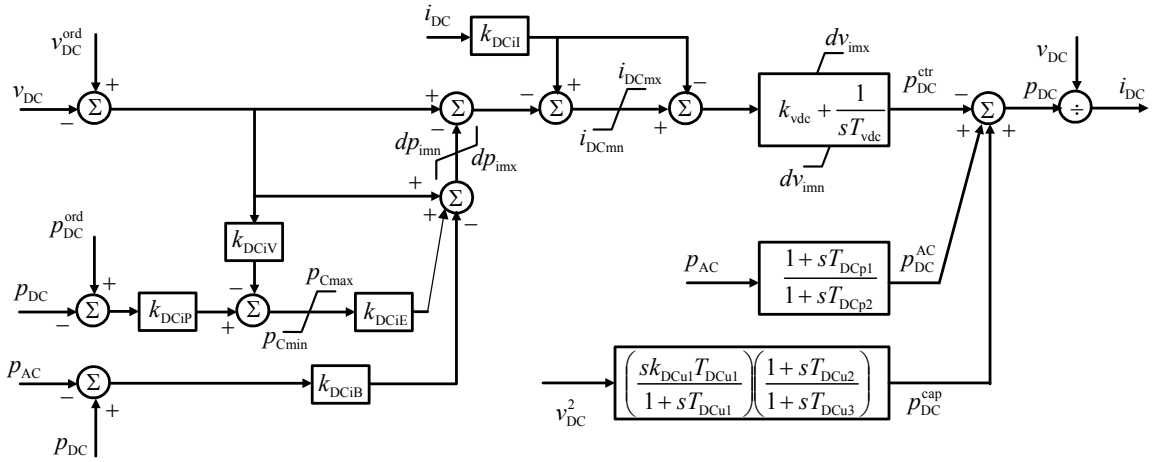

Parameter	*Value*	*Unit*	*Parameter*	*Value*	*Unit*
k_{DCiV}	0.7487	pu	k_{vdc}	2.9172	pu
k_{DCiP}	0.6467	pu	T_{vdc}	0.00064	s
k_{DCiE}	0.2000	pu	dv_{imx}	0.4000	pu
k_{DCiB}	0.1658	pu	dv_{imn}	-0.4000	pu
k_{DCiI}	0.0500	pu	T_{DCp1}	0.0050	s
dp_{imx}	0.0900	pu	T_{DCp2}	0.0547	s
dp_{imn}	-0.0900	pu	k_{DCu1}	0.0500	pu
i_{DCmx}	$1.5.kp_{vs}.k_{DCiI}$	pu	T_{DCu1}	0.0500	s
i_{DCmn}	$-1.5.kp_{vs}.k_{DCiI}$	pu	T_{DCu2}	0.5508	s
			T_{DCu3}	0.3091	s

Figure A.1. 2 Proposed generic RMS model/ DC quantity control loop

A.2 Test network for RMS model validation

The data used for modeling the generators and controllers are given below. All parameters are in a per unit in basic of power and voltage rating of the generators. Time constants are in seconds.

Table A.2. 1 *Parameters of the modeled generators*

Param.	**Unit**	**G1**	**G2**	**G3**	**G4**	**G5**
S_n	MVA	900	900	900	900	2000
P_n	MW	765	765	765	765	1800
V_n	kV	20	20	20	20	20
cos Φ_n		0.85	0.85	0.85	0.85	0.90
f_n	Hz	50	50	50	50	50
T_M	sec	11.00	13.00	12.35	10.35	13.80
r_a	p.u.	0.0025	0.0025	0.0025	0.0025	0.0041
$x_{a\sigma}$	p.u.	0.2000	0.2000	0.2000	0.2000	0.2975
T_d"	s	0.0350	0.0350	0.0350	0.0350	0.0350
x_d"	p.u.	0.2500	0.2500	0.2500	0.2500	0.3150
T_d'	s	1.3330	1.3330	1.3330	1.3330	1.1860
x_d'	p.u.	0.3000	0.3000	0.3000	0.3000	0.4807
x_d	p.u.	1.8000	1.8000	1.8000	1.8000	2.7171
T_q"	s	0.0186	0.0186	0.0186	0.0186	0.0350
x_q"	p.u.	0.2500	0.2500	0.2500	0.2500	0.3461
T_q'	s	0.1580	0.1580	0.1580	0.1580	0.2880
x_q'	p.u.	0.5500	0.5500	0.5500	0.5500	0.9972
x_q	p.u.	1.7000	1.7000	1.7000	1.7000	2.5827

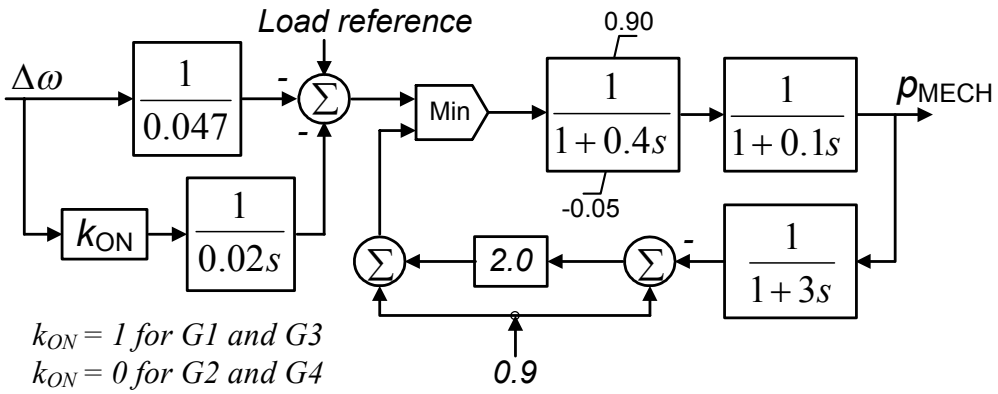

Figure A.2. 1 *Governor for G1, G2, G3 and G4*

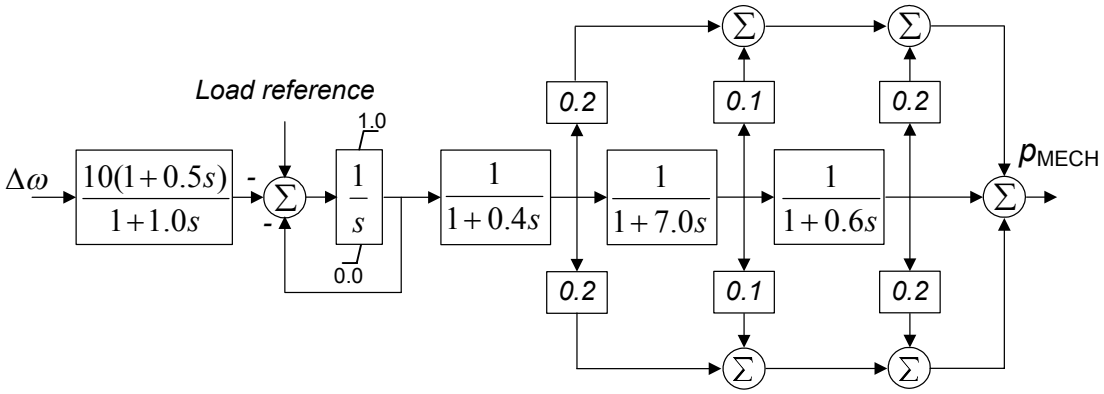

Figure A.2. 2 *Governor for G5*

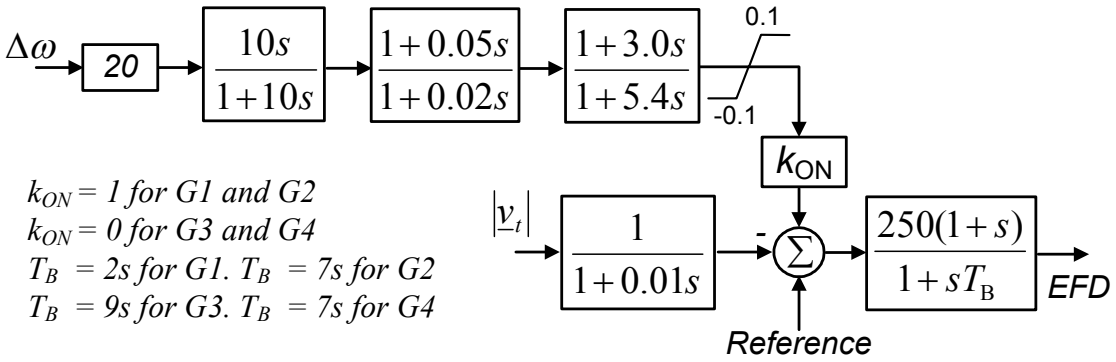

Figure A.2. 3 *AVR+PSS for G1, G2, G3 and G4*

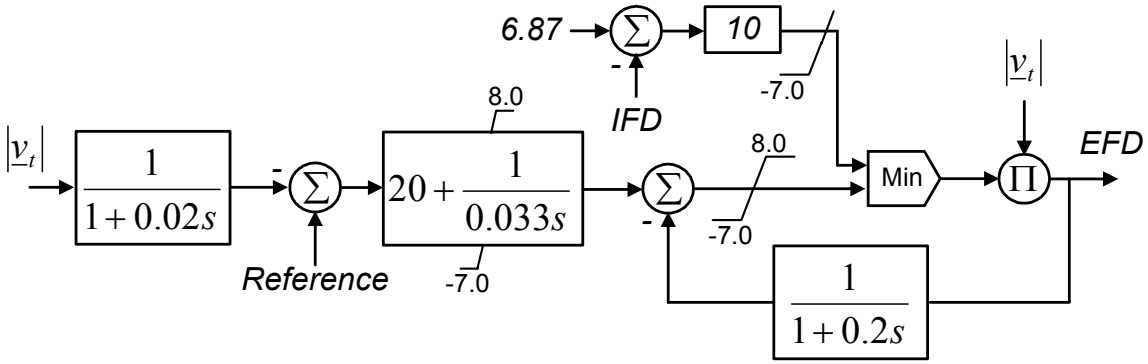

Figure A.2. 4 *AVR for G5*

A.3 Linearized model of MMC-VSC-HVDC system

In this thesis, a linearized model of a MMC-VSC-HVDC system for small-signal stability analysis can be developed based on the generic RMS model of the MMC-VSC-HVDC system proposed in the chapter 3. The linearized model emanate from linearized equations of each MMC-VSC station and the DC grid. The linearized model of each MMC-VSC station is categorized into two modules: AC and DC side modules. Each module is represented as an separate state-space model. The AC-side module comprises of linearized models of AC-side model and control module. The DC-side module includes linearized models of the current source and DC-side control module. The DC-grid linearized model is derived from the stability model in which each DC branch is modeled by Π equivalent using only resistance and capacitance elements. The combination of all linearized modules of MMC-VSC stations and the DC-grid linearized model results in the state-space model of the MMC-VSC-MTDC system. The structure of the linearized model of a Z-terminal MMC-VSC-MTDC system is described as follows. The linearized model structure described here has similarities with those previously presented in [24-26].

A.3.1 AC-side module of a MMC-VSC station

The representation of a AC-side module of i-th MMC-VSC on the terminal voltage-oriented d-q frame can be described in Laplace form as follows:

$$\begin{cases} v_{\mathrm{Sd,i}} = v_{\mathrm{Cd,i}} - r_{\mathrm{S,i}} i_{\mathrm{Sd,i}} + \omega_0 l_{\mathrm{S,i}} i_{\mathrm{Sq,i}} - l_{\mathrm{S,i}} (s i_{\mathrm{Sd,i}}) \\ v_{\mathrm{Sq,i}} = v_{\mathrm{Cq,i}} - r_{\mathrm{S,i}} i_{\mathrm{Sq,i}} - \omega_0 l_{\mathrm{S,i}} i_{\mathrm{Sd,i}} - l_{\mathrm{S,i}} (s i_{\mathrm{Sq,i}}) \end{cases} \tag{A.1}$$

where $l_{\mathrm{S,i}} = l_{\mathrm{C,i}}/2$; s is the Laplace operator, ω_0 is the fundamental frequency of the AC grid in radians/s.

The inner current controller of i-th MMC-VSC, which uses PI controllers to compute reference controlled voltages ($v_{\mathrm{Cd,i}}$ and $v_{\mathrm{Cq,i}}$), can be expressed in Laplace form using the following equations:

$$\begin{cases} v_{\mathrm{Cd,i}} = v_{\mathrm{Sd,i}} + r_{\mathrm{S,i}} i_{\mathrm{Sd,i}} - \omega_0 l_{\mathrm{S,i}} i_{\mathrm{q,i}}^{\mathrm{ref}} + \left(k_{\mathrm{pd,i}} + \dfrac{1}{s T_{\mathrm{id,i}}} \right) (i_{\mathrm{d,i}}^{\mathrm{ref}} - i_{\mathrm{Sd,i}}) \\ v_{\mathrm{Cq,i}} = v_{\mathrm{Sq,i}} + r_{\mathrm{S,i}} i_{\mathrm{Sq,i}} + \omega_0 l_{\mathrm{S,i}} i_{\mathrm{d,i}}^{\mathrm{ref}} + \left(k_{\mathrm{pq,i}} + \dfrac{1}{s T_{\mathrm{iq,i}}} \right) (i_{\mathrm{q,i}}^{\mathrm{ref}} - i_{\mathrm{Sq,i}}) \end{cases} \tag{A.2}$$

where $k_{\mathrm{pd,i}}$ and $T_{\mathrm{id,i}}$ as well as $k_{\mathrm{pq,i}}$ and $T_{\mathrm{iq,i}}$ are the gains and time constants of the PI controllers on the d and q axis's.

Combining(A.1) & (A.2) gives:

$$\begin{cases} si_{\mathrm{Sd,i}} = -\omega_0 (i_{\mathrm{q,i}}^{\mathrm{ref}} - i_{\mathrm{Sq,i}}) + (1/l_{\mathrm{Si}}) \left(k_{\mathrm{pd,i}} + \dfrac{1}{sT_{\mathrm{id,i}}} \right) (i_{\mathrm{d,i}}^{\mathrm{ref}} - i_{\mathrm{Sd,i}}) \\ si_{\mathrm{Sq,i}} = +\omega_0 (i_{\mathrm{d,i}}^{\mathrm{ref}} - i_{\mathrm{Sd,i}}) + (1/l_{\mathrm{Si}}) \left(k_{\mathrm{pq,i}} + \dfrac{1}{sT_{\mathrm{iq,i}}} \right) (i_{\mathrm{q,i}}^{\mathrm{ref}} - i_{\mathrm{Sq,i}}) \end{cases} \tag{A.3}$$

Introducing two new state variables $x_{\mathrm{d,i}}$ and $x_{\mathrm{q,i}}$ and linearizing (A.3) results in:

$$\begin{cases} \Delta \dot{i}_{\mathrm{Sd,i}} = -\omega_0 (\Delta i_{\mathrm{q,i}}^{\mathrm{ref}} - \Delta i_{\mathrm{Sq,i}}) + (1/l_{\mathrm{S,i}})(x_{\mathrm{d,i}} + k_{\mathrm{pd,i}} (\Delta i_{\mathrm{d,i}}^{\mathrm{ref}} - \Delta i_{\mathrm{Sd,i}})) \\ \Delta \dot{i}_{\mathrm{Sq,i}} = +\omega_0 (\Delta i_{\mathrm{d,i}}^{\mathrm{ref}} - \Delta i_{\mathrm{Cd,i}}) + (1/l_{\mathrm{S,i}})(x_{\mathrm{q,i}} + k_{\mathrm{pq,i}} (\Delta i_{\mathrm{q,i}}^{\mathrm{ref}} - \Delta i_{\mathrm{Sq,i}})) \\ \dot{x}_{\mathrm{d,i}} = (1/T_{\mathrm{id,i}})(\Delta i_{\mathrm{d,i}}^{\mathrm{ref}} - \Delta i_{\mathrm{Sd,i}}) \\ \dot{x}_{\mathrm{q,i}} = (1/T_{\mathrm{iq,i}})(\Delta i_{\mathrm{q,i}}^{\mathrm{ref}} - \Delta i_{\mathrm{Sq,i}}) \end{cases} \tag{A.4}$$

where $\dot{x} = sx$.

The equation (A.4) may be rewritten as:

$$\dot{\mathbf{x}}_{\mathrm{ACI,i}} = \mathbf{A}_{\mathrm{ACI,i}} \mathbf{x}_{\mathrm{ACV,i}} + \mathbf{B}_{\mathrm{ACI,i}} \Delta i_{\mathrm{d,i}}^{\mathrm{ref}} + \mathbf{C}_{\mathrm{ACI,i}} \Delta i_{\mathrm{q,i}}^{\mathrm{ref}} \tag{A.5}$$

where $\mathbf{x}_{\mathrm{ACI,i}} = (\Delta i_{\mathrm{Sd,i}}\ \Delta i_{\mathrm{Sq,i}}\ x_{\mathrm{d,i}}\ x_{\mathrm{q,i}})^{\mathrm{T}}$ and the superscript T denotes the transposition. The reference currents $\Delta i_{\mathrm{d,i}}^{\mathrm{ref}}$ and $\Delta i_{\mathrm{q,i}}^{\mathrm{ref}}$ are the output of the active power balance and reactive power controls, respectively. Different control schemes can be applied in these outer controllers. DC power $\Delta p_{\mathrm{DC,i}}$, active power Δp_{ACi}, reactive power Δq_{ACi}, AC terminal voltage magnitude $\Delta \left| \underline{v}_{\mathrm{S,i}} \right|$ and ordered reactive power $\Delta q_{\mathrm{AC,i}}^{\mathrm{ord}}$ can be the inputs of these outer controllers. In general, the linearized model of the two outer controllers can be illustrated in the following generally-deducted Laplace forms:

$$\begin{aligned} \dot{\mathbf{x}}_{\mathrm{PAC,i}} = \mathbf{A}_{\mathrm{PAC,i}} \mathbf{x}_{\mathrm{PAC,i}} + \mathbf{B}_{\mathrm{PAC,i}} \Delta p_{\mathrm{DC,i}} \\ + \mathbf{C}_{\mathrm{PAC,i}} \Delta p_{\mathrm{AC,i}} + \mathbf{D}_{\mathrm{PAC,i}} \Delta \left| \underline{v}_{\mathrm{S,i}} \right| \end{aligned} \tag{A.6}$$

$$\begin{aligned} \dot{\mathbf{x}}_{\mathrm{QAC,i}} = \mathbf{A}_{\mathrm{QAC,i}} \mathbf{x}_{\mathrm{QAC,i}} + \mathbf{B}_{\mathrm{QAC,i}} \Delta i_{\mathrm{d,i}}^{\mathrm{ref}} \\ + \mathbf{C}_{\mathrm{QAC,i}} \Delta q_{\mathrm{AC,i}} + \mathbf{D}_{\mathrm{QAC,i}} \Delta \left| \underline{v}_{\mathrm{S,i}} \right| + \mathbf{E}_{\mathrm{QAC,i}} \Delta q_{\mathrm{AC,i}}^{\mathrm{ord}} \end{aligned} \tag{A.7}$$

where $\mathbf{x}_{\mathrm{PAC,i}} = (x_{\mathrm{P,i1}} \ldots x_{\mathrm{P,iN}}\ \Delta i_{\mathrm{d,i}}^{\mathrm{ref}})^{\mathrm{T}}$ is the vector of N state variables and the output of the active power balance control; $\mathbf{x}_{\mathrm{QAC,i}} = (x_{\mathrm{Q,i1}} \ldots x_{\mathrm{Q,iM}}\ \Delta i_{\mathrm{q,i}}^{\mathrm{ref}})^{\mathrm{T}}$ is the vector of M state variables and output of the reactive power control.

The inputs of these outer controllers can be generally expressed through state variables $\Delta \mathbf{i}_{\mathrm{dq,i}} = (\Delta i_{\mathrm{Sd,i}}\ \Delta i_{\mathrm{Sq,i}})^{\mathrm{T}}$ and the AC terminal voltage on real/imaginary stationary frame (*RI*-axis) $\Delta \mathbf{v}_{\mathrm{RIi}} = (\Delta v_{\mathrm{SR,i}}\ \Delta v_{\mathrm{SI,i}})^{\mathrm{T}}$ as below:

$$\begin{cases} \Delta p_{\mathrm{AC,i}} = \mathbf{K}_{\mathrm{IP,i}} \Delta \mathbf{i}_{\mathrm{dq,i}} + \mathbf{K}_{\mathrm{UP,i}} \Delta \mathbf{v}_{\mathrm{RI,i}} \\ \Delta q_{\mathrm{AC,i}} = \mathbf{K}_{\mathrm{IQ,i}} \Delta \mathbf{i}_{\mathrm{dq,i}} + \mathbf{K}_{\mathrm{UQ,i}} \Delta \mathbf{v}_{\mathrm{RI,i}} \\ \Delta \left| \underline{v}_{\mathrm{S,i}} \right| = \mathbf{K}_{\mathrm{IU,i}} \Delta \mathbf{i}_{\mathrm{dq,i}} + \mathbf{K}_{\mathrm{UU,i}} \Delta \mathbf{v}_{\mathrm{RI,i}} \end{cases} \tag{A.8}$$

Substituting (A.8) for (A.6), (A.7), and then combining them with (A.5) gives the complete AC-side module of i-th MMC-VSC linearized model:

$$\dot{\mathbf{x}}_{\mathrm{ACV}i} = \mathbf{A}_{\mathrm{ACV}i} \mathbf{x}_{\mathrm{ACV}i} + \mathbf{B}_{\mathrm{ACV}i} \Delta p_{\mathrm{DC}i} + \mathbf{C}_{\mathrm{ACV}i} \Delta \mathbf{v}_{\mathrm{RI},i} + \mathbf{D}_{\mathrm{ACV}i} \Delta q_{\mathrm{AC},i}^{\mathrm{ord}} \tag{A.9}$$

where $\mathbf{x}_{\mathrm{ACV}i} = ((\mathbf{x}_{\mathrm{ACI}i})^{\mathrm{T}} (\mathbf{x}_{\mathrm{PAC}i})^{\mathrm{T}} (\mathbf{x}_{\mathrm{QAC}i})^{\mathrm{T}})^{\mathrm{T}}$; the coefficient matrices in (A.9) are determined as shown in Fig. A.3.1.

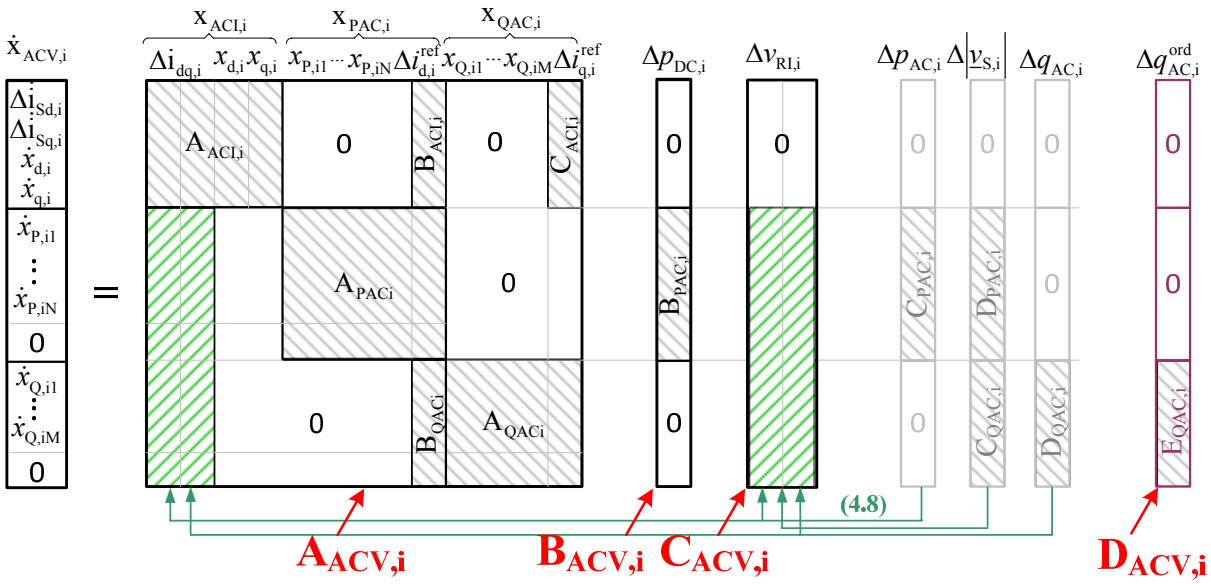

Figure A.3. 1 *AC-side module of i-th MMC-VSC linearized model*

A.3.2 DC-side module of a MMC-VSC station

A DC-side module of i-th MMC-VSC linearized model is achieved by linearizing the DC control module. The controller output is $\Delta p_{\mathrm{DC,i}}$ which is the input for the linearized model of the DC grid. Inputs of this controller considered in this work are $\Delta p_{\mathrm{AC,i}}$, $\Delta v_{\mathrm{DC,i}}$ and ordered active power $\Delta p_{\mathrm{DCi}}^{\mathrm{ord}}$. The linearized expression for linearized model of the DC side of i-th MMC-VSC may be then written as follows:

$$\dot{\mathbf{x}}_{\mathrm{DCI}i} = \mathbf{A}_{\mathrm{DCI}i} \mathbf{x}_{\mathrm{DCI}i} + \mathbf{B}_{\mathrm{DCI}i} \Delta v_{\mathrm{DC},i} + \mathbf{C}_{\mathrm{DCI}i} \Delta p_{\mathrm{AC},i} + \mathbf{D}_{\mathrm{DCI}i} \Delta p_{\mathrm{DC},i}^{\mathrm{ord}} \tag{A.10}$$

where $\mathbf{x}_{\mathrm{DCI}i} = (x_{\mathrm{D},i1} \ldots x_{\mathrm{D},iG} \, \Delta p_{\mathrm{DC}i})^{\mathrm{T}}$ is a vector including the controller state variables and an algebraic variable $\Delta p_{\mathrm{DC,i}}$.

By applying (A.8) for the term $\Delta p_{\mathrm{AC,i}}$, equation (A.10) can be rewritten as:

$$\dot{\mathbf{x}}_{\mathrm{DCI}j} = \mathbf{A}_{\mathrm{DCI}j}\mathbf{x}_{\mathrm{DCI}j} + \mathbf{B}_{\mathrm{DCI}j}\Delta v_{\mathrm{DC},j} + \mathbf{E}_{\mathrm{DCI}j}\Delta \mathbf{v}_{\mathrm{RI},j} + \mathbf{F}_{\mathrm{DCI}j}\Delta \mathbf{i}_{\mathrm{dq},i} + \mathbf{D}_{\mathrm{DCI}j}\Delta p^{\mathrm{ord}}_{\mathrm{DC},j} \tag{A.11}$$

A.3.3 DC-grid module of the MMC-VSC-HVDC linearized model

The DC grid can be represented in the stability model in which each DC branch is modeled by Π model using only resistance and capacitance elements. A DC-grid module can be expressed as follows:

$$\dot{\mathbf{x}}_{\mathrm{DCN}} = \mathbf{A}_{\mathrm{DCN}}\mathbf{x}_{\mathrm{DCN}} + \mathbf{B}_{\mathrm{DCN}}\Delta \mathbf{p}_{\mathrm{DCN}} \tag{A.12}$$

where $\mathbf{x}_{\mathrm{DCN}} = (\Delta v_{\mathrm{DC},1}\Delta v_{\mathrm{DC},2}...\Delta v_{\mathrm{DC}K})^{\mathrm{T}}$ is the state variable vector associated with the voltages on the capacitor elements of the DC grid model and $\Delta \mathbf{p}_{\mathrm{DCN}} = (\Delta p_{\mathrm{DC},1}\Delta p_{\mathrm{DC},2}...\Delta p_{\mathrm{DC}Z})^{\mathrm{T}}$ is the vector of power at the DC terminals of the MMC-VSC stations.

A.3.4 Complete linearized model of the MMC-VSC-HVDC system

To construct the state-space equations of the MMC-VSC-MTDC system, equations (A.9), (A.11) and (A.12) are combined as shown in Fig. A.3.2. The combination can be expressed as:

$$\dot{\mathbf{x}}_{\mathrm{MTDC}} = \mathbf{A}_{\mathrm{MTDC}}\mathbf{x}_{\mathrm{MTDC}} + \mathbf{B}_{\mathrm{MTDC}}\Delta \mathbf{v}_{\mathrm{RIZ}} + \mathbf{E}_{\mathrm{MTDC}}\Delta \mathbf{p}^{\mathrm{ord}}_{\mathrm{DCZ}} + \mathbf{F}_{\mathrm{MTDC}}\Delta \mathbf{q}^{\mathrm{ord}}_{\mathrm{ACZ}} \tag{A.13}$$

where $\mathbf{x}_{\mathrm{MTDC}} = (...(\mathbf{x}_{\mathrm{ACV}i})^{\mathrm{T}}.....(\mathbf{x}_{\mathrm{DCN}})^{\mathrm{T}}.....(\mathbf{x}_{\mathrm{DCI}i})^{\mathrm{T}}...)^{\mathrm{T}}$.

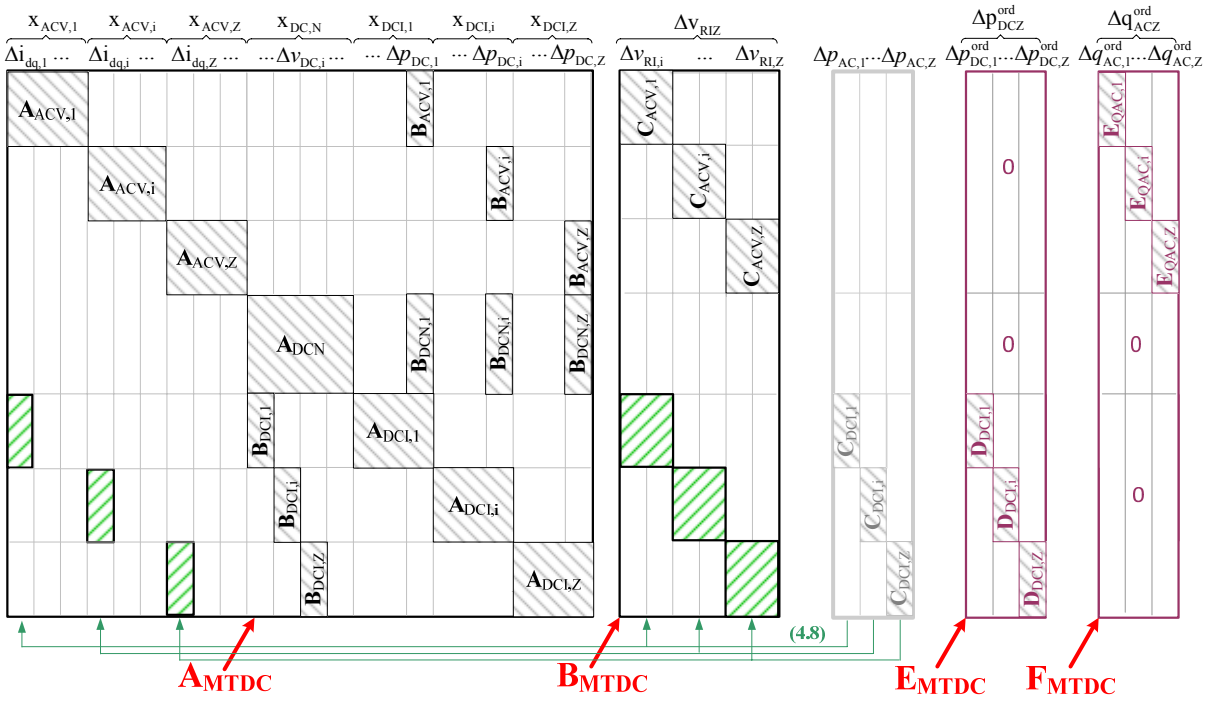

Figure A.3. 2 *Linearized model of the MMC-VSC-MTDC system*

At this stage, the non-state-space variables in $\mathbf{x}_{\mathrm{MTDC}}$ should be eliminated. $\mathbf{x}_{\mathrm{MTDC}}$ becomes a pure state variable vector $\mathbf{x}_{\mathrm{Z}}$, which includes all state-space variables of the linearized model of the MMC-VSC-MTDC system. Now, the state-space equation of the MMC-VSC-MTDC system can be created as:

$$\dot{\mathbf{x}}_{\mathrm{Z}} = \mathbf{A}_{\mathrm{Z}}\mathbf{x}_{\mathrm{Z}} + \mathbf{B}_{\mathrm{Z}}\Delta\mathbf{v}_{\mathrm{RIZ}} + \mathbf{E}_{\mathrm{Z}}\Delta\mathbf{p}_{\mathrm{DCZ}}^{\mathrm{ord}} + \mathbf{F}_{\mathrm{Z}}\Delta\mathbf{q}_{\mathrm{ACZ}}^{\mathrm{ord}} \tag{A.14}$$

The current injection $\Delta\mathbf{i}_{\mathrm{RI,i}} = (\Delta i_{\mathrm{SR,i}}\ \Delta i_{\mathrm{SI,i}})^{\mathrm{T}}$ of the MMC-VSC-HVDC at i-th converter station into the AC system can be generally expressed through $\Delta\mathbf{i}_{\mathrm{dq,i}} = (\Delta i_{\mathrm{Sd,i}}\ \Delta i_{\mathrm{Sq,i}})^{\mathrm{T}}$ and $\Delta\mathbf{v}_{\mathrm{RI,i}}$ as following:

$$\Delta\mathbf{i}_{\mathrm{RI,i}} = \mathbf{K}_{\mathrm{II,i}}\Delta\mathbf{i}_{\mathrm{dq,i}} + \mathbf{K}_{\mathrm{UI,i}}\Delta\mathbf{v}_{\mathrm{RI,i}} \tag{A.15}$$

Coupling the current injections of Z converter stations gives the current injection expression for the MMC-VSC-HVDC system to the AC system as:

$$\Delta\mathbf{i}_{\mathrm{RIZ}} = \mathbf{C}_{\mathrm{Z}}\Delta\mathbf{x}_{\mathrm{Z}} + \mathbf{D}_{\mathrm{Z}}\Delta\mathbf{v}_{\mathrm{RIZ}} \tag{A.16}$$

Neglecting changes in the reference values for active/reactive powers (last two terms in (A.14)), the complete state-space system can then be given by combining (A.14) and (A.16) as follows:

$$\begin{bmatrix} \dot{\mathbf{x}}_{\mathrm{Z}} \\ \Delta\mathbf{i}_{\mathrm{Z}} \end{bmatrix} = \begin{bmatrix} \mathbf{A}_{\mathrm{Z}} & \mathbf{B}_{\mathrm{Z}} \\ \mathbf{C}_{\mathrm{Z}} & \mathbf{D}_{\mathrm{Z}} \end{bmatrix} \begin{bmatrix} \mathbf{x}_{\mathrm{Z}} \\ \Delta\mathbf{v}_{\mathrm{RIZ}} \end{bmatrix} \tag{A.17}$$

Figure 3.6 illustrates the schematic diagram of the proposed linearized model for a point-to-point MMC-VSC-HVDC system. It also reveals the linkage between linearized modules and the MMC-VSC-HVDC system with the interconnected ac system. This flexible structure can easily be adapted for modeling multi-terminal MMC-VSC-HVDC systems.

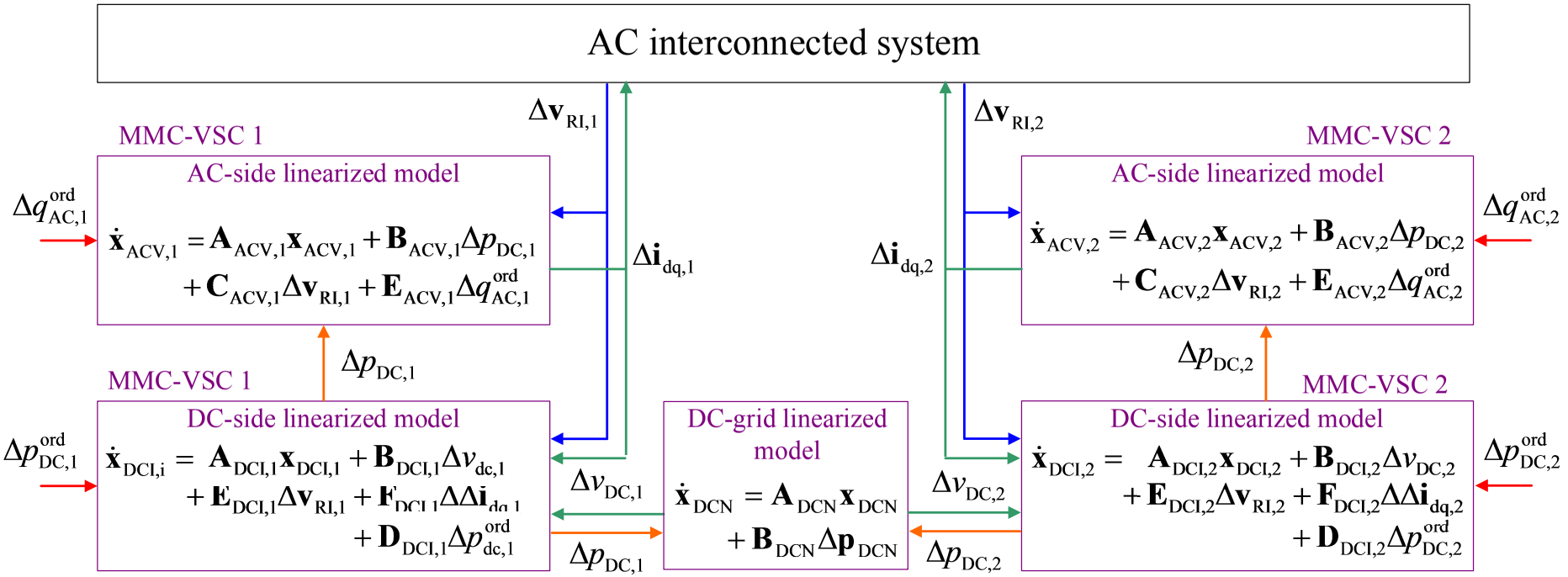

$\Delta \mathbf{i}_{dq,i} = (\Delta i_{d,i}\ \Delta i_{q,i})^T$ Direct and quadrature terminal current vector

$\Delta \mathbf{v}_{RI,i} = (\Delta v_{R,i}\ \Delta v_{I,i})^T$ Real and imaginary terminal voltage vector

$\mathbf{x}_{ACV,i} = (\Delta i_{d,i}\ \Delta i_{q,i}\ ...x_{ACV,i}...)^T$ State variable vector including terminal current and AC control module state variables

$\mathbf{x}_{DCI,i} = (...x_{DCI,i}\ ...\ \Delta p_{DC,i})^T$ State variable vector including DC control module state variables and an algebraic variable $\Delta p_{DC,i}$

$\mathbf{x}_{DCN} = (\Delta v_{DC,1}\ \Delta v_{DC,2})^T$ State variable vector associated with capacitor voltages of the dc grid model

$\Delta \mathbf{p}_{DCN} = (\Delta p_{DC,1}\ \Delta p_{DC,2})^T$ Algebraic variable vector of DC power

the superscript T denotes transposition

Figure A.3. 3 Linearized model structure of a MMC-VSC-HVDC system

A.4 Setting parameters of the optimal POD options

Table A.4. 1 Setting parameters of the optimal POD options

POD option	Setting parameter							
	Input (bus angle)	Output (channel)	k_W (pu)	T_W (s)	T_1 (s)	T_2 (s)	T_3 (s)	T_4 (s)
P-BEST-L Best local	ϕ_{B7}	P-VSC1	2.000	7.529	0.028	0.020	2.000	1.190
	ϕ_{B9}	P-VSC2	-1.463	17.278	1.058	1.854	0.644	1.058
	ϕ_{B9}	P-VSC2	1.305	4.404	0.701	0.047	0.632	0.906
Q-BEST-L Best local	ϕ_{B7}	Q-VSC1	0.659	1.969	2.000	0.134	0.020	0.431
	ϕ_{B9}	Q-VSC2	-2.000	0.200	1.155	1.497	1.362	0.020
	ϕ_{B9}	Q-VSC2	-0.851	0.200	0.020	2.000	0.965	0.020
P-BEST-G Best global	ϕ_{B6}	P-VSC1	1.851	16.311	1.306	1.907	0.657	0.020
	ϕ_{B10}	P-VSC2	2.000	20.000	0.655	0.059	1.983	1.469
	ϕ_{B11}	P-VSC3	2.000	0.200	0.880	2.000	2.000	0.504
Q-BEST-G Best global	ϕ_{B6}	Q-VSC1	1.834	0.873	0.020	1.906	2.000	0.103
	ϕ_{B10}	Q-VSC2	1.985	12.245	1.683	0.539	0.567	0.121
	ϕ_{B11}	Q-VSC2	1.506	12.820	2.000	0.589	0.195	1.806
PQ-BEST-L Best local	ϕ_{B7}	P-VSC1	-2.000	18.004	0.338	1.882	1.603	0.020
	ϕ_{B9}	Q-VSC2	-0.810	17.481	2.000	2.000	1.622	2.000
	ϕ_{B9}	P-VSC2	0.971	5.900	1.475	0.020	0.552	1.391
PQ-BEST-G Best global	ϕ_{B6}	P-VSC1	2.000	7.529	0.028	0.020	2.000	1.190
	ϕ_{B10}	Q-VSC2	-1.463	17.278	1.058	1.854	0.644	1.058
	ϕ_{B11}	P-VSC3	1.305	4.404	0.701	0.047	0.632	0.906

A.5 Test network for the primary frequency control analysis

The data used for modeling the generators and controllers are given below. All parameters are in a per unit in basic of power and voltage rating of the generators. Time constants are in seconds. No POD controller is applied for the MMC-VSC-MTDC system.

Table A.5. 1 *Parameters of the modeled generators*

Param.	**Unit**	**G1**	**G3**	**G5**
S_n	MVA	2000	2000	2000
P_n	MW	765	765	1800
V_n	kV	20	20	20
$\cos \Phi_n$		0.85	0.85	0.90
f_n	Hz	50	50	50
T_M	sec	11.00	12.35	13.80
r_a	p.u.	0.0025	0.0025	0.0041
$x_{a\sigma}$	p.u.	0.2000	0.2000	0.2975
T_d"	s	0.0350	0.0350	0.0350
x_d"	p.u.	0.2500	0.2500	0.3150
T_d'	s	1.3330	1.3330	1.1860
x_d'	p.u.	0.3000	0.3000	0.4807
x_d	p.u.	1.8000	1.8000	2.7171
T_q"	s	0.0186	0.0186	0.0350
x_q"	p.u.	0.2500	0.2500	0.3461
T_q'	s	0.1580	0.1580	0.2880
x_q'	p.u.	0.5500	0.5500	0.9972
x_q	p.u.	1.7000	1.7000	2.5827

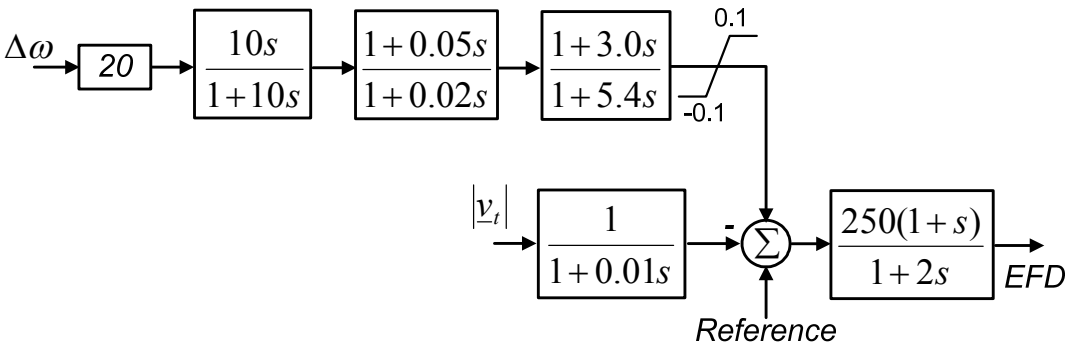

Figure A.5. 1 *AVR+PSS for G1 and G3*

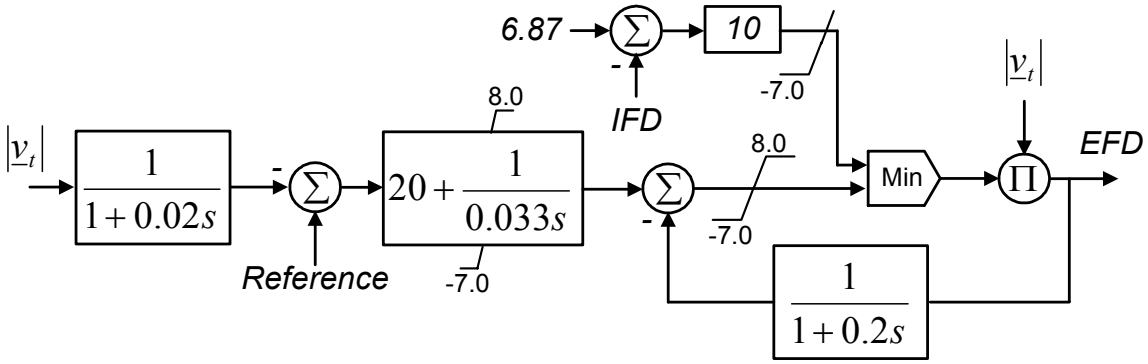

Figure A.5. 2 *AVR for G5*

A.6 Test network for control coordination analysis

Table A.6. 1 *Line parameters*

From Bus	To Bus	Name	Length factor	Resistance (Ohm)	Impedance (Ohm)	Capacitance (nF)	V_N (kV)
BUS25	BUS02	L02-25	1.0	8.330	10.240	330.0	345.0
BUS02	BUS01	L01-02	1.0	4.170	48.920	1560.0	345.0
BUS02	BUS03	L02-03	1.0	1.550	17.970	570.0	345.0
BUS03	BUS18	L03-18	1.0	1.310	15.830	480.0	345.0
BUS18	BUS17	L17-18	1.0	0.830	9.760	290.0	345.0
BUS17	BUS27	L17-27	1.0	1.550	20.590	720.0	345.0
BUS27	BUS26	L26-27	1.0	1.670	17.500	530.0	345.0
BUS25	BUS26	L25-26	1.0	3.810	38.450	1140.0	345.0
BUS26	BUS28	L26-28	1.0	5.120	56.420	1740.0	345.0
BUS28	BUS29	L28-29	1.0	1.670	17.970	550.0	345.0
BUS26	BUS29	L26-29	1.0	6.780	74.390	2290.0	345.0
BUS17	BUS16	L16-17	1.0	0.830	10.590	300.0	345.0
BUS16	BUS15	L15-16	1.0	1.070	11.190	380.0	345.0
BUS16	BUS19	L16-19	2.5	1.900	23.200	680.0	345.0
BUS16	BUS21	L16-21	1.0	0.950	16.070	560.0	345.0
BUS16	BUS24	L16-24	1.0	0.360	7.020	150.0	345.0
BUS21	BUS22	L21-22	2.5	0.950	16.670	570.0	345.0
BUS24	BUS23	L23-24	2.5	2.620	41.660	800.0	345.0
BUS15	BUS14	L14-15	1.0	2.140	25.830	820.0	345.0
BUS03	BUS04	L03-04	1.0	1.550	25.350	490.0	345.0
BUS04	BUS14	L04-14	1.0	0.950	15.350	310.0	345.0
BUS04	BUS05	L04-05	1.0	0.950	15.240	300.0	345.0
BUS05	BUS06	L05-06	1.0	0.240	3.090	100.0	345.0
BUS06	BUS07	L06-07	1.0	0.710	10.950	250.0	345.0
BUS07	BUS08	L07-08	1.0	0.480	5.480	170.0	345.0
BUS05	BUS08	L05-08	1.0	0.950	13.330	330.0	345.0
BUS08	BUS09	L08-09	1.0	2.740	43.210	850.0	345.0
BUS01	BUS39	L01-39	1.0	1.190	29.760	1670.0	345.0
BUS39	BUS09	L09-39	1.0	1.190	29.760	2670.0	345.0
BUS06	BUS11	L06-11	1.0	0.830	9.760	310.0	345.0
BUS14	BUS13	L13-14	1.0	1.070	12.020	380.0	345.0
BUS11	BUS10	L10-11	1.0	0.480	5.120	160.0	345.0
BUS13	BUS10	L10-13	1.0	0.480	5.120	160.0	345.0
BUS22	BUS23	L22-23	1.0	0.710	11.430	410.0	345.0

Table A.6. 2 *Load parameters*

Bus name	P (MW)	Q (MVAr)
BUS03	322.0	2.4
BUS04	500.0	184.0
BUS07	233.8	84.0
BUS08	522.0	176.0
BUS12	8.5	88.0
BUS15	320.0	153.0
BUS16	529.0	32.3
BUS18	158.0	30.0
BUS20	680.0	103.0
BUS21	474.0	115.0
BUS23	247.5	84.6
BUS24	308.6	-92.2
BUS25	224.0	47.2
BUS26	139.0	17.0
BUS27	281.0	75.5
BUS28	206.0	27.6
BUS29	283.5	26.9
BUS31	9.2	4.6
BUS39	1104.0	250.0

Table A.6. 3 *Transformer parameters*

From Bus	To Bus	Name	Sn (MVA)	Upn (kV)	Upr (kV)	Usn (kV)	Usr (kV)	urk (%)	uk (%)
BUS25	BUS37	T37	100.0	345.0	353.630	10.0	10.0	0.060	2.320
BUS02	BUS30	T30	100.0	345.0	353.630	10.0	10.0	0.000	1.810
BUS29	BUS38	T38	100.0	345.0	353.630	10.0	10.0	0.080	1.560
BUS22	BUS35	T35	100.0	345.0	353.630	10.0	10.0	0.000	1.430
BUS06	BUS31	T31	100.0	345.0	369.150	10.0	10.0	0.000	2.500
BUS12	BUS11	T11-12	100.0	345.0	347.070	345.0	345.0	0.160	4.350
BUS12	BUS13	T12-13	100.0	345.0	347.070	345.0	345.0	0.160	4.350
BUS10	BUS32	T32	100.0	345.0	369.150	10.0	10.0	0.000	2.000
BUS19	BUS20	T19-20	100.0	345.0	365.700	345.0	345.0	0.070	1.380
BUS20	BUS34	T34	100.0	345.0	348.110	10.0	10.0	0.090	1.800
BUS19	BUS33	T33	100.0	345.0	369.150	10.0	10.0	0.070	1.420
BUS23	BUS36	T36	100.0	345.0	345.000	10.0	10.0	0.050	2.720

Table A.6. 4 *Generator loadings*

Param.	**G30**	**G31**	**G32**	**G33**	**G34**	**G35**	**G36**	**G37**	**G38**	**G39**
v_G (pu)	1.004	0.982	0.975	0.990	0.990	1.020	1.030	1.028	1.026	0.990
ϕ_G (deg)	18.6	0.0	10.2	21.0	22.2	15.0	20.9	17.0	20.5	1.0
P_G (MW)	850.0	97.0	650.0	680.0	660.0	650.0	660.0	540.0	830.0	1000.0
Q_G (MVAr)	144.9	239.2	255.7	129.6	142.3	138.4	72.9	129.5	82.6	87.9

Table A.6. 5 *Generator dynamic parameters*

Name	**Unit**	**G30**	**G31**	**G32**	**G33**	**G34**	**G35**	**G36**	**G37**	**G38**	**G39**
S_n	MVA	1000	1000	1000	1000	1000	1000	1000	1000	1000	10000
U_n	kV	10	10	10	10	10	10	10	10	10	345
T_M	sec	8.40	6.06	7.16	5.72	5.20	6.96	5.28	4.86	6.99	10.00
r_a	p.u.	0.0000	0.0000	0.0000	0.0000	0.0000	0.0600	0.0000	0.0100	0.0000	0.0000
$x_{a\sigma}$	p.u.	0.1350	0.3550	0.3500	0.3500	0.5450	0.2250	0.3250	0.2850	0.3500	0.0350
T_d"	s	0.0000	0.0000	0.0000	0.0000	0.0000	0.0000	0.0000	0.0000	0.0000	0.0000
x_d"	p.u.	0.3099	0.6999	0.5299	0.4399	1.3199	0.4999	0.4899	0.5699	0.5699	0.0599
T_d'	s	10.2000	6.5600	5.7000	5.6900	5.4000	7.3000	5.6600	6.7000	4.7900	7.0000
x_d'	p.u.	0.3100	0.7000	0.5300	0.4400	1.3200	0.5000	0.4900	0.5700	0.5700	0.0600
x_d	p.u.	1.6000	2.9560	2.5600	2.6260	6.7600	2.5460	2.9560	2.9600	2.1160	0.2600
T_q"	s	0.0000	0.0000	0.0000	0.0000	0.0000	0.0000	0.0000	0.0000	0.0000	0.0000
x_q"	p.u.	0.6898	1.6999	0.8799	1.6599	1.6599	0.8099	1.8599	0.9099	0.5899	0.0799
T_q'	s	0.0000	1.5000	1.5000	1.5000	0.4400	0.4000	1.5000	0.4100	1.9600	0.7000
x_q'	p.u.	0.6899	1.7000	0.8800	1.6600	1.6600	0.8100	1.8600	0.9100	0.5900	0.0800
x_q	p.u.	0.6900	2.8200	2.3700	2.5800	6.2000	2.4100	2.9200	2.8000	2.0500	0.1900

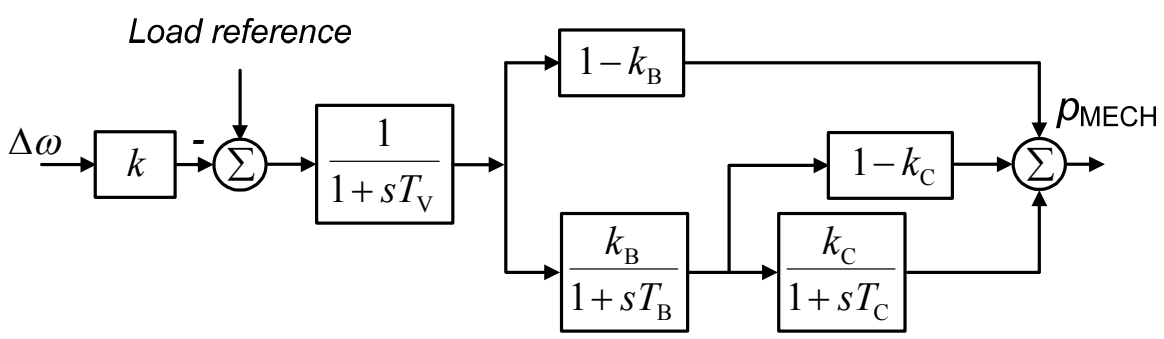

Figure A.6. 1 *Governor block diagram*

Table A.6. 6 *Setting parameters for generator governors*

Param.	**G30**	**G31**	**G32**	**G33**	**G34**	**G35**	**G36**	**G37**	**G38**
k (pu)	4.200	2.200	0.870	15.920	17.440	5.120	3.900	2.148	3.312
T_V (s)	0.200	0.450	3.000	0.240	3.000	0.120	0.200	3.000	0.380
k_B (pu)	0.500	1.000	1.000	1.000	1.000	1.000	1.000	1.000	1.000
T_B(s)	0.400	0.100	5.000	0.180	5.000	0.150	0.180	3.000	0.100
k_C (pu)	0.500	0.755	1.000	0.798	1.000	0.533	0.500	1.000	0.720
T_C(s)	0.965	54.000	5.000	10.000	5.000	9.640	7.500	4.000	6.000

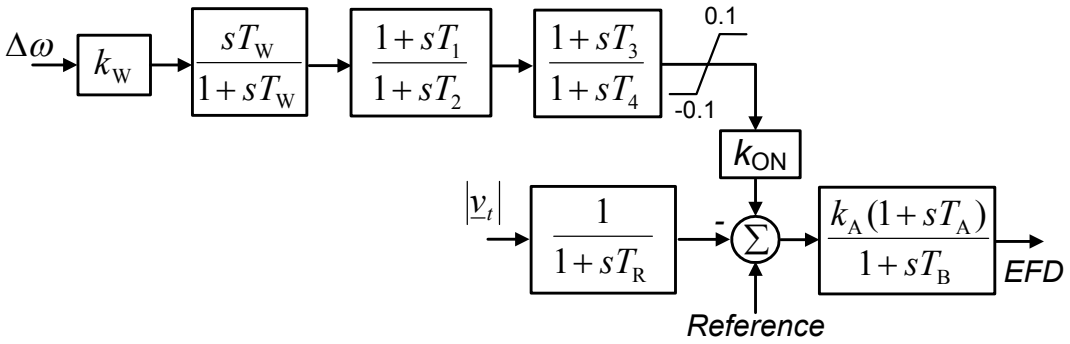

Figure A.6. 2 *AVR+PSS block diagram*

Table A.6. 7 *Setting parameters for AVR + PSS*

Name	**G30**	**G31**	**G32**	**G33**	**G34**	**G35**	**G36**	**G37**	**G38**
T_R (s)	0.010	0.010	0.010	0.010	0.010	0.010	0.010	0.010	0.010
k_A (pu)	200.000	150.000	150.000	100.000	100.000	100.000	100.000	300.000	300.000
T_A (s)	1.000	1.500	1.500	1.000	1.000	1.000	1.000	1.000	1.000
T_B (s)	2.000	2.500	2.500	3.000	3.000	3.000	3.000	2.000	2.000
k_{ON} (pu)	1	1	1	1	0	1	1	1	1
k_W (pu)	5.500	4.000	4.000	2.000	4.500	-4.500	2.787	6.000	8.000
T_W (s)	9.511	20.000	0.200	15.709	4.370	20.000	20.000	0.200	8.507
T_1 (s)	2.000	2.000	0.020	2.000	2.000	0.020	2.000	0.247	1.666
T_2 (s)	0.509	0.020	0.025	0.020	0.020	1.747	1.004	2.000	0.476
T_3 (s)	1.649	2.000	1.729	0.025	2.000	1.622	2.000	0.437	2.000
T_4 (s)	0.408	0.126	0.262	0.066	1.178	0.025	0.020	0.108	0.885

Table A.6. 8 *Setting parameters for PFS controllers*

VSC	VSC droop kVP (pu)	***Setting parameters for PFS controller***					
		α_{DC} (pu)	k_{PFS0} (MW/Hz)	T_P (s)	T_{AN} (s)	R_N (pu)	R_L (pu)
1	0.162	1.0	918.9	8.436	11.474	0.317	1.00
2	0.315	1.0	918.0	8.270	11.395	0.290	1.00
3	0.669	1.0	917.1	8.271	11.459	0.295	1.00

Table A.6. 9 *Setting parameters for FVS controllers*

VSC station	***Setting parameters for FVS controller***					
	k_{FVS} (pu)	T_1 (s)	T_1 (s)	T_2 (s)	T_3 (s)	T_4 (s)
1&2&3	-20	30	0.5	3.5	1.2	2.5

Table A.6. 10 *Setting parameters of the optimal POD options*

POD option	Setting parameter							
	Input (bus angle)	Output (channel)	k_W (pu)	T_W (s)	T_1 (s)	T_2 (s)	T_3 (s)	T_4 (s)
POD on Q channel	ϕ_{B19}- ϕ_{B16}	Q-VSC1	-14.169	5.639	1.375	0.628	0.875	1.521
	ϕ_{B19}- ϕ_{B16}	Q-VSC1	15.000	10.033	1.371	0.605	1.923	1.546
	ϕ_{B19}- ϕ_{B16}	Q-VSC1	-3.768	20.000	1.973	0.749	0.046	0.105
	ϕ_{B22}- ϕ_{B16}	Q-VSC3	-3.873	13.329	2.000	1.657	0.020	2.000
	ϕ_{B22}- ϕ_{B16}	Q-VSC3	-14.062	1.141	2.000	2.000	0.020	2.000
	ϕ_{B22}- ϕ_{B16}	Q-VSC3	1.722	8.682	0.927	0.020	0.374	2.000
POD on P channel	ϕ_{B19}- ϕ_{B16}	P-VSC1	-8.547	0.200	1.248	0.020	0.125	1.817
	ϕ_{B19}- ϕ_{B16}	P-VSC1	0.455	5.744	1.373	1.552	0.621	1.717
	ϕ_{B19}- ϕ_{B16}	P-VSC1	1.356	12.434	0.206	0.252	0.020	1.007
	ϕ_{B22}- ϕ_{B16}	P-VSC3	-4.374	10.749	1.574	1.971	1.690	2.000
	ϕ_{B22}- ϕ_{B16}	P-VSC3	-9.549	0.200	0.605	0.917	0.569	0.119
	ϕ_{B22}- ϕ_{B16}	P-VSC3	5.170	17.212	1.911	2.000	1.567	0.762

Curriculum Vitae

Ngọc-Tuấn Trịnh

Born September 04, 1980 in Nghe-An, Vietnam.

Education

1998-2003	Bachelor of Science Electrical Power Engineering Hanoi University of Technology Hanoi, Vietnam
2005-2008	Master of Science Electrical Power Engineering RWTH Aachen University Aachen, Germany
2012-2016	Doctor of Engineering Science Institute of Electrical Power Systems Duisburg-Essen University Duisburg, Germany

Work History

2003 - 2005	Technician Department of Procurement, Northern Power Project Management Board (NPPMB) Electricity of Viet Nam (EVN), Vietnam.
2012 - 2016	Researcher Institute of Electrical Power Systems (EAN) University Duisburg-Essen, Germany.
since 2008	Consultant Power Technologies International (PTI), Siemens AG Erlangen, Germany.

Electrical Engineering